IMPROVEMENTS IN CATALYSIS FOR THE COPOLYMERIZATION OF ETHYLENE WITH POLAR COMONOMERS

BY

BRIAN VAN DYKE

THESIS

Submitted in partial fulfillment of the requirements
for the degree of Master of Science in Chemistry
in the Graduate College of the
University of Illinois Urbana-Champaign, 2022

Urbana, Illinois

Adviser:

Associate Professor Damien Guironnet

ABSTRACT

Polyolefins are the most abundant polymer by volume, making up over half of the 300 million tons of plastics produced in 2015. This is not without a reason: polyolefins such as polypropylene and polyethylene (PE) have numerous applications and advantages in processability, chemical resistance, strength, and low toxicity. Much work has been done on developing organometallic catalysts capable of synthesizing polyolefins, however there are still some remaining challenges in the field relating to the incorporation of polar comonomers These challenges can be addressed through in improvements in late-transition metal catalysis, and three will be approached in this work: the copolymerization of polar olefins with ethylene, the non-alternating copolymerization of ethylene and carbon monoxide (CO), and the stereocontrolled copolymerization of propylene with vinyl silyl ethers (VSEs).

The copolymerization of ethylene with polar olefins greatly improves the adhesion properties of nonpolar commodity polyolefins, producing cutting-edge materials with novel physical properties and potential applications. While much progress has been made in this field of polyolefin catalysis, the structure-function relationships that govern catalyst properties such as activity, polar monomer incorporation and molecular weight control are still non-trivial. To shed light on the relationships, we set out to examine nickel- and palladium-catalyzed polyolefin synthesis with new *N*-acylamidine based ligands. These ligands are easily accessible through a modular three-step synthesis that allow for the facile tuning of ligand steric and electronic properties. By modulating these ligand features and examining their effect on catalytic activity, insight of structure-function relations can be obtained.

A variety of *N*-acylamidine ligands were synthesized containing Acyl, thiobenzoyl, and phosphoryl chelating moieties. While the palladium-methyl complexes of these ligand were able to be synthesized and isolated, none showed significant activity towards ethylene homopolymerization, preventing any investigation into copolymerizations with polar olefin monomers. Attempts to synthesize the nickel-methyl analogues were unsuccessful. The inability of these ligands to both polymerize ethylene and support a nickel-methyl species was attributed to poor coordination strength, as observed by decomposition under polymerization/metalation conditions. Attempts to improve coordination strength through synthesizing tetradentate bis-*N*-acyl amidines were unsuccessful, as well as metalation attempts with group (IV) metals.

The chemical stability of its hydrocarbon backbone of PEs makes it mostly unsensitive to hydrolysis or photodegradation, leading to rampant plastic pollution. Increasing the rate of photodegradation of these materials is possible through the incorporation of carbonyl monomers from the copolymerization of ethylene and CO. Late transition metal catalysts can copolymerize ethylene and CO to form photodegradable polyketones. The significantly stronger coordination of carbon monoxide over ethylene results in the formation of a purely alternated polyketone that has dissimilar physical properties to commodity polyolefins. A few catalysts have been developed to synthesize HDPE analogs with <5% CO – Pd-Phosphinosulfonates, Ni-Phosphinophenolates, and Pd-diphosphazane monoxide catalysts. However, these catalysts exhibit low polymerization activity. We report the utilization of a highly-active biaryl-substituted Pd-phosphinosulfonate catalyst for the non-alternating copolymerization of CO and ethylene.

Polyethylene with CO content varying between 0.1-50% CO were synthesized with up to 170x higher activity and 15x larger M_n than the commercial cationic Pd-bisphosphine complexes. Fine analysis of the polymer microstructure at low CO content suggests that the copolymerization

does not follow the classical random Mayo-Lewis model. At low CO content, greater than statistical amount of alternated ketone segments are present in the polymer. We attribute this to a penultimate monomer effect, which may be either kinetic (insertion rate) or thermodynamic (monomer coordination) in origin. Attempts to elucidate the origins of this effect using copolymerization parameters were proved to be mathematically impossible and attempts to determine them were compounded by an extreme sensitivity to CO by the Pd-Phosphinosulfonate complex.

$PEX_{b,}$ a crosslinked ethylene/vinyl silyl ether (VSE) copolymer, is used in construction applications as a piping material and wire insulator. However, the isotactic polypropylene (iPP) analogue of PEX_b has not been reported and could potentially be an impactful material by merit of the higher strength of iPP compared to HDPE. The ethylene/VSE copolymer cross-linked to form PEX_b can be synthesized using diimine-supported cationic nickel-methyl complexes, which usually lack stereocontrol in polypropylene polymerization due to facile “chain-walking” (consecutive β-hydride elimination/re-insertion). In 2005, Coates and coworkers reported an axially-shielded diimine nickel(II) bromide complex capable of suppressing chain-walking and polymerizing propylene in a stereocontrolled manner. However, this complex requires a alkyl aluminum initiator, which is incompatible with polar comonomers. We set out to synthesize a cationic nickel methyl complex supported by this axially shielded diimine to enable the stereocontrolled copolymerization of propylene with VSEs. The nickel (II) dimethyl complex of this ligand was able to be isolated and characterized by nuclear magnetic resonance spectroscopy. Future work will be directed toward the synthesis of the final cationic Nickel methyl complex and copolymerization studies.

ACKNOWLEDGMENTS

I would like to take this opportunity to thank my advisor, Damien Guironnet, for giving me a second chance at my graduate studies and letting me join his group after a mental health crisis ended my time in my previous group. He has been extremely understanding of my circumstances and has consistently advocated for what is best for my future career, even in the midst of scientific failure. I could not have asked for a better group of engineers and chemists to work with in the Guironnet lab. I'd like to thank them for providing camaraderie, valuable scientific discussion, cat-sitting, gym partnership, and convincing me that I like some wine, as long as it tastes like whiskey. I'd also like to that Kyle Webb down in the electric shop for equipment repairs/entertaining discussions of geopolitics and Dean Olsen for helping me with all my NMR needs.

I also must thank my friends and family for constantly being my support system throughout four and a half tumultuous years in my graduate studies, despite being half a country away. My best friends, Gunther Druker and Brendan Cherry, for always being there for me, joining me in camping adventures and getting dragged along to death metal shows. I especially thank my Dad for calling me every single night to talk about repairing injection blow-molding equipment and the Philadelphia Eagles, regardless if either are doing well. I'd like to thank Mandy Taisto, a mentor, friend, and kindred spirit who convinced me to follow my dreams even thought the end didn't seem clear. My mental health team, Carol Baxter, Valorie Groves, and Cheryl Zaabel for helping fix the weird flesh computer inside my head. Finally, my cat, Arnie, who can't read this but will continue to be adorable and headbutt me later

Dedicated to Wally Van Dyke

TABLE OF CONTENTS

CHAPTER 1: INTRODUCTION

Polyolefins are the most abundant polymer by volume, making up over half of the 300 million tons of plastics produced in 2015.[1] This is not without a reason: polyolefins such as polypropylene and polyethylene (PE) have numerous applications and advantages in processability, chemical resistance, strength, and low toxicity.[2] Much work has been done on developing organometallic catalysts capable of synthesizing polyolefins, but there are still a few remaining challenges in polyolefin synthesis (**Figure 1**).

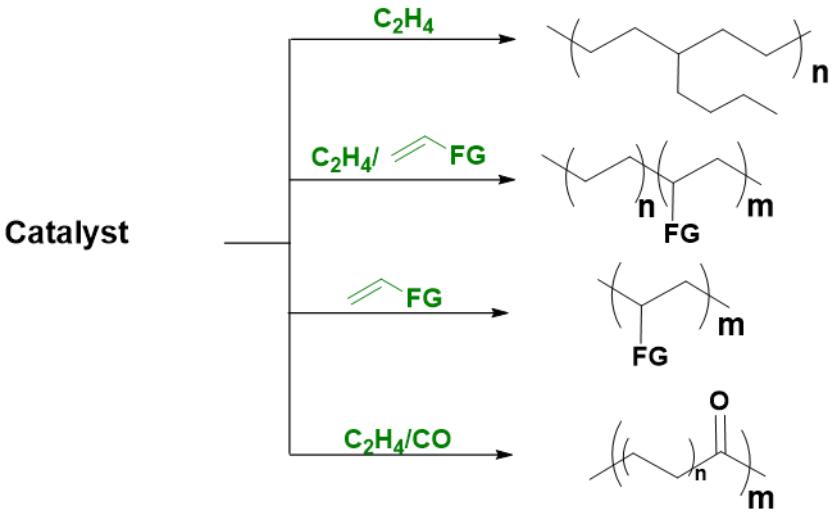

Figure 1. *Challenges in polyolefin synthesis*

These challenges include the copolymerization of polar comonomers, the non-alternating copolymerization of CO, the synthesis of low-density polyethylene at low pressures (10 vs. 10^3 bar C_2H_4), and the stereoselective polymerization of polar comonomers.[3-5] To be addressed, all of these will require the development of new catalysts. The goal of this project is to design new ligands for the copolymerization of ethylene with polar monomers.

By nature of being a hydrocarbon, polyolefins such as PE are very nonpolar. This becomes a problem during adhesion, as polar adhesives cannot stick to non-polar polymer surface. One method to solve this problem is by incorporating polar groups along the polymer backbone through

copolymerization. This conceptually simple solution is made very difficult by the high oxophilicity of the early-transition metal catalysts. Ziegler-Natta, Phillips and metallocene catalysts do not tolerate polar functionalities. This is due to κ-coordination of the polar functionality to the metal center, which prevents insertion into the alkene bond (**Figure 2**).[6] In contrast, late transition metals

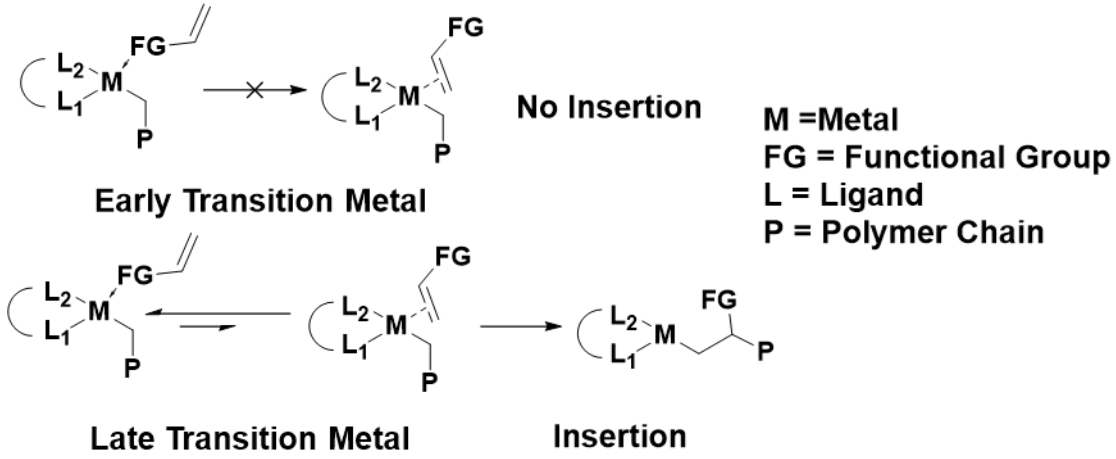

Figure 2. *Coordination modes of polar olefin monomers*

catalysts are compatible with polar monomer as they experience more of an equilibrium between κ- and π-coordination.

Much work has been done on developing late-transition metal catalysts for the copolymerization with polar comonomers.[7] A major breakthrough occurred in the mid-1990s with Brookhart's cationic Pd(II) diimine catalyst (**Figure 3A**).[8] These complexes were able to copolymerize vinyl comonomers with ethylene to produce highly branched copolymers. The polar

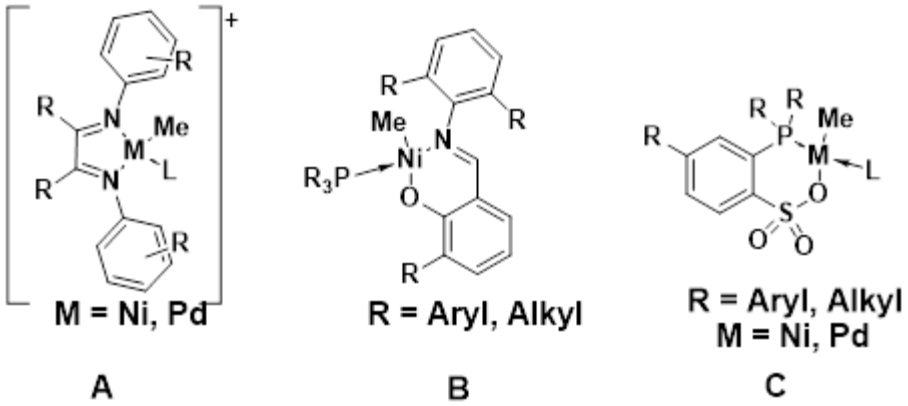

Figure 3. *Major late-transition metal catalyst for the copolymerization of polar olefins and ethylene*

monomers are mostly located on the ends of these branches, which are formed via chain-walking. Diimine complexes can copolymerize acrylates but could not handle more challenging monomers such as vinyl acetate, acrylonitrile, and vinyl ethers.[9] The next big hit came from Grubbs and coworkers in 1998 with their neutral Ni(II)-phenoxyimine catalyst (**Figure 3B**).[10] This catalyst produced linear copolymers at 6 times the activity of the diimine system but was limited to functionalized norbornene monomers. A further advance was made in 2002 by Drent and coworkers with the phosphinosulfonate ligand.[11] The neutral Pd complexes generated from this ligand (**Figure 3C**) yield highly linear copolymers between acrylates and ethylene and have shown to be competent with a wide range of polar comonomers. Incorporation of acrylate up to 50% has been reported with these catalysts.[12] While much work has been done in this field, many of these catalysts suffer from low activity compared to their industrial counterparts (10^3 vs 10^{10} g $mmol^{-1}h^{-1}$), preventing their commercial implementation. To address the remaining challenges in polyolefin synthesis, new catalysts must be developed.

CHAPTER 2: *N*-ACYLAMIDINE LIGANDS AS A NEW PLATFORM FOR TRANSITION METAL-CATALYZED OLEFIN POLYMERIZATION

2.1 Motivation

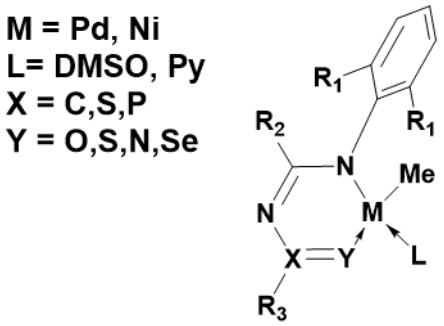

Figure 4. *Late-transition metal N-Acylamidine complexes*

My approach to improve on ethylene/polar comonomer copolymerization catalysis is a novel class of *N*-Acylamidine ligands (**Figure 4**). While there has been N,O ligands developed for Pd or Ni catalyzed insertion polymerization in the past, namely the Grubbs phenoxyimine ligands,[10, 13] as well as ligands based off of the amidine backbone,[14] this system is unique because of the versatility of its modular synthesis. The ligand is made from three components, an aniline, nitrile and acyl chloride. The functionalities of these components can be varied to investigate the impact of sterics and electronics on catalyst activity. After elucidating these structure-function relationships, we can ideally design a catalyst to overcome specific challenges in polyolefin synthesis.

2.2 Synthesis, characterization, and activity of N-acylamidine Pd and Ni complexes

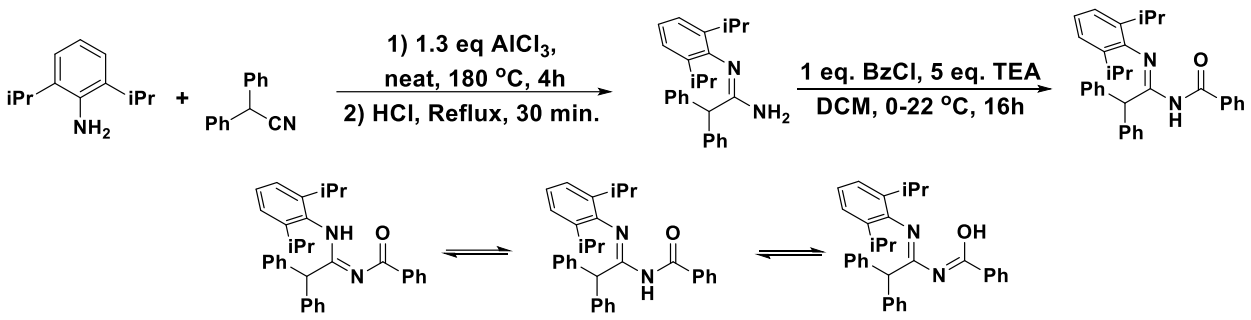

Scheme 1. *Synthesis of N-Acylamidines*

The first *N*-acylamindine ligand ($DippBzPh_2$) were synthesized in a two-step procedure as shown in Scheme 1. First, the amidine component was synthesized in an $AlCl_3$-catalyzed condensation from 2,6-diisopropylaniline and 2,2-diphneylacetonitrile with 63% yield. This amidine was further acylated with benzoyl chloride to provide a mixture of three products as identified by ^1H NMR (**Figure 5**) and thin-layer chromatography. These products appeared

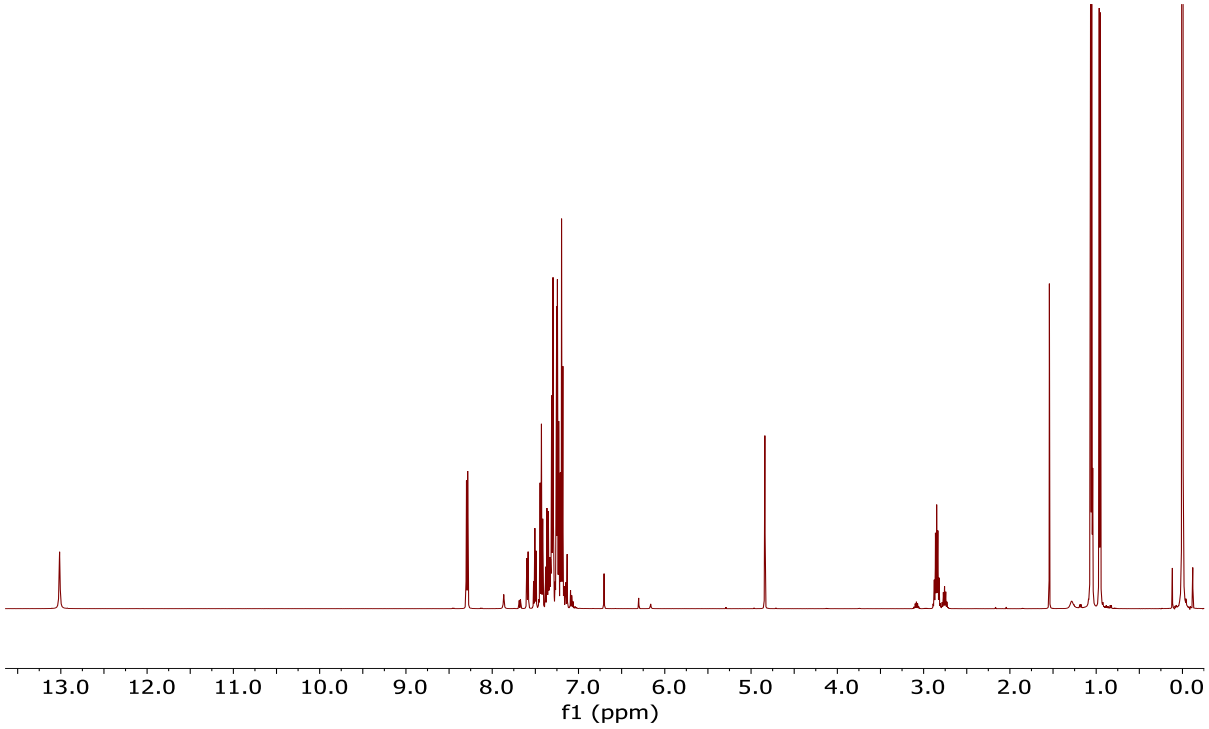

Figure 5*. ^1H NMR ($CDCl_3$, 1% v/v TMS, 25 °C, 500 MHz) of $DippBzPh_2$*

inseparable after multiple chromatography and recrystallization methods were attempted. Mass spectrometry of the sample contained a single peak, m/z = 475.3 (**Figure 6**). This suggests the

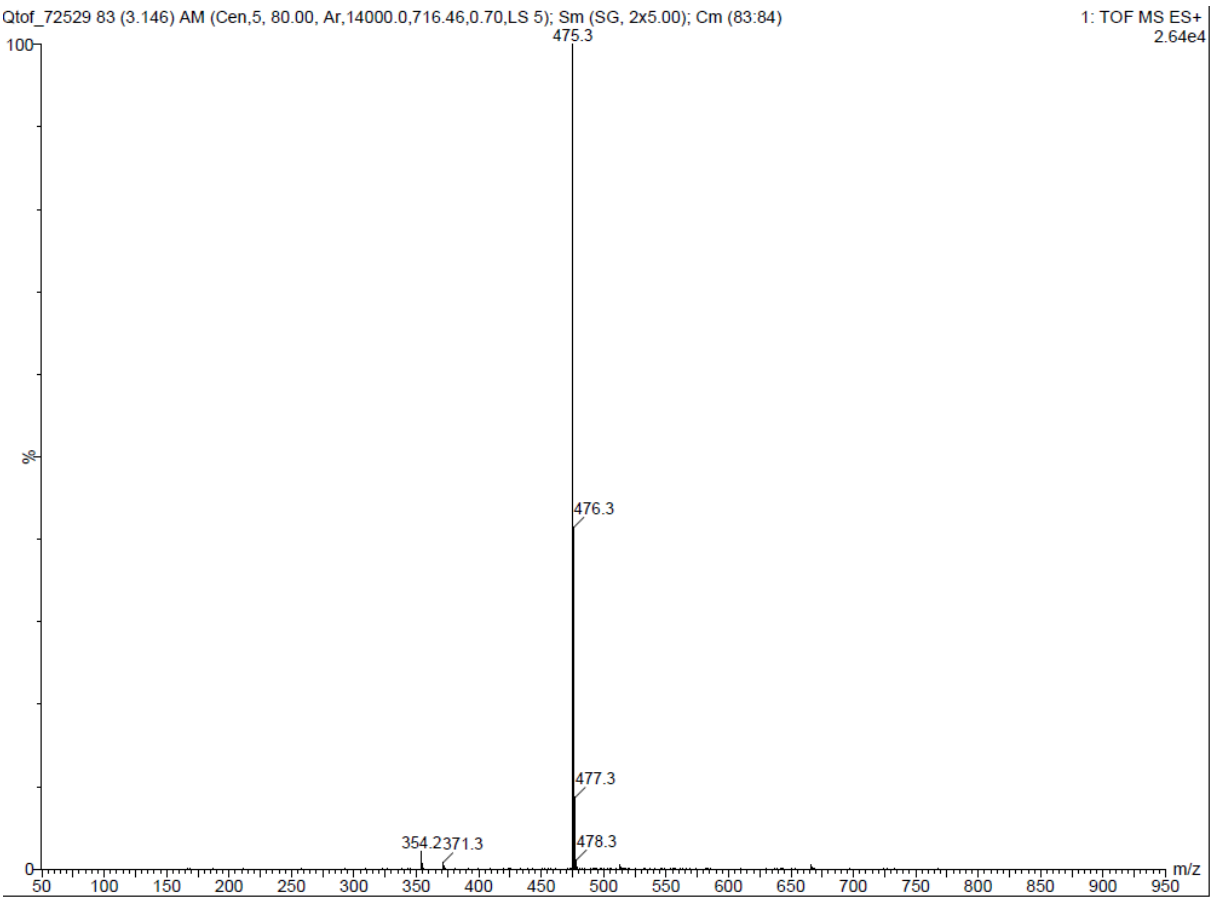

Figure 6. *ESI-MS of DippBzPh*$_2$

three products are isomeric to each other. Würthwein and coworkers demonstrated that *N*-acylamidines exist as a set of three tautomers, as shown in Scheme 1.[15] To confirm the existence of tautomers, the mixture was deprotonated with 1 equivalent of KH. Upon deprotonation the three characteristic isopropyl methine peaks (δ = 2.73, 2.83, 2.97 ppm) in the ^{1}H NMR were replaced

by a single peak (δ = 3.05 ppm), confirming the presence of tautomers (**Figure 7)**. The final yield of the acylation was determined to be 79%, for an overall synthetic yield of 49.8%.

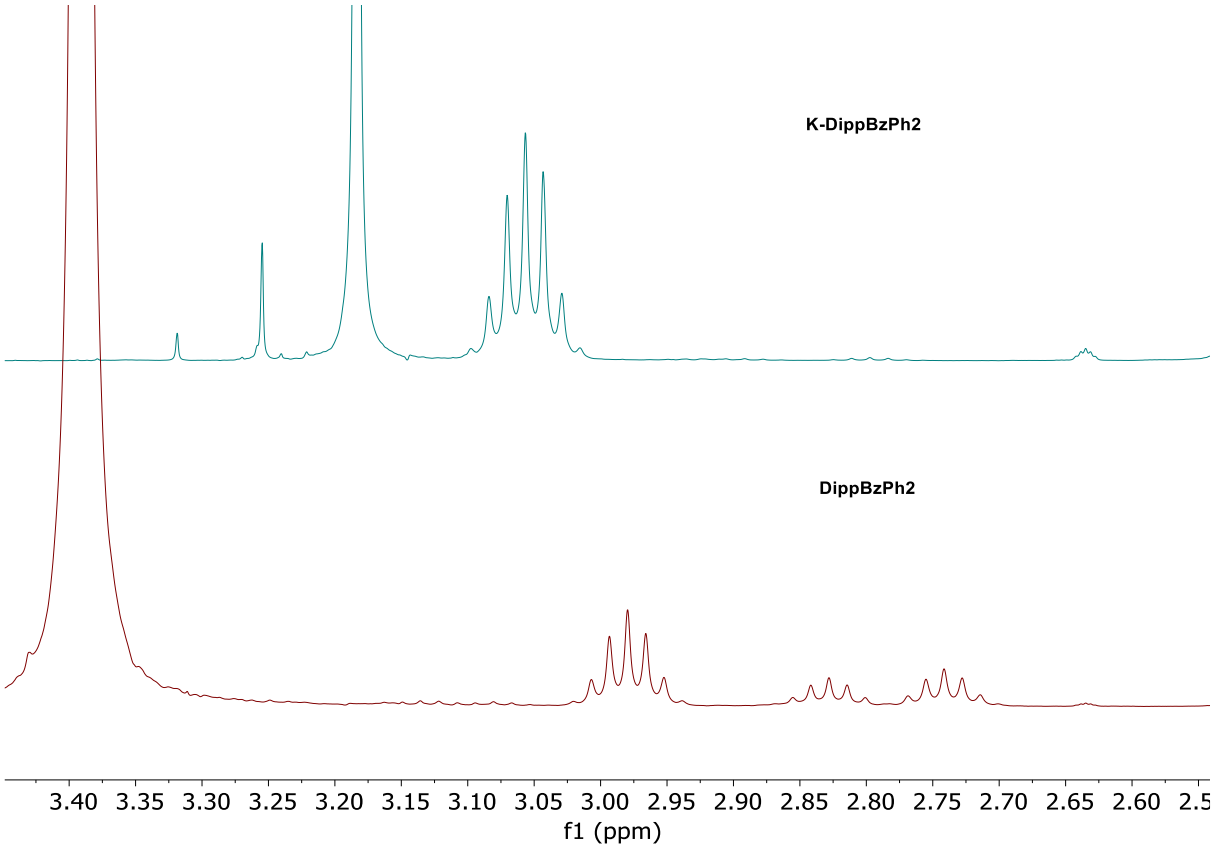

Figure 7*. ^{1}H NMR (d_6-DMSO, 25 °C, 500 MHz) of K-DippBzPh$_2$ isopropyl C-H signals (top, green) and ^{1}H NMR (d_6-DMSO, 25 °C, 400 MHz) of DippBzPh$_2$ tautomer mixture isopropyl C-H signals*

The purified DippBzPh$_2$ ligand was treated with a slight excess (1.1 eq.) of (tmeda)PdMe$_2$ and excess DMSO (10 eq) to synthesize DippBzPh$_2$PdMe(dmso). DMSO was chosen as an

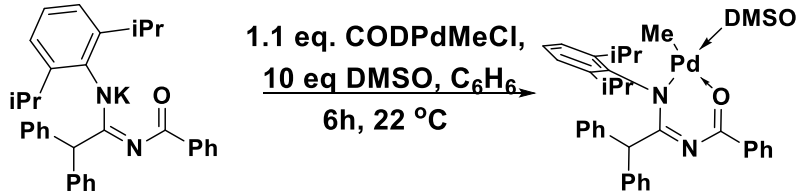

Scheme 2*. Synthesis of DippBzPh$_2$PdMe(dmso)*

ancillary ligand because of its weak coordination strength and therefore lower competition with olefin monomers.[12] Unfortunately, this complexation method was unsuccessful, as the NH proton of the ligand could not protonate (tmeda)PdMe$_2$. Instead, an alternate salt metathesis method was

utilized to synthesize DippBzPh$_2$PdMe(dmso). DippBzPh$_2$ was first deprotonated with KH, then the purified potassium salt was treated with a slight excess CODPdMeCl in the presence of excess DMSO (**Scheme 2**). This method proved successful, producing DippBzPh$_2$PdMe(dmso) in 55.6% yield. ^{1}H NMR characterization (**Figure 8**) showed a Pd methyl singlet at 0.67 ppm, as well as two separate isopropyl methyl doublets at 0.81 and 1.44 ppm, indicating hindered rotation of the diisopropylphenyl ring, and characteristic benzylic (s, 1H, 5.37 ppm) and isopropyl methine (sept.; 2H, 3.30 ppm).

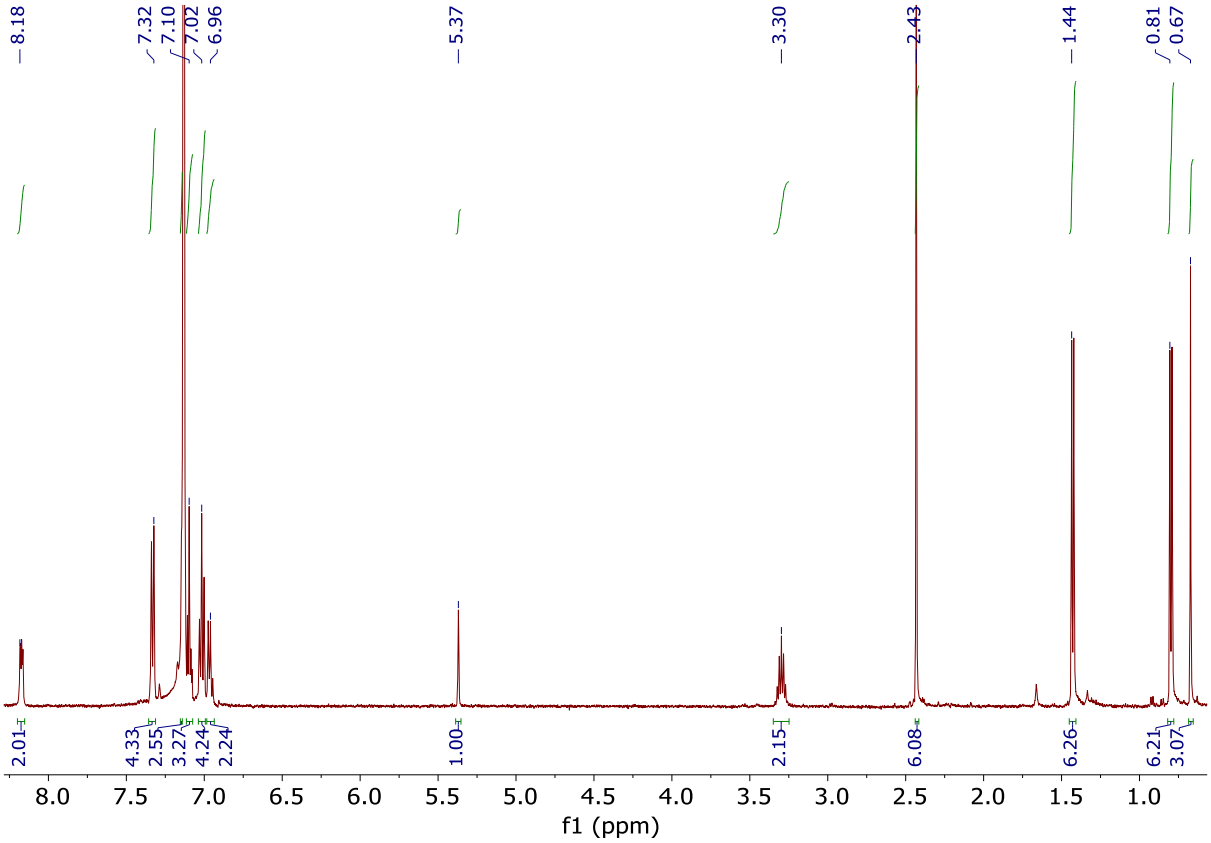

Figure 8. *^{1}H NMR (C_6D_6, 25 ^{o}C, 500 MHz) of DippBzPh$_2$PdMe(dmso)*

DippBzPh$_2$ was treated with NiMe$_2$(tmeda) in the presence of excess pyridine at -28 ^{o}C (**Scheme 3**) and was allowed to warm to room temperature over the course of the reaction,

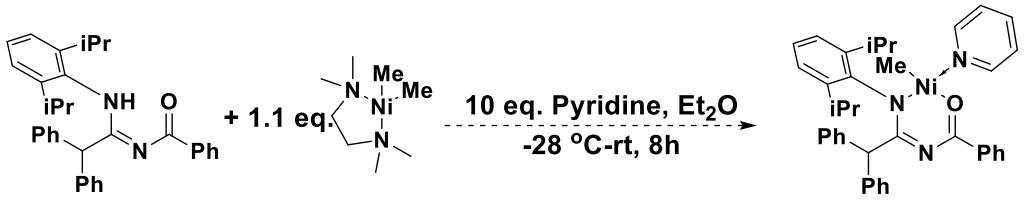

***Scheme 3**. Attempted synthesis of DippBzPh$_2$NiMe(py)*

monitored by ^{1}H NMR (**Figure 9**). While a new singlet at -0.76 ppm appeared, indicative of a new NiMe species, the complex quickly degraded and was not isolated.

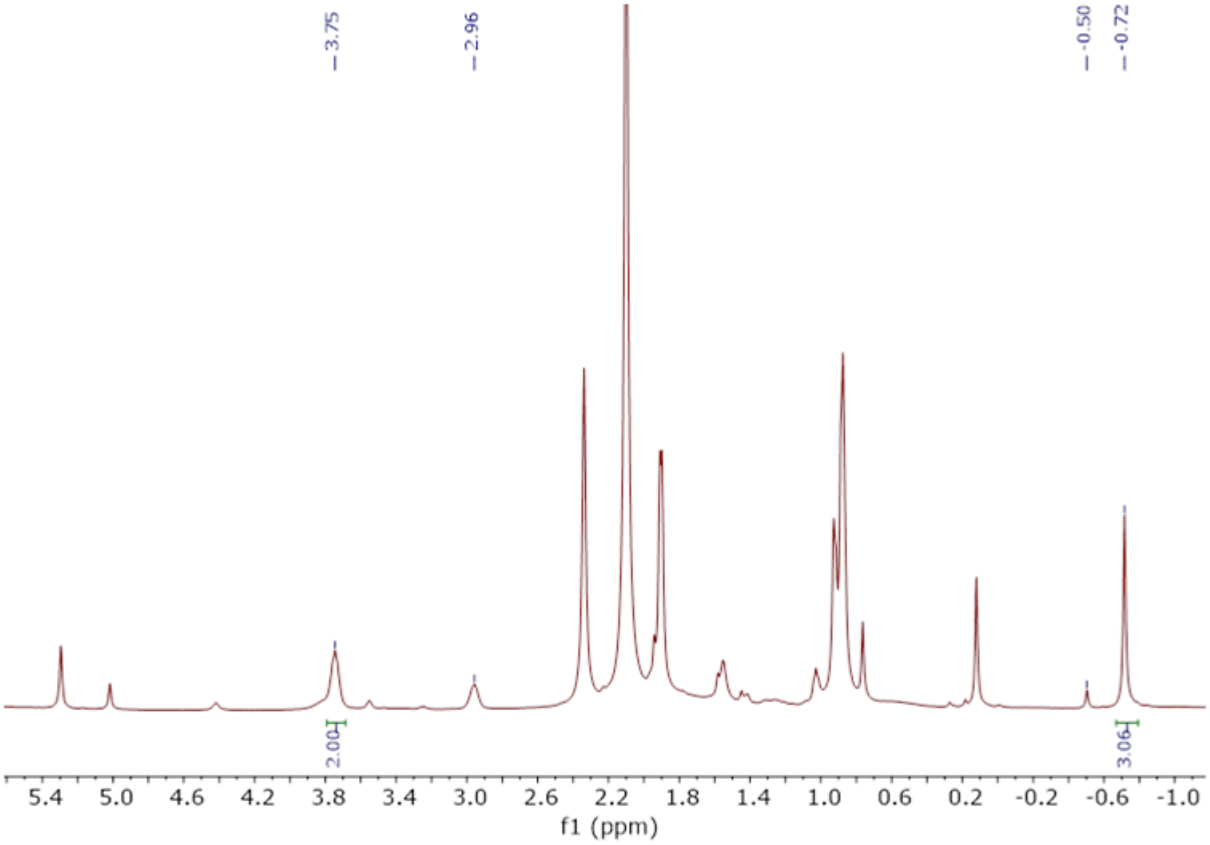

***Figure 9.** ^{1}H NMR (C$_6$D$_6$, 25 ^{o}C, 500 mHz) of DippBzPh$_2$ treated with (tmeda)NiMe$_2$*

Following the successful synthesis of DippBzPh$_2$PdMe(dmso), ethylene polymerization activity was investigated. A Buchi High-pressure reactor was loaded with 20.5 μmol of catalyst and deoxygenated, anhydrous toluene (PhMe) and charged with 5 bar of ethylene. After 30

minutes, the polymerization was stopped, and the contents of the reactor examined. No trace of polyethylene was produced. A range of temperatures (25-85 ^{o}C, **Table 1**) were investigated, yet

Table 1. *Polymerization data for DippBzPh$_2$ complexes*

Trial #	***Metal***	***$P_{ethylene}$***	***Temp ^{o}C***	***Yield (mg)***
1	Pd	5	25	0
2	Pd	5	45	0
3	Pd	5	65	0
4	Pd	5	85	0
5	Ni [1]	5	25	35
6	Ni [1]	5	65	40
7	Ni [1]	5	85	199
8	Ni [1]	40	65	75
9	Ni [1]	40	65	69
10	Ni [1]	40	65	49
11	Ni [1]	40	85	96

1: in-situ synthesized catalyst, 20 µmol NiMe$_2$(tmeda) + 20 µmol ligand

the catalyst failed to yield polymer at any of the temperatures listed. Noticeable amounts of Pd black were isolated at the end of each polymerization, indicating catalyst decomposition.

Additionally, *in situ* Ni-catalyzed polymerizations were performed by injecting DippBzPh$_2$ and (tmeda)NiMe$_2$. At 5 bar, these polymerizations did produce a small amount of waxy polymer, with increasing yields at higher temperatures (**Table 1**). Increasing the ethylene pressure to 40 bar caused no significant change in polymer yield. Again, evidence of catalyst decomposition was observed with the production of Ni black during the polymerization. This low polymerization activities combined with the difficulty to synthesize and isolate the targeted catalysts suggest that DippBzPh$_2$ is too weak of a ligand to support a Pd or Ni center during polymerizations.

2.3 Synthesis of stronger L-donor ligands and corresponding Pd and Ni Complexes

***Scheme 4**. Synthesis of DippSBzPh$_2$*

To improve the coordination strength of the *N*-Acylamidine ligands, two new ligands were synthesized with stronger sigma donor: DippSBzPh$_2$, a thiobenzoyl derivative, and DippPOOPh$_2$Ph$_2$, a phosphoryl amidine. We hypothesized that the stronger sigma donor will increase catalyst stability thus improving overall polymerization activity. DippSBzPh$_2$ was

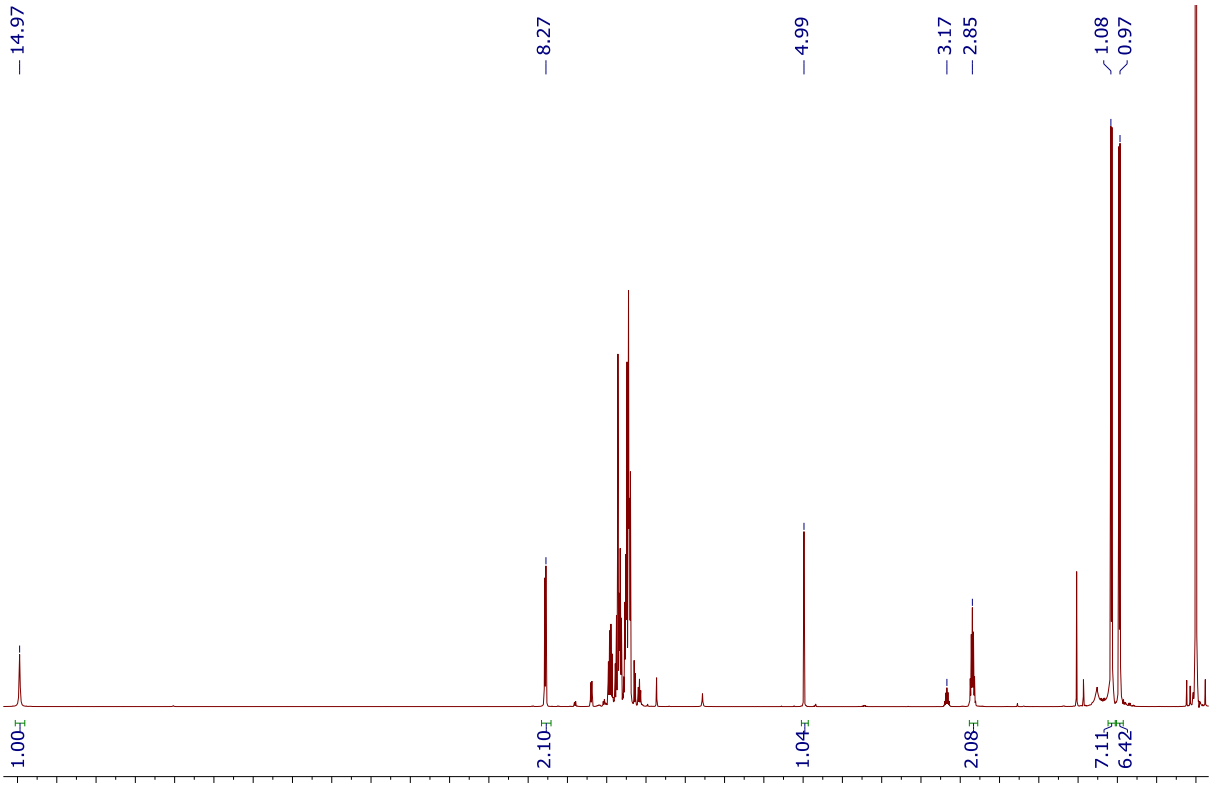

***Figure 10.** ^{1}H NMR (CDCl$_3$, 25 °C, 500 MHz) of DippSBzPh$_2$*

synthesized by thiating DippBzPh$_2$ with 0.5 eq. of Lawesson's reagent, in 55% yield (**Scheme 4**). The purified product exists as a mixture of two tautomers. ^{1}H NMR characterization (**Figure 10**) shows a far downfield NH peak at 15 ppm, a benzylic methine singlet at 4.99 ppm, and isopropyl peaks at 2.85 (2H, CH, major tautomer) 1.08 and 0.97 (3H each, CH$_3$, major tautomer).

DippSBzPh$_2$ was treated with (tmeda)PdMe$_2$ in the presence of excess pyridine to synthesize the corresponding PdMe(py) complex in 74% yield. The ^{1}H NMR of this complex (**Figure 11**) has a downfield PdMe peak at 0.87, as well as new isopropyl peaks at 0.77, 1.00 ppm (Methyl) and 3.42 ppm (methine). The NH peak disappeared, indicating deprotonation. Attempts to synthesize the DMSO analogue from both (tmeda)PdMe$_2$ and CODPdMeCl were unsuccessful, with the desired complex decomposing during purification.

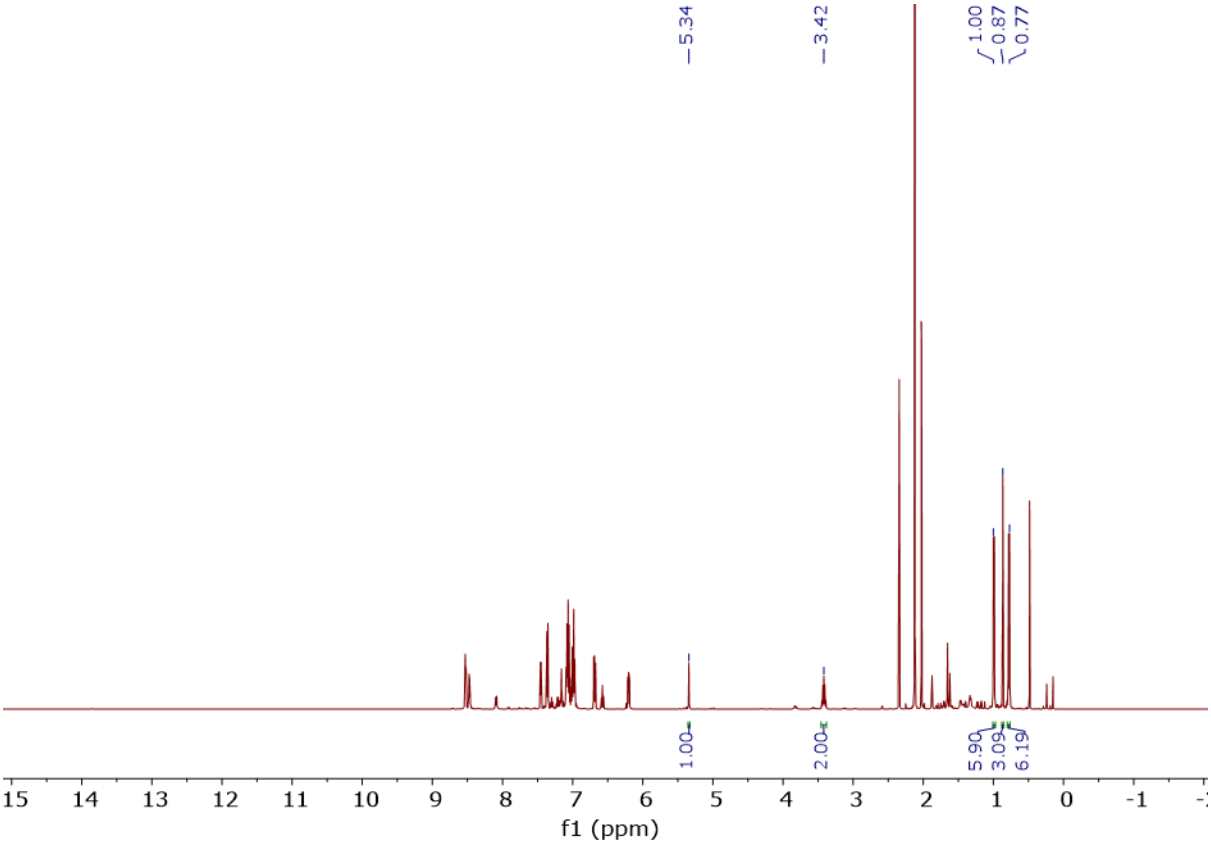

Figure 11. *^{1}H NMR (C_6D_6, 25 ^{o}C, 500 MHz) of DippSBzPh$_2$PdMe(py)*

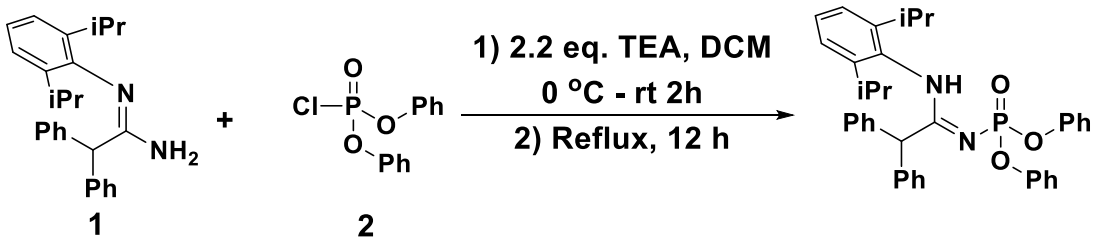

Scheme 5. *Synthesis of DippPOOPh$_2$Ph$_2$*

DippPOOPh$_2$Ph$_2$ was synthesized by treating amidine (**1**) with phosphoric chloride (**2**) in 69% yield (**Scheme 5**). The NH peak of the ligand is more upfield than the other two ligands, appearing at 10.81 ppm (**Figure 12)**. The phosphorylated amidine exists as a pair of tautomers, as

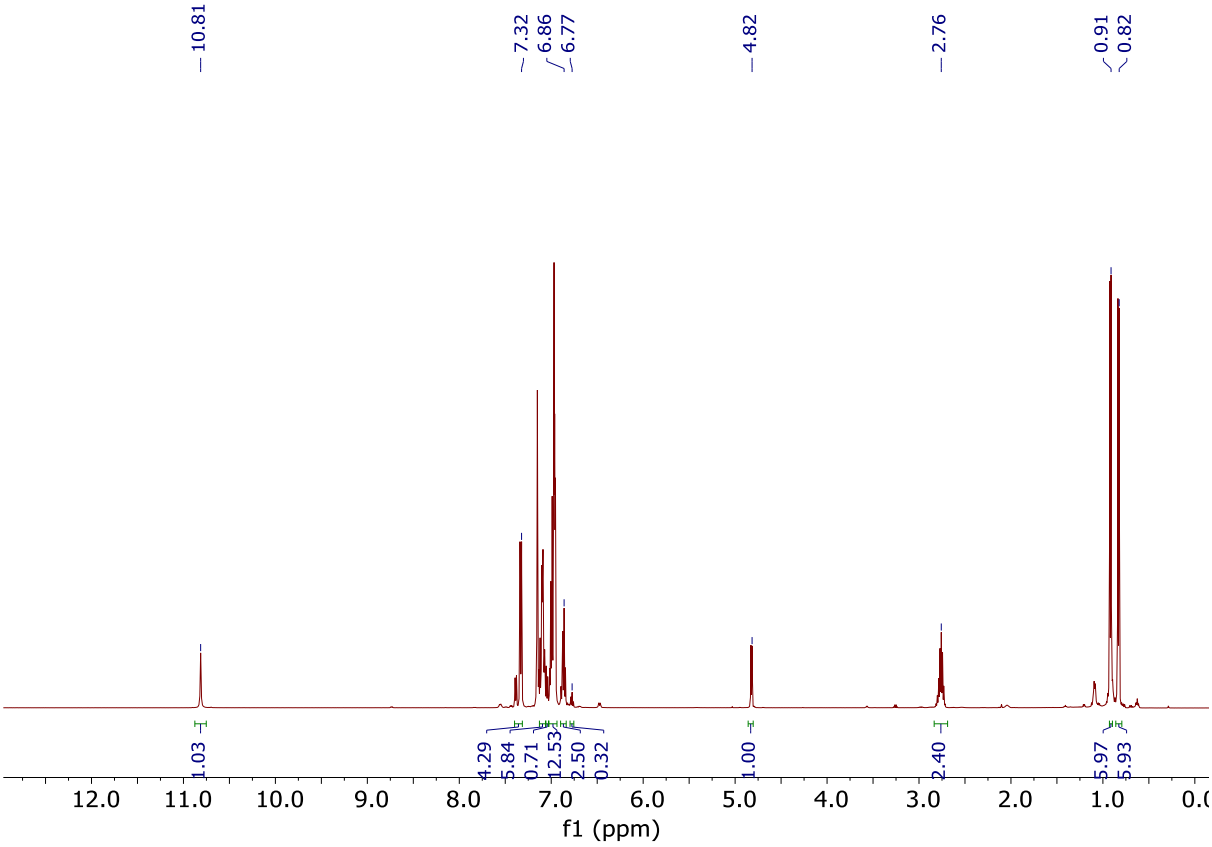

Figure 12*. ^{1}H NMR (CDCl$_3$, 25 °C, 500 MHz) of DippPOOPhPh$_2$*

evidenced by two separate signals in the ^{31}P NMR at 0.5 and -6.7 ppm (**Figure 13**), and a single species with m/z = 603.28 (**Figure 14)**.

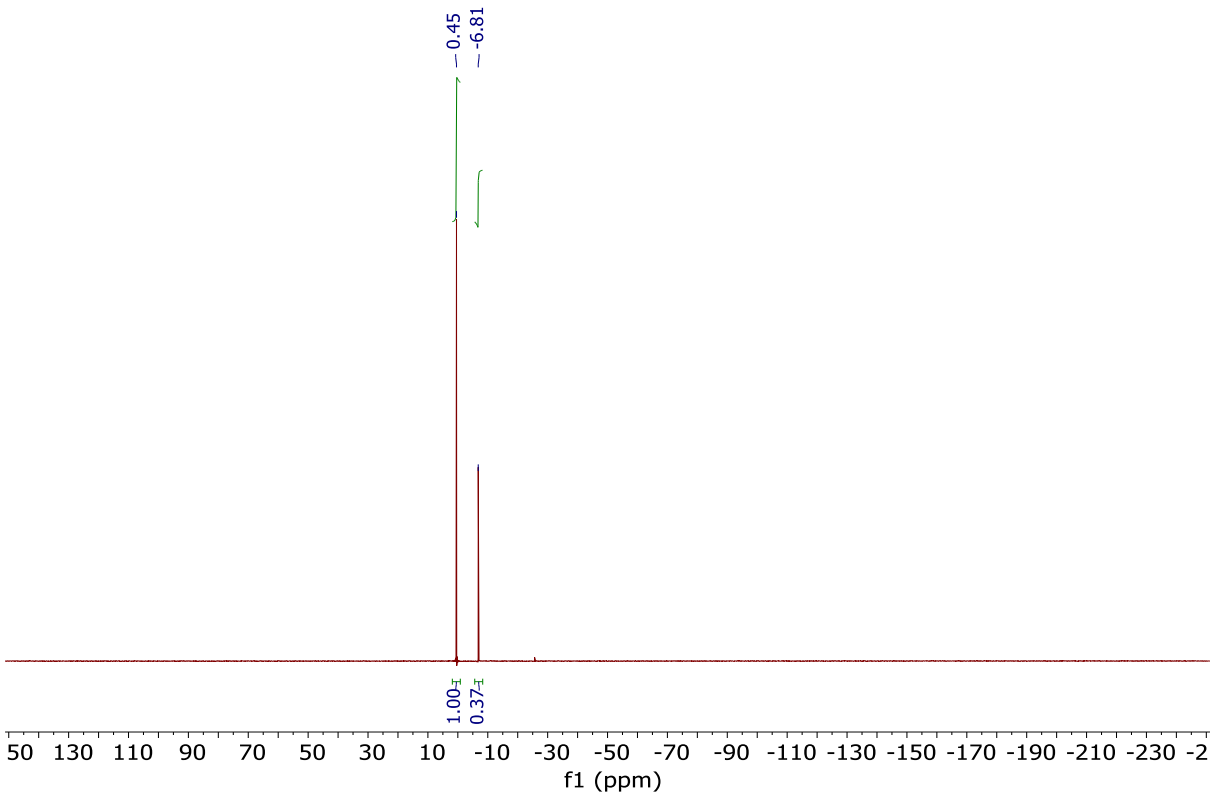

Figure 13. *^{31}P NMR ($CDCl_3$, 25 °C, 500MHz) of $DippPOOPh_2Ph_2$*

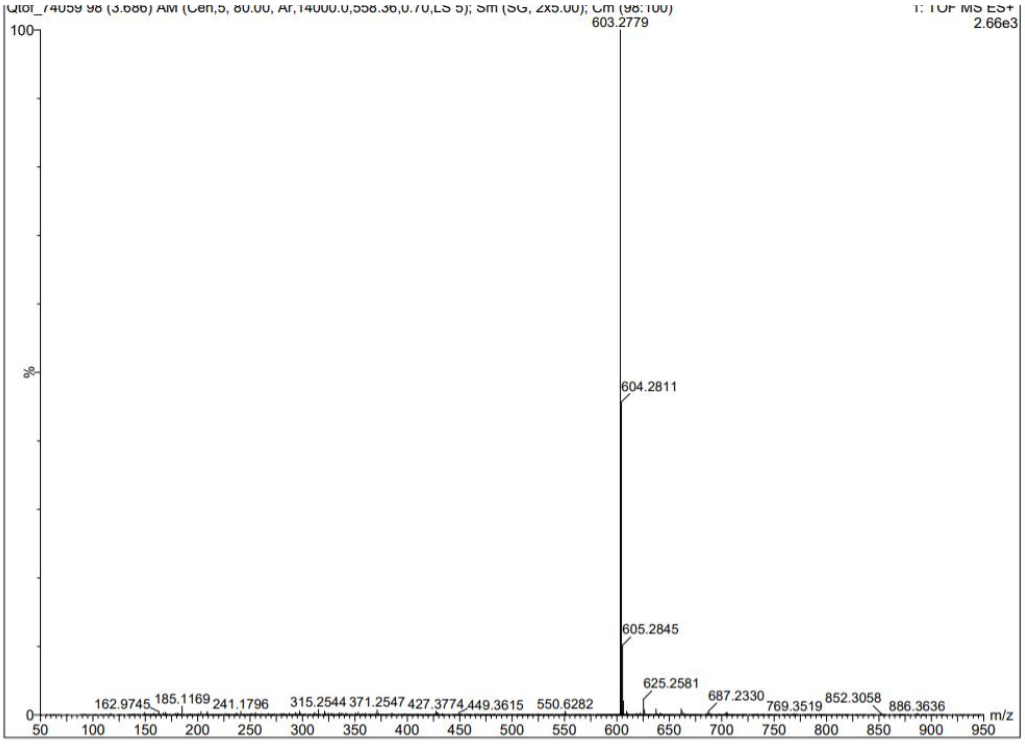

Figure 14. *ESI-MS of $DippPOOPh_2Ph_2$*

DippPOOPh$_2$Ph$_2$ was deprotonated with KH, then treated with CODPdMeCl in the presence of excess DMSO to synthesize DippPOOPh$_2$Ph$_2$PdMe(dmso) in 16% yield. This low yield is likely the result of decomposition, as Pd black formation was observed throughout purification. The isolated complex was characterized by ^{1}H NMR. Like DippSBzPh$_2$PdMe(py), DippPOOPh$_2$Ph$_2$PdMe(dmso) exhibits a downfield PdMe peak at 0.90 ppm, between the isopropyl methyl peaks at 1.49 and 0.83 ppm. The Isopropyl and benzylic methine peaks also shifted from 3.42 to 3.36 ppm and 4.82 to 5.14 ppm, respectively. The isolated complex was characterized by ^{1}H NMR (**Figure 15**).

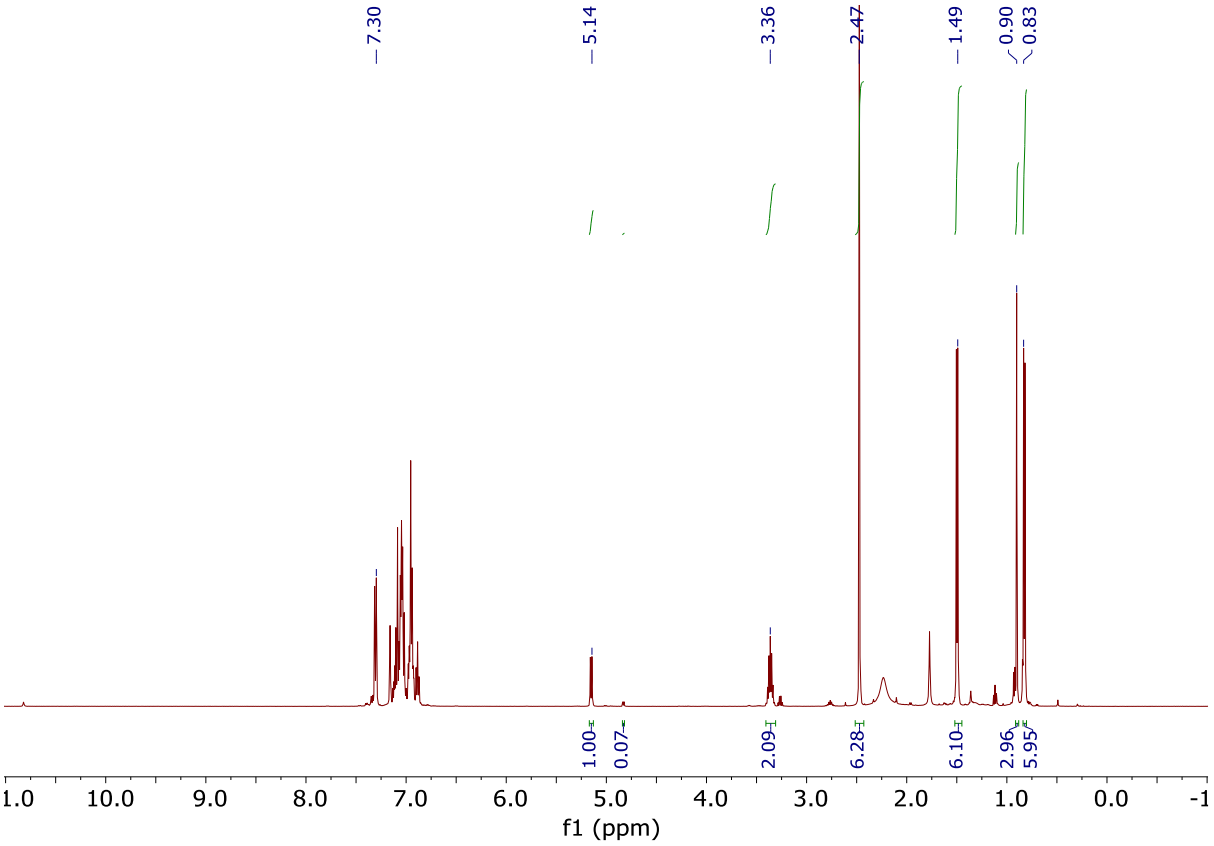

Figure 15. *^{1}H NMR (C_6D_6, 25 ^{o}C, 500 MHz) of DippPOOPh$_2$Ph$_2$PdMe(dmso)*

Like DippSBzPh$_2$PdMe(py), DippPOOPh$_2$Ph$_2$PdMe(dmso) exhibits a downfield PdMe peak at 0.90 ppm, between the isopropyl methyl peaks at 1.49 and 0.83. This was supported by ^{1}H-^{13}C HSQC NMR spectra, where a cross peak at 16.0 ppm in the ^{13}C NMR trace can be observed.

The Isopropyl and benzylic methine peaks also shifted from 3.42 to 3.36 and 4.82 to 5.14, respectively.

The newly synthesized ligands (DippSBzPh$_2$ and DippPOOPh$_2$Ph$_2$) were treated with excess (tmeda)NiMe$_2$ and pyridine at -28 ^{o}C to synthesize the corresponding Ni-Me complexes. This led to a complex mixture of products, observed from multiple isopropyl methine peaks in the ^{1}H NMRs. Unfortunately, with both ligands, the nickel complexes could not be isolated. Additionally, the complexes started to degrade within 30 minutes in solution. Attempts to stabilize the complexes by using a stronger ancillary ligand, 2,6-lutidine, were similarly unsuccessful.

In order to assess the polymerization activity of the synthesized Pd complexes, both catalysts were subjected 40 bar of ethylene in a high pressure Buchi reactor. No activity for either Pd complexes was observed. Large amounts of Pd black were observed after both polymerizations, indicating catalyst decomposition. Similarly, *in situ* polymerizations with each ligand and (tmeda)NiMe$_2$ were unsuccessful at producing polymer. From these observations, and the difficulty synthesizing both Pd and Ni complexes, we can conclude that the studied *N*-Acylamidine ligands are not sufficiently stable enough to be active towards ethylene polymerizations, let alone copolymerizations with polar comonomers.

2.4 Synthesis of early transitions metal complexes with N-Acylamidine ligands

The lack of success with late transition metals led us to explore the use of early transition metals with our novel ligands. Early transition metal complexes often have higher olefin polymerization activity that late transition metals, however, the high oxophilicity of commonly used d^0 transition metals such as Ti(IV), Zr(IV), and Hf(IV) prevents them from copolymerizing with polar vinyl monomers.[16] Thus, our goals with any early transition complexes we make will shift towards getting high activity towards ethylene polymerizations. The desired complexes draw

similarities to phenoxyimine complexes, namely the FI catalysts developed by Fujita and coworkers.[14] When combined with an alkylaluminum co-catalysts, these complexes have polymerized ethylene with activities up to 60 kg PE mmol(metal)$^{-1}$h^{-1} and have made copolymers with alkyl-substituted olefins.[18]

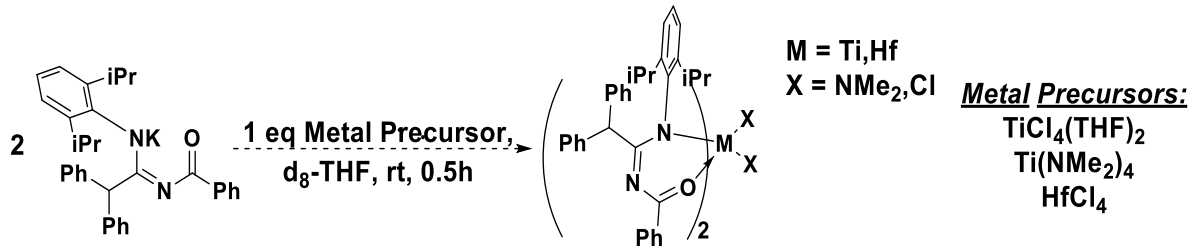

***Scheme 6**. Attempted synthesis of Group IV bis-DippBzPh$_2$ complexes*

To synthesize Ti *N*-Acyl amidine complexes, two equivalents of K-DippBzPh$_2$ were treated with a single equivalent of TiCl$_4$(thf)$_2$ at room temperature as shown in Scheme 6. Two equivalents of bidentate *N*-Acylamidine were used to accommodate the expected octahedral geometry of the Ti-complex. The reaction was monitored by ^{1}H NMR. However, within 30 minutes after the addition of TiCl$_4$(THF)$_2$, only DippBzPh$_2$ was observed, as indicated by the amidine NH peak at 13.3 ppm (**Figure 16**). This decomposition is evidence that our ligand is too weak to stabilize the desired metal complex. Similar attempts with Ti(NMe$_2$)$_4$ resulted in a complex mixture of products, from which a new complex could not be isolated and characterized.

Attempts to metalate with $HfCl_4$ were hampered by the precursor's poor solubility in benzene and THF.

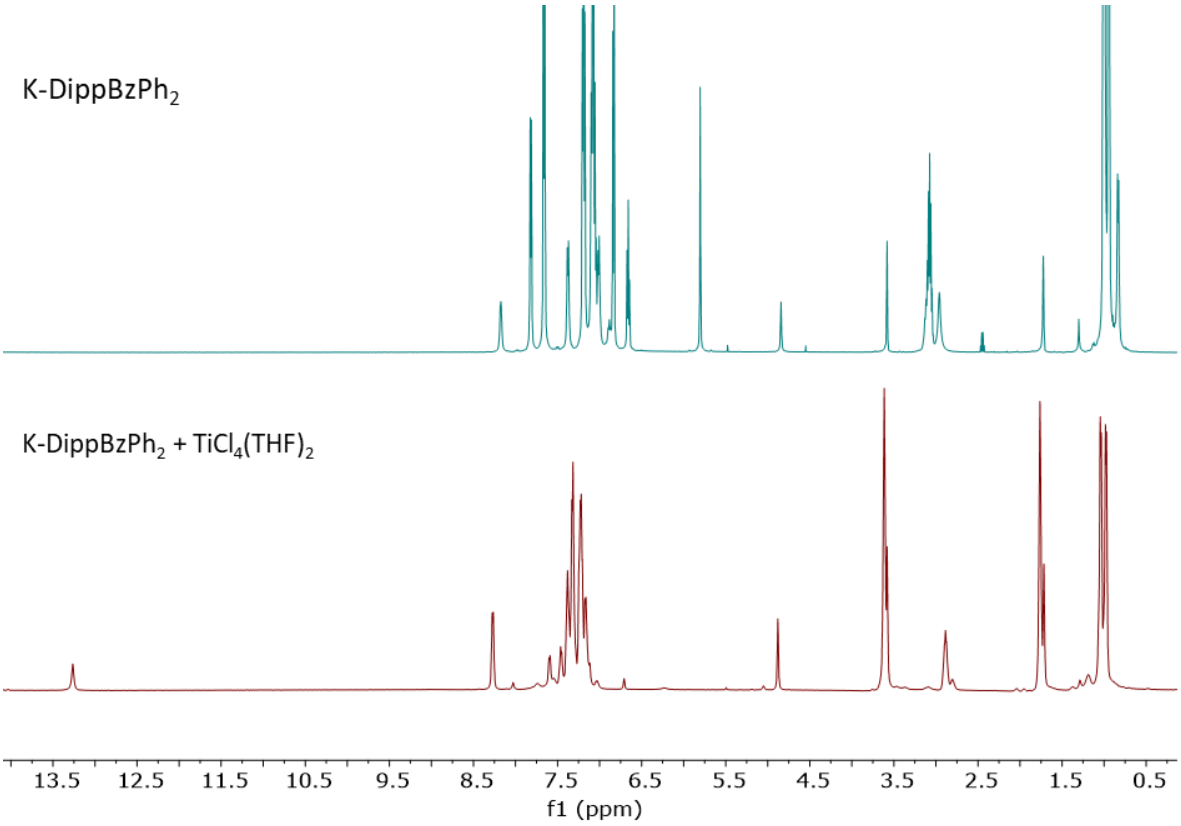

Figure 16. *^{1}H NMR (C_6D_6, 25 °C, 500 MHz) of attempted $(DippBzPh_2)_2TiCl_2$ synthesis. Top: deprotonated $DippBzPh_2$. Bottom: deprotonated $DippBzPh_2$ after treatment with $TiCl_4(THF)_2$ for 30 min.*

To increase the coordination strength, we redesigned our ligands to take advantage of a stronger chelate effect, going from a bidentate to a tetradentate system. Following modified literature procedures,[19] imidoyl chloride (**2**) is treated with KNCO to form the corresponding

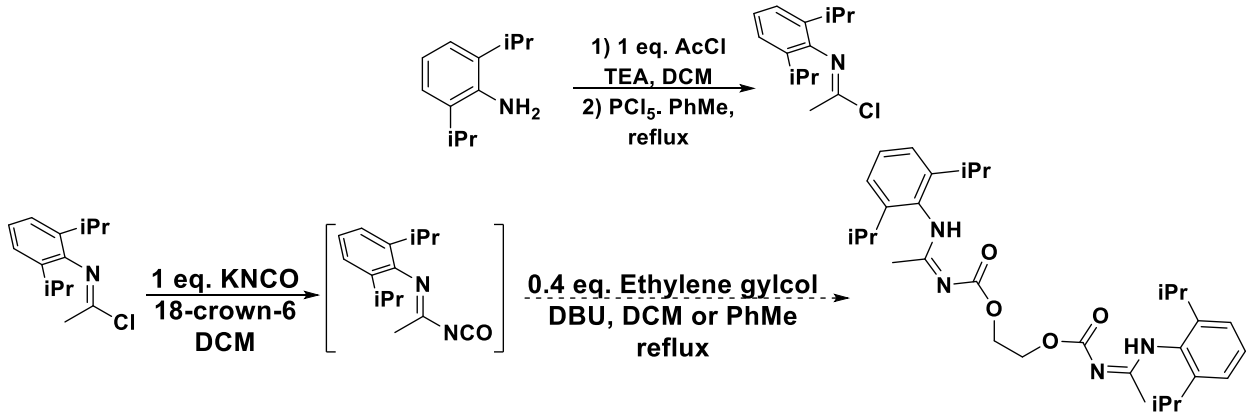

Scheme 7*. Attempted synthesis of diurethane-linked bis-N-acylamidine ligands*

isocyanate *in situ*, which is then attacked by ethylene glycol in the presence of catalytic base to for a diurethane (**Scheme 7**). Ultimately, this reaction was unsuccessful. Evidence of the isocyanate and monourethane are seen in the ESI-MS (**Figure 17**), indicating the first step of the reaction is

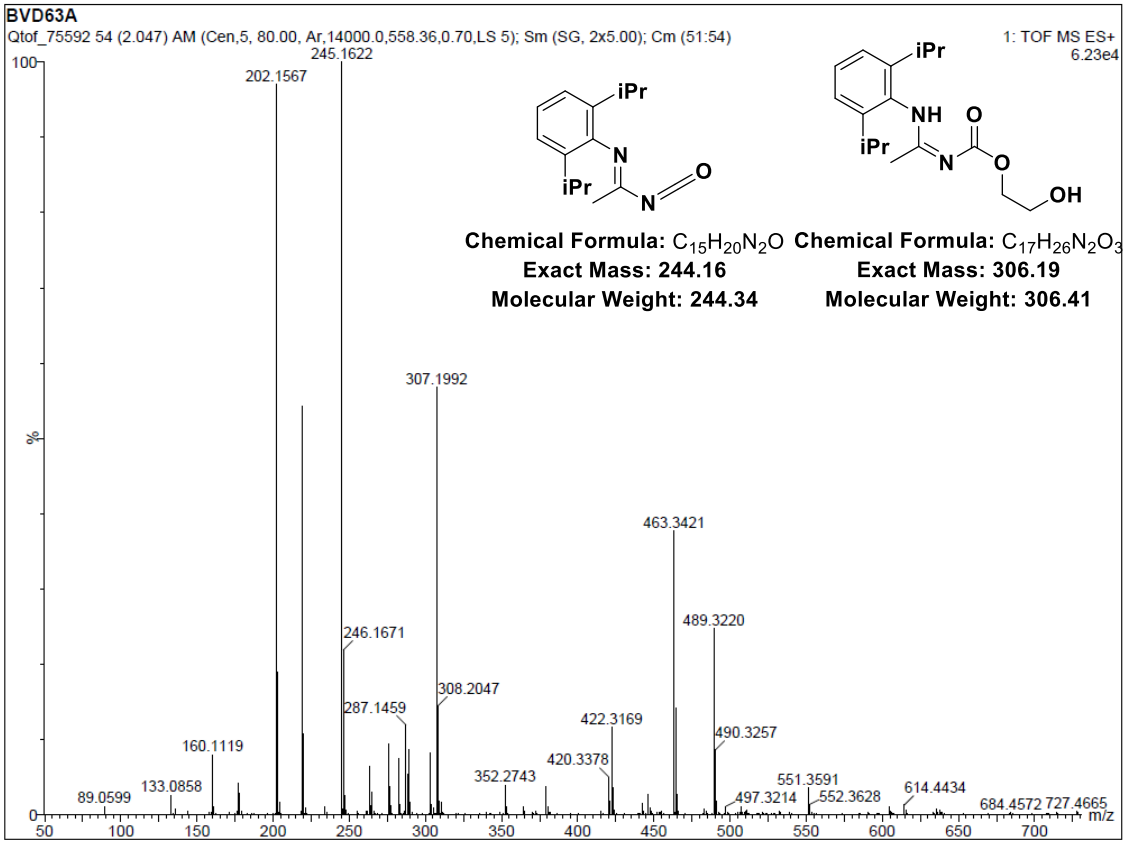

***Figure 17**. ESI-MS of crude diurethane ligand synthesis reaction mixture*

successful, however it does not appear that the monourethane product is nucleophilic enough to attack a second isocyanate. Changing the solvent from dichloromethane (DCM) to PhMe and increasing the temperature were unsuccessful in improving conversion, as was attempting to synthesize the corresponding diurea with a more nucleophilic secondary amine. Using 0.4 eq. of diol (relative to **2**) was also unsuccessful at producing diurethane product.

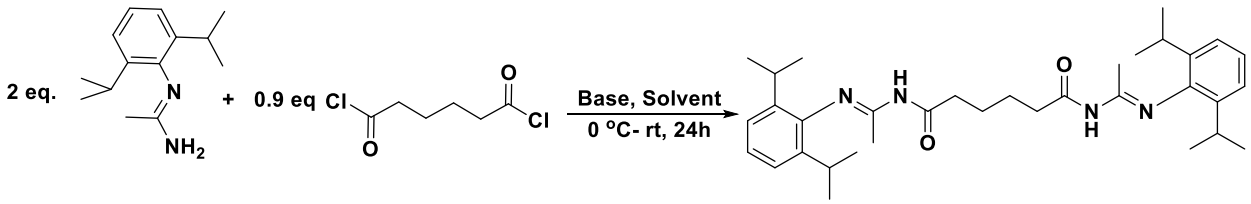

Scheme 8. *Synthesis of adipyl acid-linked bis-N-acylamidine*

The failure of this synthesis motivated a second synthetic approach to accessing *bis-N*-acylamidines, acylating two amidines with adipyl acid chloride, as shown in **Scheme 8**. This reaction produced small amounts of the desired product, as observed by ESI-MS, but in insignificant quantities to isolate (**Figure 18**). The major impurity was remaining starting amidine (m/z = 219.18). Additionally, significant amounts of diimide (m/z = 329.22) and amide (m/z = 506.37) product were observed in the MS. This implies that the low reactivity is due to the adipyl

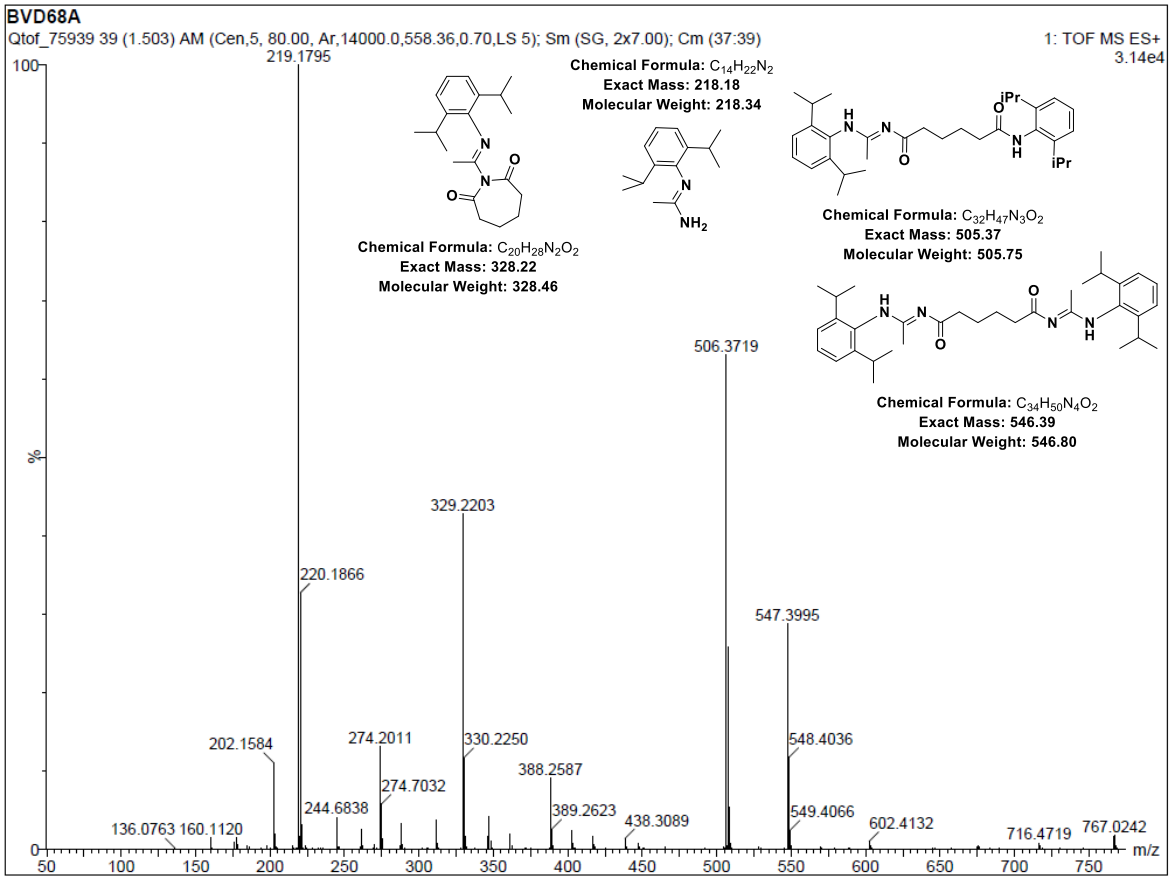

Figure 18. *ESI-MS of crude bis-N-Acylamidine synthesis reaction mixture with adipyl acid chloride and TEA*

acid being consumed by exhaustive acylation of the amidine, and amine impurities from the starting material or amidine degradation, respectively. Changing the base from triethylamine to potassium *tert*-butoxide or diisopropylethylamine failed to improve the yield. Additionally, changing the solvent from DCM to THF or PhMe failed to improve the conversion.

CHAPTER 3: PENULTIMATE MONOMER EFFECT IN LATE TRANSITION METAL-CATALYZED ETHYLENE/CARBON MONIXIDE COPOLYMERIZATIONS

3.1 Motivation

Polyethylene (HDPE, LLDPE, LDPE, EPDM, UHMWPE) is by volume the most important plastic in the world as it represents ca. 33% of the world's plastic production.[1] Due to its low cost, this also means PE makes up for an even larger fraction of plastic pollution, accounting for 25 million tons of waste annually in the United States alone.[20] The accumulation of this plastic waste leads to environmental pollution that is extremely damaging to natural ecosystems.

One way to reduce the amount of polyolefin waste being produced is to accelerate its degradation into biologically consumable small molecules. PE degradation begins with the oxidation of alkane chains in the polymer to ketone functionalities (**Scheme 9**).[21] After oxidation, the C-C bond between the carbonyl and C_α can be cleaved by excited oxygen to generate Norrish radicals.[22] These radical species rearrange into small-molecule olefins, ketones, and aldehydes that can readily be digested by microorganisms.[23] Due to the inertness of the hydrocarbon backbone in polyethylene, this process occurs on the scale of hundreds of years.[21]

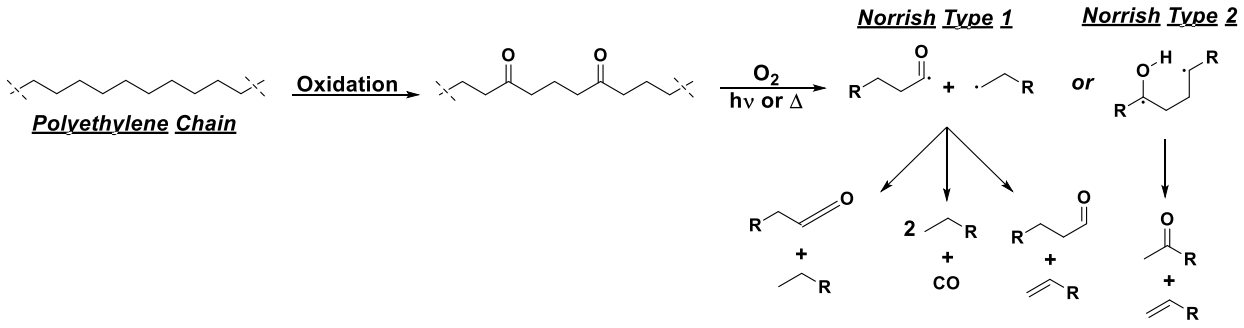

Scheme 9*. Oxidative degradation of polyolefins*

One way to speed up polyethylene degradation up would be to replace the original polyethylene plastic with a polyketone made directly from ethylene and carbon monoxide (CO). Radical polymerizations have been used to produce branched PE with isolated, in-chain ketone units (**Scheme 10**).[24] These polymers had similar physical properties to commercial LDPE yet were observed to degrade at significantly faster rates in the presence of both natural light and UV irradiation. Reducing the CO content to 5-10 mol% in the PE backbone improves adhesion and hardness without sacrificing its processability.[25]

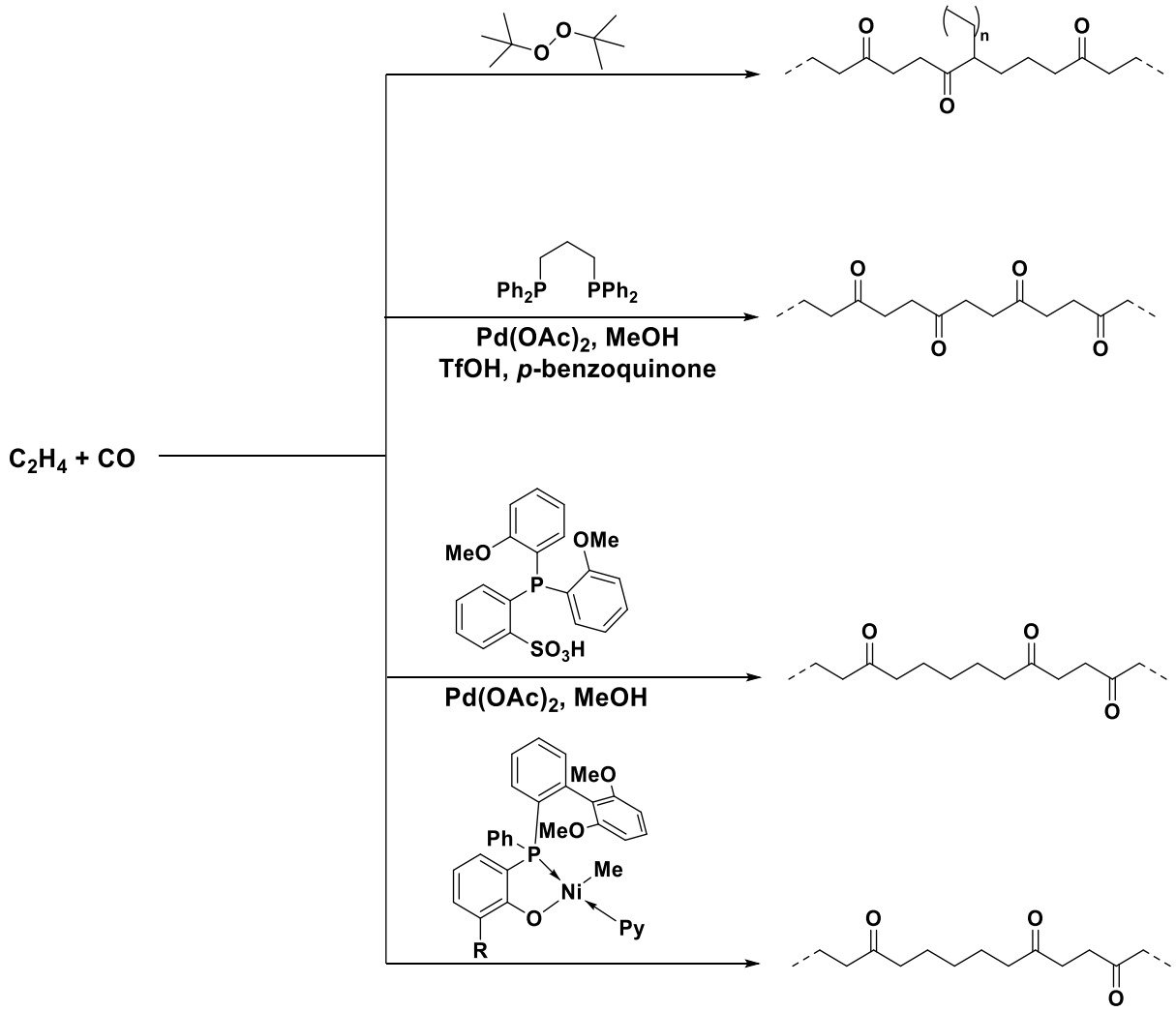

***Scheme 10**. Overview of polyketone synthesis*

This has been an attractive goal in transition-metal catalyzed polyolefin synthesis for decades, with the first copolymerization of ethylene and CO being reported in 1941.[26] Single-site

transition metal catalyzed polyketone synthesis allows for precise control over the copolymer architecture and microstructure that is not available in free-radical polymerizations. While the first of these types of polymerizations were performed with nickel (II) salts,[24] the bulk of research shifted towards cationic palladium (II) systems supported by a variety of neutral bidentate [P,P], [N,N], and [P,O] ligands.[27] A breakthrough cationic Pd bisphosphine system was reported by Drent[28] and commercialized by Shell-Carlion[29] in the early 1990's. It was a combination of $Pd(OAc)_2$, a bidentate bisphosphine ligand, triflic acid, and 1,4-benzoquinone (**Scheme 10**), and was capable of producing perfectly alternating copolymers of CO and ethylene. The addition of the protic acid and oxidant serve to regenerate the initiating Pd-H species and prevent competition between monomers and anionic counterions. However, the resulting polymer is very brittle and has a T_m = 260 ^oC, making it far removed from a polymer like HPDE in material properties. This is due to strong dipole-dipole interactions between the alternating in-chain ketone moieties.[30]

In 2002, Drent and coworkers reported the first transition metal catalyst system capable of making non-alternating polyketones, a combination of $Pd(OAc)_2$ and a Phosphinosulfonate ancillary ligand (L1) that forms a neutral Pd(II)-phosphinosulfonato complex *in situ* (**Scheme 10)**.[31] Mechanistic studies suggest that a variety of electronic and steric effects imparted by the phosphinosulfonate ligand are responsible for allowing consecutive insertions of ethylene. These

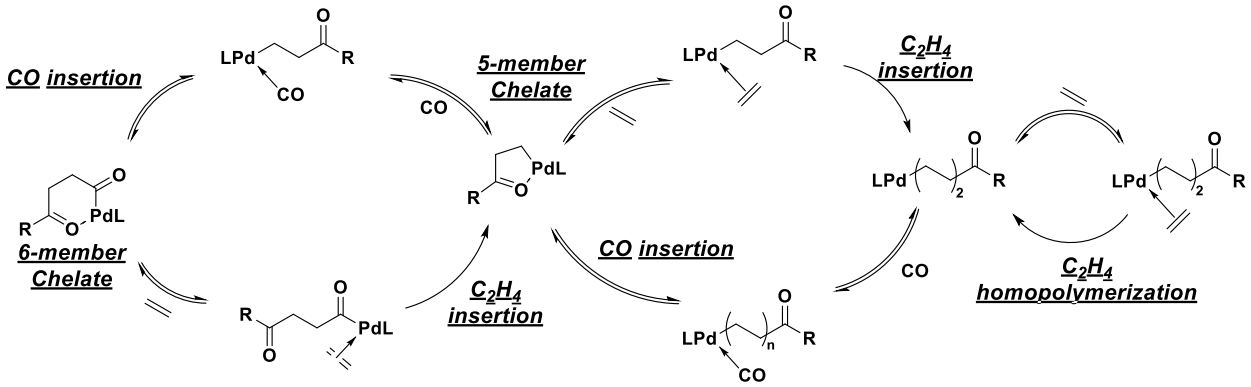

Scheme 11. *Propagation mechanism of non-alternating ethylene/CO copolymerization*

effects are proposed to destabilize a proposed 5-member chelate resting state (**Scheme 11**) allowing ethylene to coordinate to the Pd center.[32-33]

The first isolated Pd-phosphinosulfonate complexes capable of non-alternating ethylene/CO copolymerizations were reported by Rieger and coworkers in 2005 and were able to produce copolymers with 20 mol% CO.[34] Using a semi-batch reactor, Müller and coworkers were able to synthesize non-alternating PKs with 1-30 mol% CO.[35] However, despite these advances in reducing the mol% CO, L1-Pd complexes suffer from low activity (200 $g*mmolPd^{-1}*h^{-1}$) and M_n (3-6000 g/mol).

Very recently, there has been a renaissance in new catalysts for non-alternating ethylene/CO copolymerization. Mecking and coworkers reported Ni(II)-phosphinoenolato complexes (**Scheme 11**) that can produce high molecular weight polymers ($M_n \approx 200{,}000$ g/mol) with low CO content (1%) and increased activity.[36] These catalysts are notable because they are the first reported Ni(II) complexes capable of non-alternating ethylene/CO copolymerization. While Ni(II) complexes supported by [P,O] ligands have been reported in the past, these complexes were only capable of making diblock (polyethene)(alt-ethylene-CO)polymers.[37] However, the recently reported Ni(II) catalysts are proposed to be able to favor non-alternation due to the η^2 -coordination of a biaryl phosphine substituent axially oriented to the metal center.[38] DFT calculations suggest this steric effect weakens the 5-member chelate resting state, allowing for coordination, and consecutive insertions of ethylene. In addition to these Ni complexes, new cationic Pd(II) diphosphazane monoxide[39] and Ni(II) bisphosphine[40] catalysts have been reported to synthesize high-molecular weight non-alternating polyketones. Finally, new methods to polymerize non-alternated polyketones with highly isolated carbonyl groups using Pd-Phosphinosulfonato complexes and metal carbonyls as the CO source have been developed.[41]

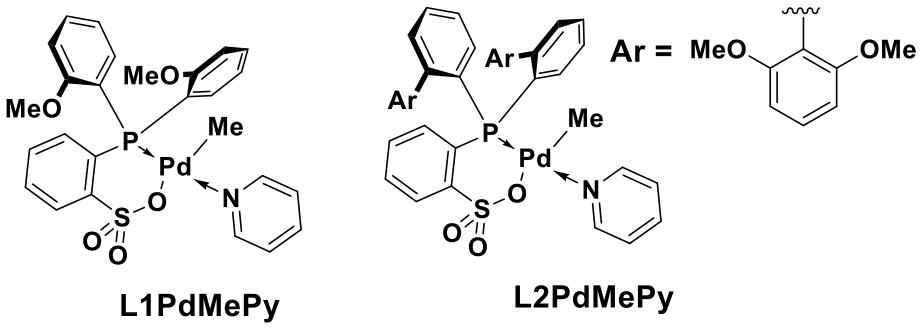

Figure 19. *Pd(II) phosphinosulfonato complexes for the non-alternating copolymerization of ethylene and CO*

In my attempts to improve upon the catalyst activity and polymer M_n of non-alternating PK's with Pd catalysts, I investigated using a more sterically hindered phosphinosulfonate ligand, L2 (**Figure 19**). In ethylene homopolymerizations, L2PdMePy showed 100-fold increase in activity and a 10-fold molecular weight of L1PdMePy.[12] L2PdMePy could also incorporate methyl acrylate in copolymerizations similar to L1-Pd complexes, suggesting that they too may be able to handle polar comonomers such as CO.[42]

3.2 Synthesis of Non-alternating polyketones with L2PdMePy

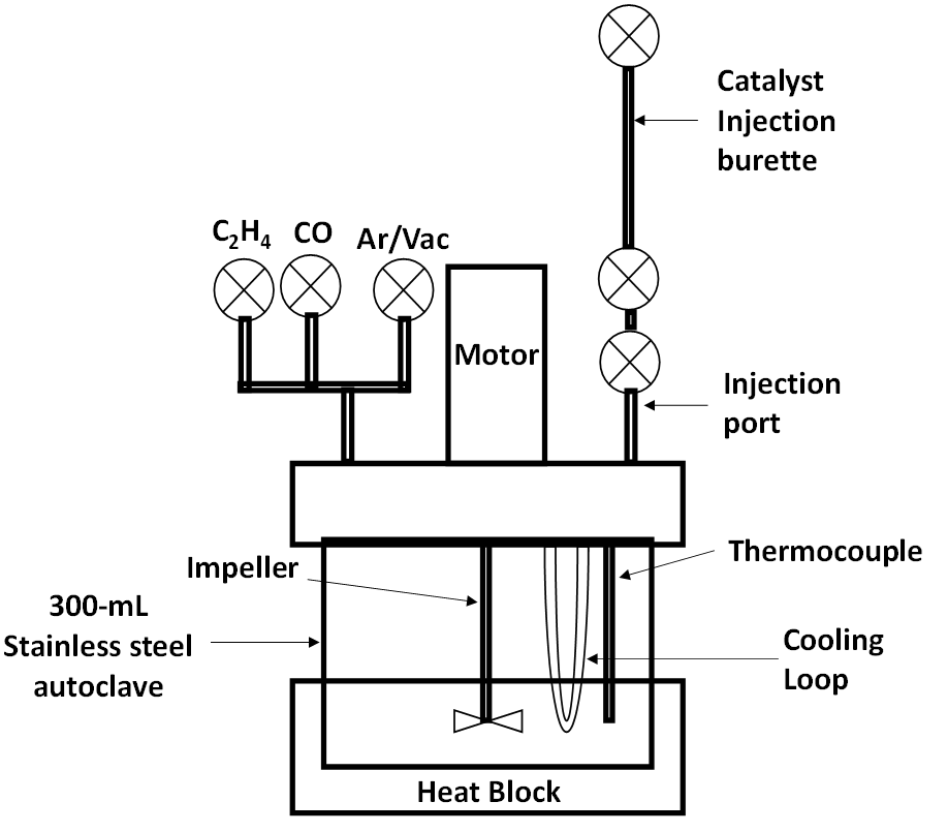

Figure 20. *Parr reactor schematic for ethylene/CO copolymerizations*

L2PdMePy was synthesized according to literature procedures in good yield (84%). ^{1}H and ^{31}P NMR spectra of the synthesized complex matched those reported in the literature, indicating a successful synthesis.[42] Ethylene/CO copolymerizations were carried out in a 300-ml Parr reactor (**Figure 20**) equipped with an overhead impeller stirrer, thermocouple, water-fed cooling loop, and ports for ethylene, CO, Ar/vacuum, and catalyst injection.

Several considerations must be made when performing an ethylene/CO copolymerization with this reactor setup. First, ethylene/CO pressurization must begin after solvent addition into the reactor, at room temperature. Then, the L2PdMePy catalyst is introduced as a solution of benzene/DCM (100:1) via a gas burette after pressurization. Catalyst addition before pressurization of ethylene/CO will lead to either catalyst death from ligand displacement by CO or ethylene homopolymerization depending on the order of pressurization. After the addition of catalyst, the reactor is heated to 110 ^{o}C. The temperature increase is accompanied by large pressure

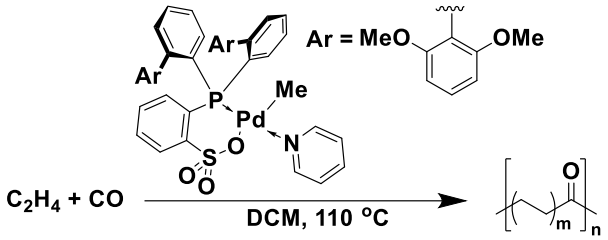

Table 2. *Ethylene/CO Copolymerization data.*

Trial #	***1***	***2***	***3***	***4***	***5***	***6***	***7***	***8***	***L1PdMeI***
Pressure ratio ($CO:C_2H_4$, bar)	1:38	0.5:28.5	1:25	1.5:24.5	2:24	3:23	5:21	1:1	1:49
Mol% CO[a]	0.3	1.8	1.1	11	25	40[c]	45[c]	50[c]	1.4
% A/NA[a,b]	0.1/0.2	0.5/2.1	0.4/1.9	7.3/10.4	20.9/23.6	46.3/39.4[c]	75.1/23.2[c]	97.0/3.0[c]	39/61
$\nu_{C=O}(cm^{-1})$	1714	1714	1710	1703	1698	1696	1691	1691	1714
Activity (g $mmol^{-1}$ h^{-1})	16,600	3300	950	250	79	40	44	10	96
M_n (g/mol)[a]	*2,500*	*4,600*	*11,000*	*42,600*	*71,000*	-	-	-	*5,000*

A. Determined by ^{1}H NMR (500 MHz, d_2-TCE, 100 ^{o}C). B. A – alternating carbonyl; NA – non-alternating carbonyl (2 consecutive C_2H_4 insertions); I -isolated carbonyl. C. ^{1}H NMR, 500 MHz, 1:9 C_6D_6:HFIP, 25^{o}C.

increase, with the overall pressure of the reactor at least doubling. The increase in pressure is theorized to help increase the solubility of ethylene in the reactor, as lower pressures only produce alternating polyketone even at the same monomer feed compositions.

L2PdMePy can synthesize a variety of non-alternating polyketones with between 0.3-and 50% CO (**Table 2**). Like L1PdMePy, large excesses of ethylene are required to make a non-alternating polyketone with even a 4:1 ethylene:CO pressure ratio producing a largely alternating polyketone (**Table 2**, entry 8). Increasing the ratio of ethylene to CO even more makes it possible to access polyketones with extremely low CO content, down to 0.3 mol% CO, pushing the limits of the ^{1}H NMR characterization techniques. L2PdMePy exhibits extremely high polymerization activity at low CO feed compositions (**Table 2,** entry 1), similar to its literature reported activity in ethylene hompolymerizations.[12] This activity is higher than L1PdMePy by a factor of 10^{4} and higher than the current highest activity ethylene/CO copolymerization catalyst[36] by a factor of 10^{3}. However, this high activity quickly drops off at higher feed compositions of CO, likely due to the increased likelihood of catalyst inhibition by CO.

Additionally, L2PdMePy is capable of producing high-molecular weight polyketones (**Table 2,** entry 5), 15-fold higher than L1PdMePy, but only at higher CO feed ratios. It should be noted that the reliability of molecular weight determination (^{1}H NMR) decreases at high molecular weights, and polyketones with higher mol % of alternating fractions are only soluble in hexafluoroisopropanol solvent mixtures, further confounding this calculation. High-temperature gel permeation chromatography is needed for more accurate molecular weight determinations.

3.3 Microstructure of synthesized polyketones

The microstructure of the polyketones produced by L2PdMePy is identical to polymers reported int the literature. Several characteristic peaks of non-alternating polyketones are present in the ^{1}H NMR (**Figure 21**). Alternating methylene hydrogen signals are present at 2.7 ppm, followed by the non-alternating (double ethylene insertions) α- and β-hydrogens at 2.4 ppm and 1.7 ppm, respectively. The non-alternating β-methylene peak overlaps with methyl branching in

the polymer, which is why it integrates at a higher value than the non-alternating α-methylene peak. Isolated polyethylene methylene signals are present between 1.3 and 1.4 ppm. Between these

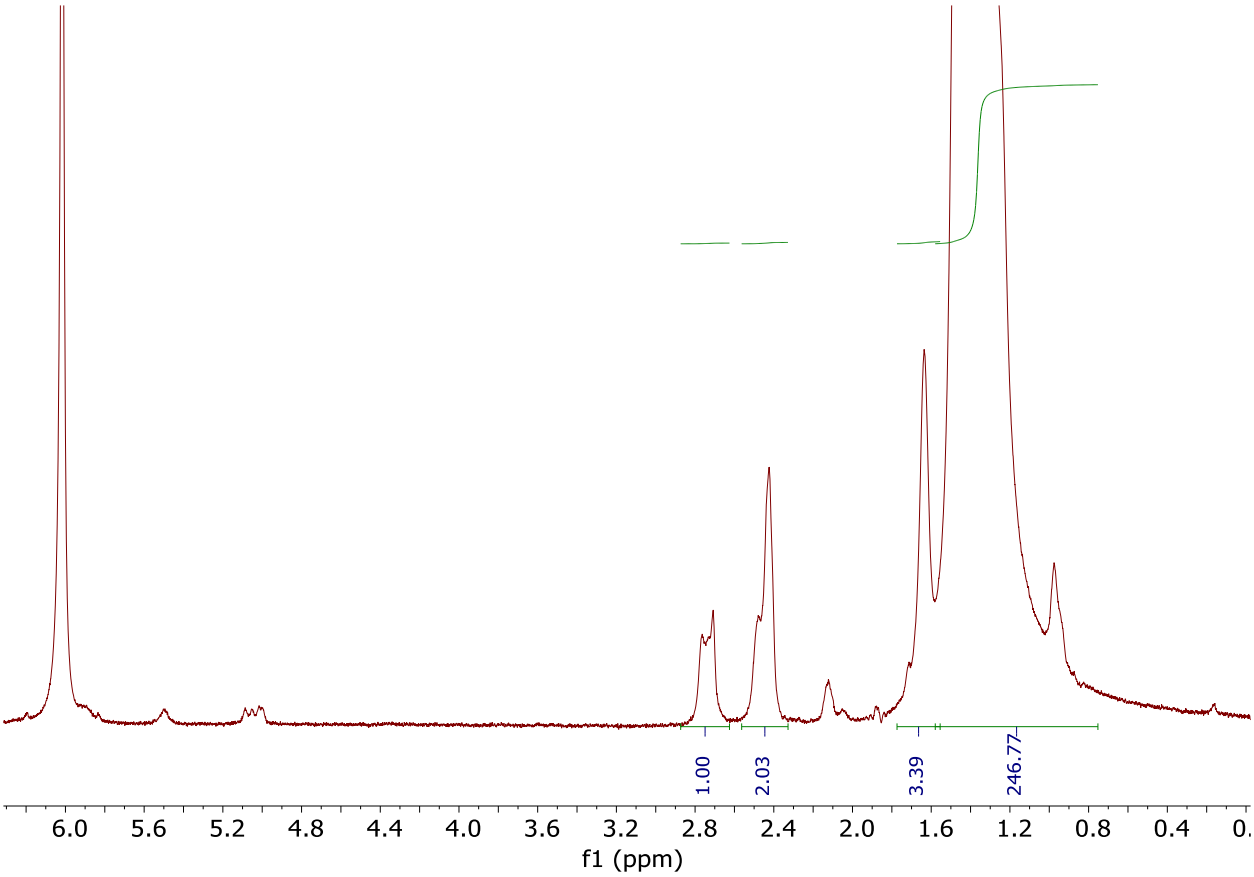

Figure 21. *^{1}H NMR of a 1% CO polyketone. 500 MHz, d_2-TCE, 100°C, 2mg/ml Cr(acac)$_3$ as a relaxation agent*

peaks, allylic methylene signals can be observed at 2.14 ppm, which combined with vinyl signals at 5.0, 5.5, and 5.9 ppm suggest that the main method of chain transfer and termination is β-hydrogen elimination from a Pd-alkyl species. The mole fraction of CO, triad fraction, and polymer M_n was calculated from these signals according to formulas reported in the literature.[35]

In addition to ^{1}H NMR, the polyketones were characterized by FT-IR spectroscopy (**Figure 21**). The shift of the carbonyl peak in the IR spectra has been demonstrated to be a function of three separate peaks corresponding to isolated, non-alternating, and alternating segments.[35] Of these signals, the alternating signal is the most red-shifted, appearing at 1691 cm^{-1}. Its lower energy compared to the non-alternating and isolated carbonyl signals is attributed to dipole-dipole

interactions between carbonyls in alternating segments. The shift of the carbonyl peak is therefore dependent on the mole fraction of CO and alternating motifs, which is observed in **Figure 22**, where the carbonyl peak blue shifts as the mole fraction of CO in the polymer decreases.

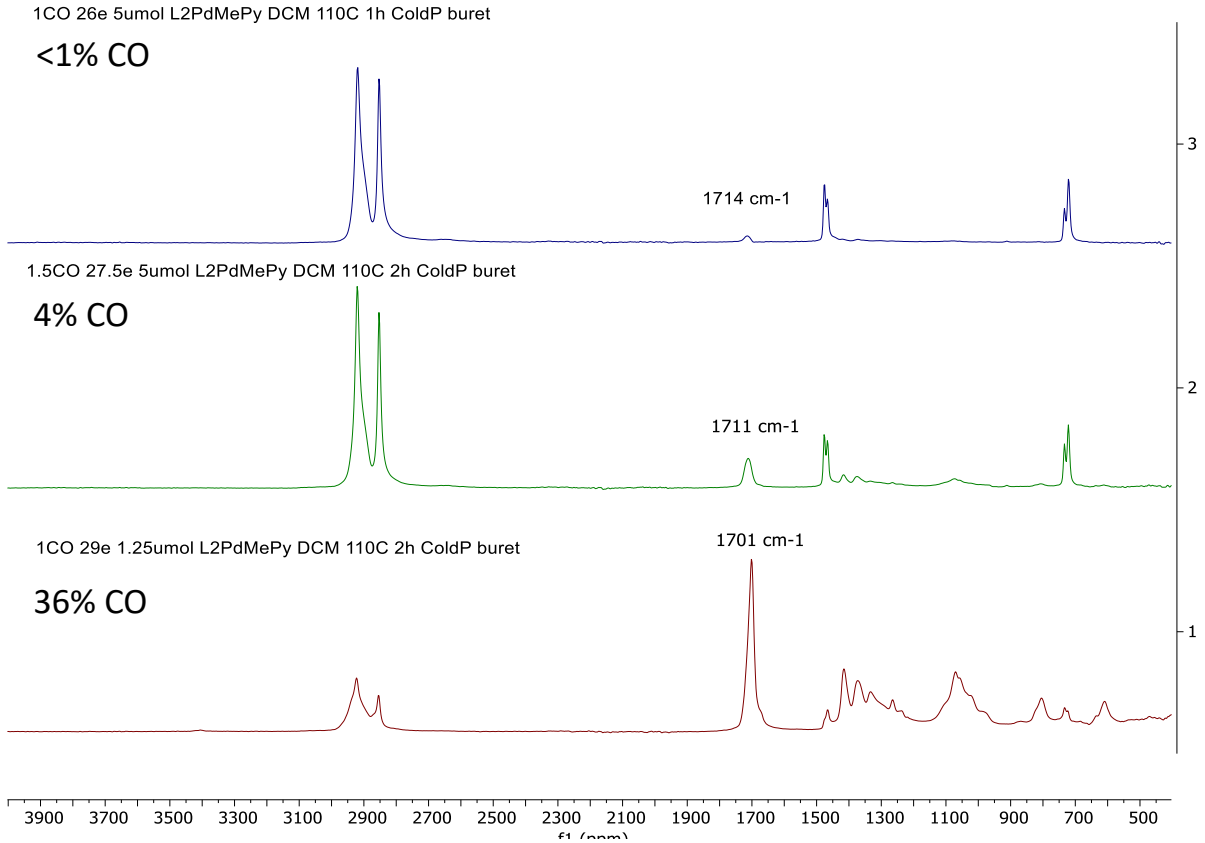

***Figure 22**. FT-IR spectra of polyketones with increasing CO content. Top-Bottom - <1% CO, 4% CO, 36% CO*

Examining the microstructure of the synthesized polyketones reveals that there is an unexpectedly high fraction of alternating sections. For example, in a polyketone with 1% CO, 0.4% of ethylene monomers are in alternating segments. This is much higher than statistically expected. In a purely random polymerization where you get a statistical distribution of CO functionalities, assuming a 1% CO polyketone is being produced, there is a 1% chance of adding CO and a 99% chance of adding ethylene to the growing polymer chain. Assuming CO is added, then there is a 100% probability that ethylene is added next, since CO cannot homopolymerize. Afterwards, to make an alternating motif, another CO must be added with a 1% probability of that

happening. Multiplying these probabilities together provides the theoretical mole fraction of alternating sections in a random copolymer – 0.01%. This is lower than what is observed by a factor of 40. The only way this distribution can occur if the probability of adding the second CO monomer is much higher than statistically expected. Since the monomer added before must be ethylene, this implies that it is the penultimate CO monomer that is imparting this bias towards adding a second CO monomer.

3.4 Evidence against blend formation

The copolymerization results for L2PdMePy initially raised doubts in the composition of the synthesized copolymers. Due to large yields of polymer, it could be assumed that the conversion of CO during the polymerization was very high. Potentially, all of the CO was being consumed in the initial stages in the polymerization in an alternating copolymer, followed by ethylene homopolymerization. Without access to high-temperature gel-permeation chromatography, two alternate methods to investigate blend formation were pursued.

First, a 1 wt% blend of an alternating polyketone and low molecular weight PE ($M_n \approx 2000$ g/mol) was mixed using coprecipitation from *ortho*-dichlorobenzene. After verifying that the polymer was quantitatively precipitated, the blend was characterized with FT-IR and ^{1}H NMR spectroscopy and compared to a 1% CO non-alternating polyketone sample.

From the FT-IR spectra shown in **Figure 23**, it is apparent that the non-alternating polyketone has a blue-shifted carbonyl signal compared to both the 1 wt% blend and the purely

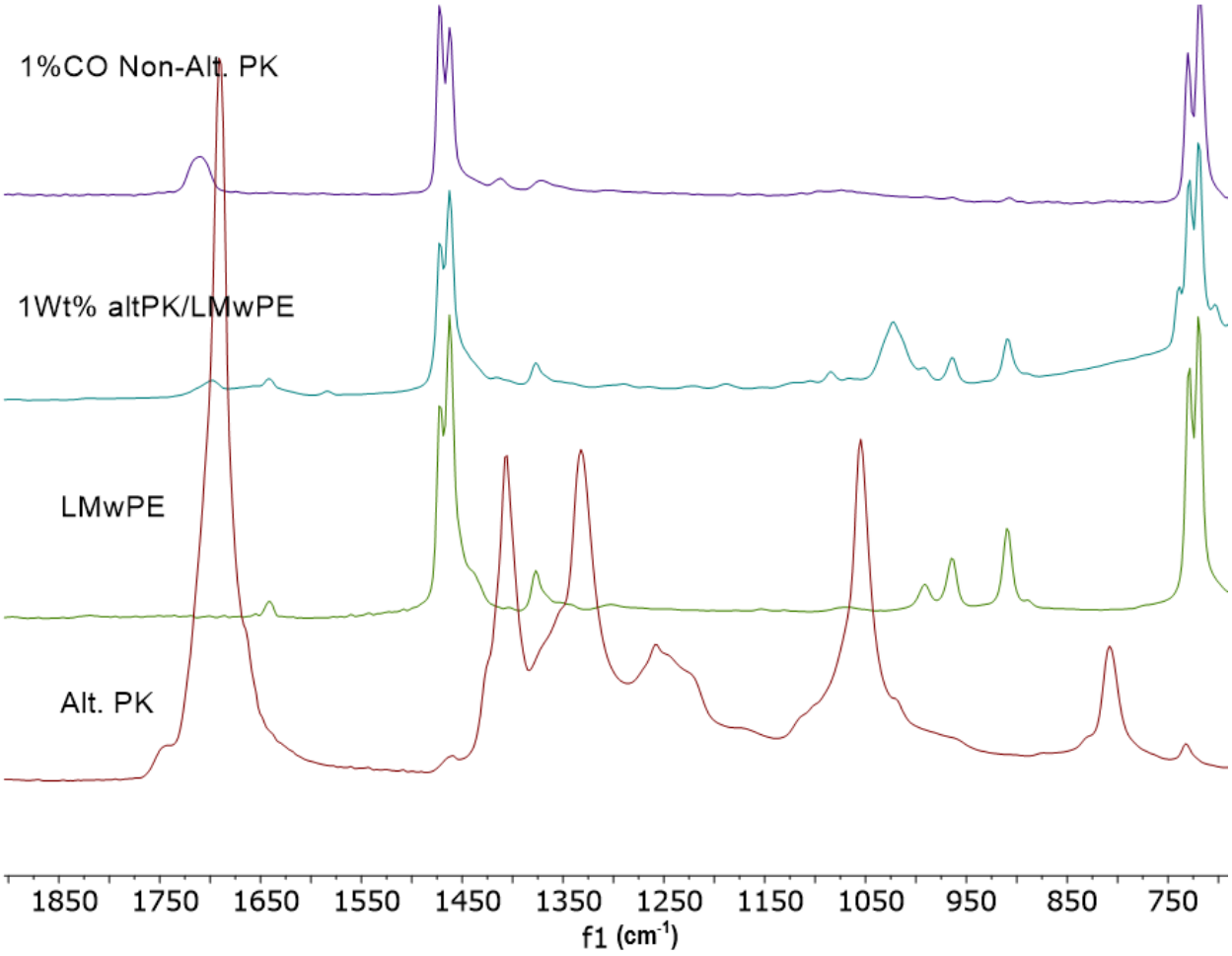

Figure 23. *Fingerprint region of the FT-IR spectra of 1% non-alternating polyketone (Blue), 1 wt% alt. polketone/PE blend (Teal), PE (green), and purely alternating polyketone*

alternating polyketone sample. While the blend does not match the alternating sample exactly, likely due to PE chains breaking up interactions between the alternating segments, the combination of the red-shifted carbonyl peak and the additional fingerprint region peaks between 900-1100 cm^{-1} that are not present in the non-alternating polymer suggest that blend formation is not occurring.

Similarly, examination of the ^{1}H NMR spectra of both the blend and the non-alternating polyketone reveals that the blend lacks methylene signals at 2.4 ppm that are characteristic of non-alternating α-methylenes (**Figure 24**).

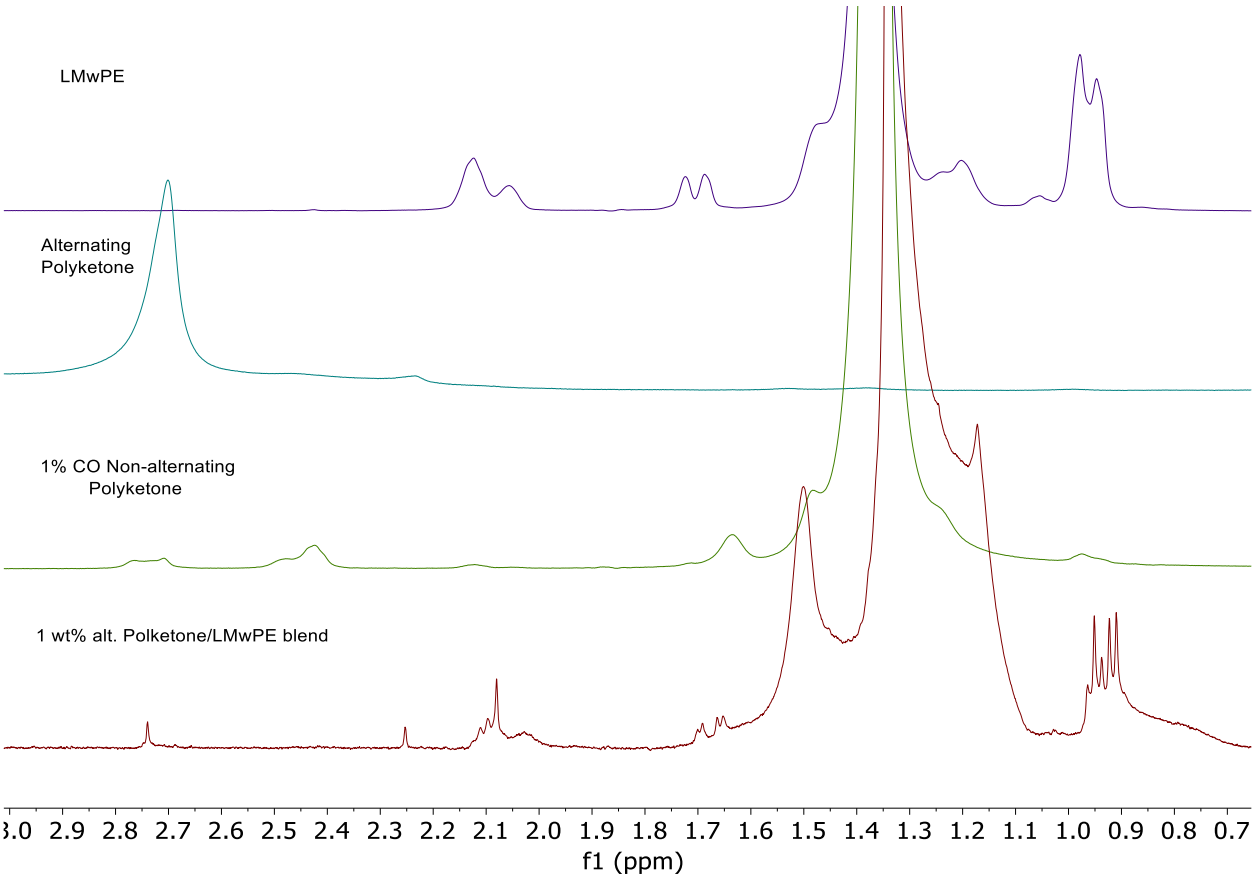

Figure 24. *Methylene region of the ^{1}H NMR spectra (500 MHz, d_2-TCE, 100°C) of LMwPE (purple), purely alternating polyketone (teal), 1% non-alternating polyketone (green), and 1 wt% alt. polyketone/PE blend (red)*

The second method used to investigate blend formation was to investigatbeing formed, e polymer composition over time. If a blend is formed, then both the CO% and alternating fraction will decrease as more polymer is being produced, as all the CO is initially consumed and is being diluted by the continuing homopolymerization of ethylene. In **Table 3,** it is evident that this is not the case. The polymer composition and microstructure remain constant as both the polymer yield and CO conversion increase. Additionally, the catalyst TON increases overtime as well, indicating that it is still active after an hour of polymerizations.

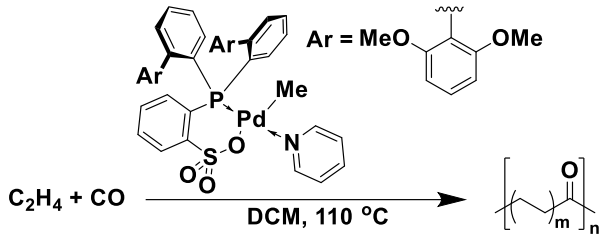

Table 3. *Ethylene/CO Copolymerization data over time.*

Yield (g)	***Time, h***	***TON (gPK/mmolPd^{-1})***	***%CO[a]***	***%alt[a]***	***%CO conv.***
4.06	0.5	1625	1.8	0.5	56
5.39	0.75	2150	1.8	0.6	75
6.53	1	2610	1.7	0.6	90

130 mg CO, 28.5 bar ethylene, 2.5 μmol L2PdMePy. A. Determined by ^{1}H NMR (500 MHz, d_2-TCE, 100 °C).

3.5 Mechanistic hypotheses for the observed alternation bias

Mechanistically, there are two potential hypotheses than can be made as to the origin of the observed alternation bias. The first explanation relates to the binding strength of the two monomers (thermodynamic in nature). In this explanation, if the ratio of binding equilibrium constants for ethylene and CO is smaller when the penultimate monomer is CO (ethylene binds weaker than CO), then CO is more likely to coordinate leading to the propagation of an alternating motif (**Scheme 12**). This can be expressed as equation 1:

$$1).\ \frac{K_{eq3}}{K_{eq4}} < \frac{K_{eq1}}{K_{eq2}}$$

Where K_{eq1} is the binding constant of ethylene to a non-alternating motif, K_{eq2} is the binding constant of CO to a non-alternating motif, K_{eq3} is the binding constant of ethylene to an alternating motif, and K_{eq4} is the binding constant of CO to an alternating motif (**Scheme 12**).

The second explanation relates to the insertion rates of the two monomers (kinetic in nature). In this explanation, if the ratio of insertion rates for ethylene and CO is smaller when the penultimate monomer is CO (ethylene inserts slower than CO), then CO is more likely to insert leading to the propagation of an alternating motif (**Scheme 12**). This can be expressed as equation 2:

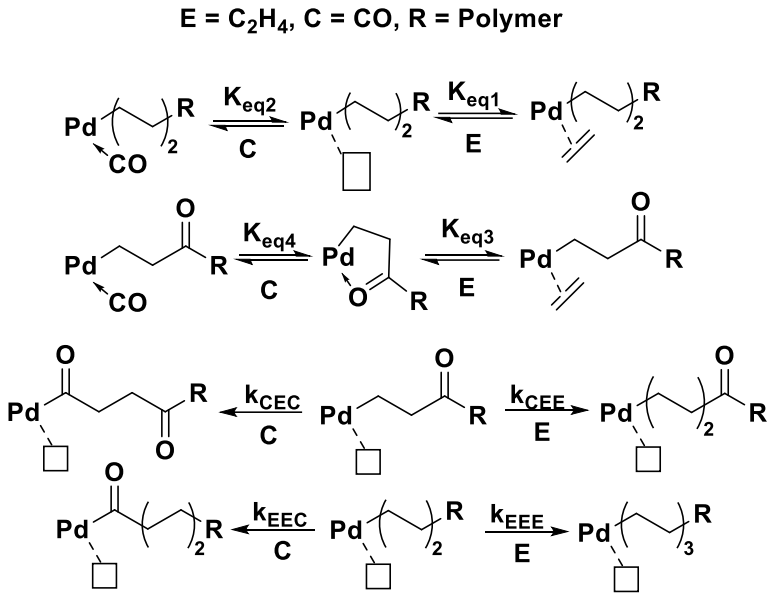

Scheme 12. *Hypothesis for the mechanistic origin of the penultimate monomer effect observed in ethylene/CO copolymerizations*

$$2).\ \frac{k_{CEE}}{k_{EEE}} < \frac{k_{CEC}}{k_{EEC}}$$

Where k_{EEE} is the insertion rate constant of ethylene to a non-alternating motif, k_{EEC} is the insertion rate constant of CO to a non-alternating motif, k_{CEE} is the insertion rate constant of ethylene to an alternating motif, and k_{CEC} is the insertion rate constant of CO to an alternating motif (**Scheme 12**).

A potential method for elucidating the mechanistic origin of this penultimate monomer effect would be to examine copolymerization parameters for the reaction. Copolymerization parameters are expressed as the ratio of rate constants for the addition each monomer to a growing

polymer chain ending in either comonomer. The Mayo-Lewis equation[43] is classically used to determine copolymerization parameters from polymer and feed composition data. The determined copolymerization parameters could eliminate one of the potential hypotheses for the observed penultimate monomer effect if the parameters are nonsensical under the assumptions of one of the hypotheses (i.e., the binding strength of CO being weaker than ethylene).

Since the penultimate monomer has to be considered in these polymerizations, a version of the Mayo-Lewis equation that takes this monomer into account must be used – The Merz-Alfrey-Goldfinger equation.[44] This equation is derived from the addition rates of each monomer to the eight different combinations of possible chains ends when taking the penultimate monomer and the final monomer into account (**Scheme 13**). Each of these reactions can be expressed as the rate laws shown on the right of **Scheme 13**.

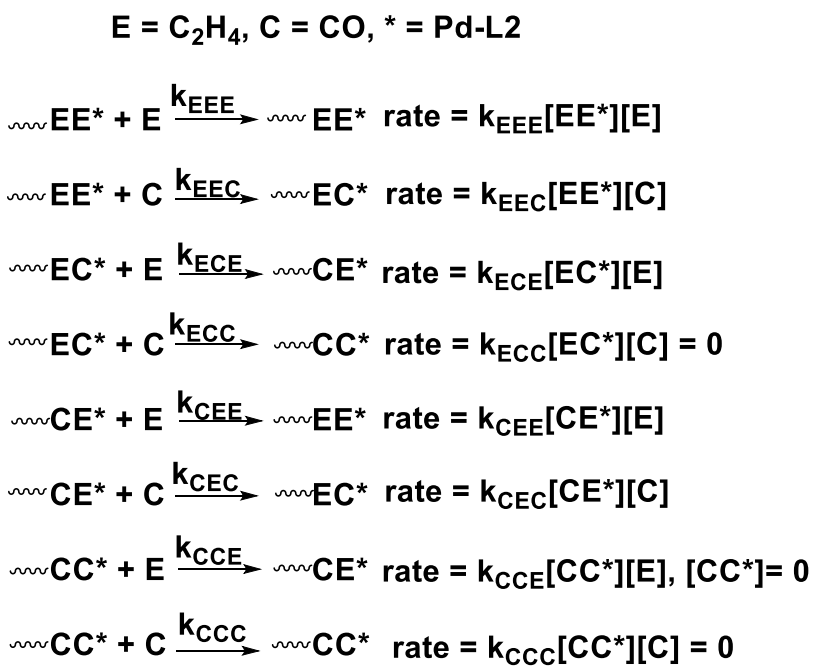

Scheme 13. *Propagation reactions used to derive the Merz-Alfrey-Goldfinger equation*

The rate laws for each of the propagation can be expressed as a function of monomer consumption in equation 3:

$$3).\ \frac{dE}{dC} = \frac{[E]}{[C]} \times \frac{k_{EEE}[EE^*] + k_{CEE}[EC^*] + k_{ECE}[CE^*] + k_{CCE}[CC^*]}{k_{EEC}[EE^*] + k_{CEC}[EC^*] + k_{ECC}[CE^*] + k_{CCC}[CC^*]}$$

The concentration of each growing chain end can be determined using the steady-state approximation, since the initiation of new chains is assumed to be much slower than propagation. Simplification of this expression yields equation 4:

$$4).\ \frac{dE}{dC} = \frac{1 + \left(\frac{k_{CEE}[E]}{k_{CEC}[C]}\right)\frac{[C] + \frac{k_{EEE}[E]}{k_{EEC}}}{\frac{k_{CEE}}{k_{CEC}}[E] + [C]}}{1 + \left(\frac{k_{ECC}[C]}{k_{ECE}[E]}\right)\frac{[E] + \frac{k_{CCC}[C]}{k_{CCE}}}{\frac{k_{ECC}}{k_{ECE}}[C] + [E]}}$$

Since CO cannot homopolymerize, $k_{ECC} = 0$, which eliminates all of the terms in the denominator, simplifying to equation 5:

$$5).\ \frac{dE}{dC} = 1 + r_1' x \left(\frac{r_1 x + 1}{r_1' x + 1}\right)$$

$$x = \frac{[E]}{[C]}$$

$$r_1 = \frac{k_{EEE}}{k_{EEC}}$$

$$r'_1 = \frac{k_{CEE}}{k_{CEC}}$$

Equation 5 relates the ratio of mole fractions of ethylene over CO in the polymer (dE/dC) and feed (x). from fitting these data, two copolymerization parameters, r_1 and r'_1 can be determined. These parameters are equal to the ratio of insertion rates of ethylene vs. CO in a non-

alternating segment (r_1) and an alternating segment (r'_1). The insertion rate hypothesis will stand if equation 2 is true, which can now be expressed as $r'_1 < r_1$.

However, the Merz-Alfrey-Goldfinger equation does not relate to the binding strengths of either monomer, so a second equation must be derived to determine copolymerization parameters assuming that the penultimate effect is on monomer coordination and not insertion rate. Assuming this is true, eight new expressions can be written for the propagation of each monomer (**Scheme 14**).

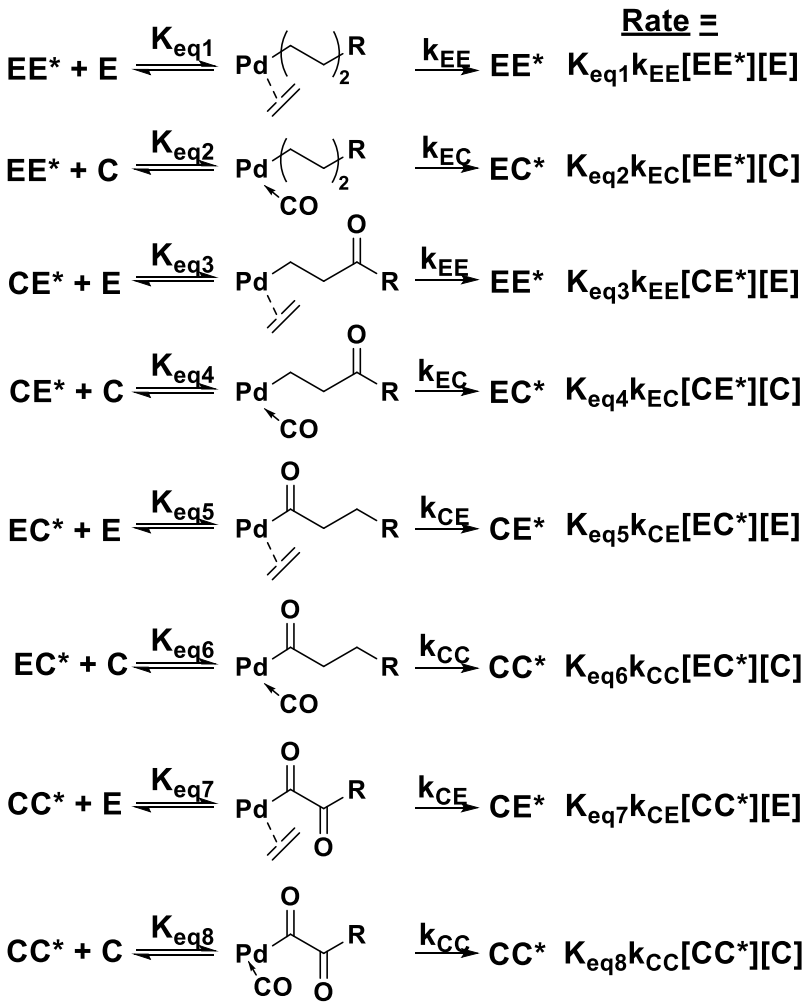

Scheme 14. *Propagation reactions used to derive the copolymerization parameter equation accounting for a penultimate effect on monomer coordination*

After combining the expressed rate laws in **Scheme 14** into a function of polymer composition, equation 6, it becomes obvious that this equation has the same mathematical form as the Merz-Alfrey-Goldfinger equation, being nearly identical to equation 3:

$$3).\ \frac{dE}{dC} = \frac{[E]}{[C]} \times \frac{k_{EEE}[EE^*] + k_{CEE}[EC^*] + k_{ECE}[CE^*] + k_{CCE}[CC^*]}{k_{EEC}[EE^*] + k_{CEC}[EC^*] + k_{ECC}[CE^*] + k_{CCC}[CC^*]}$$

$$6).\ \frac{dE}{dC} = \frac{[E]}{[C]} \times \frac{K_{eq1}k_{EE}[EE^*] + K_{eq3}k_{EE}[EC^*] + K_{eq5}k_{CE}[CE^*] + K_{eq7}k_{CE}[CC^*]}{K_{eq2}k_{EC}[EE^*] + K_{eq4}k_{EC}[EC^*] + K_{eq6}k_{CC}[CE^*] + K_{eq8}k_{CC}[CC^*]}$$

The only difference between these two equations after applying the steady-state approximation and simplifying will be the definition of the copolymerization parameters, which will now include the monomer binding equilibrium constants:

$$r_1 = \frac{K_{eq1}k_{EE}}{K_{eq2}k_{EC}}$$

$$r_1' = \frac{K_{eq3}k_{EE}}{K_{eq4}k_{EC}}$$

These parameters are equal to the ratio of binding constants of ethylene vs. CO in a non-alternating segment (r_1) and an alternating segment (r'_1), multiplied by the ratio of insertion rates of ethylene vs. CO into a Pd-alkyl species. The insertion rate hypothesis will stand if equation 1 is true, which can now be expressed as $r'_1 < r_1$. Since this outcome is identical to the conditions that must be met to uphold the insertion rate hypothesis, this method cannot be used to eliminate either hypothesis.

3.6 Extreme CO sensitivity of L2PdMePy

Despite not being a useful method to gain mechanistic insight into the alternation bias observed in late transition metal-catalyzed ethylene/CO copolymerizations, determining the

copolymerization parameters of this reaction could be useful for industrial applications and scale-up. Utilizing the same polymerization methods as before, a variety of ethylene/CO feed compositions were used to make a suite of non-alternating polyketones. The composition of these polymers was determined by ^{1}H NMR. Feed compositions were determined gravimetrically by pressurizing a simplified reactor chamber filled with dichloromethane and recording the mass difference afterwards. The polymer compositions (ratio of ethylene and CO mole fractions) were plotted against determined feed compositions and fit with the Merz-Alfrey-Goldfinger equation using ExcelSolver (**Figure 25**). The X^2 of the fit was determined and used as a metric of goodness of fit.

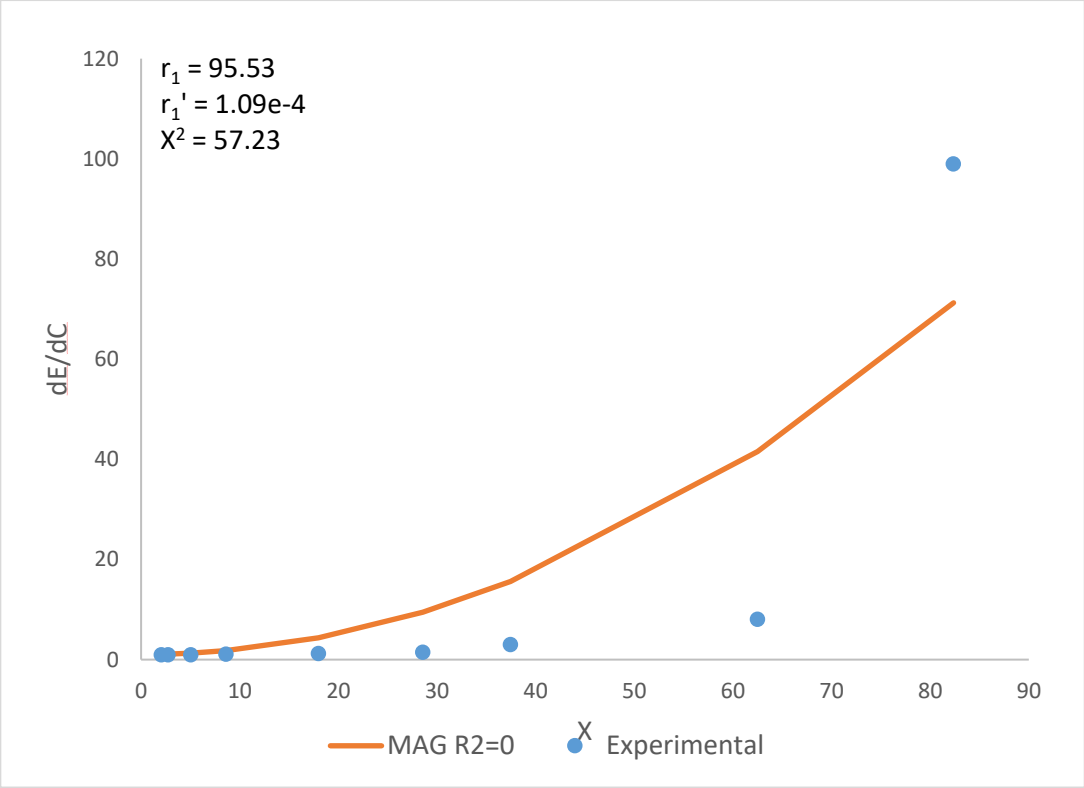

***Figure 25**. Ratio of ethylene : CO mole fractions in synthesized polyketones (dE/dC) as a function of ratio of ethylene : CO mole fractions in the monomer feed (X). Experimental values shown in blue, ExcelSolver fit (Merz-Alfrey-Goldinger equation) in orange*

With a minimized X^2 of 57.23, the Merz-Alfrey-Goldfinger fit of these data does not reject the null hypothesis and is therefore statistically insignificant. Examination of the data reveals that

the fit is highly dependent on the final data point, with both high ratios of ethylene/CO mole fractions in the feed and copolymer. More data is needed in this region to improve the quality of the fit. However, the changes in the mass of CO added in this region are miniscule, which prompted a redesign of the reactor setup to better quantify small quantities of CO (**Figure 26**).

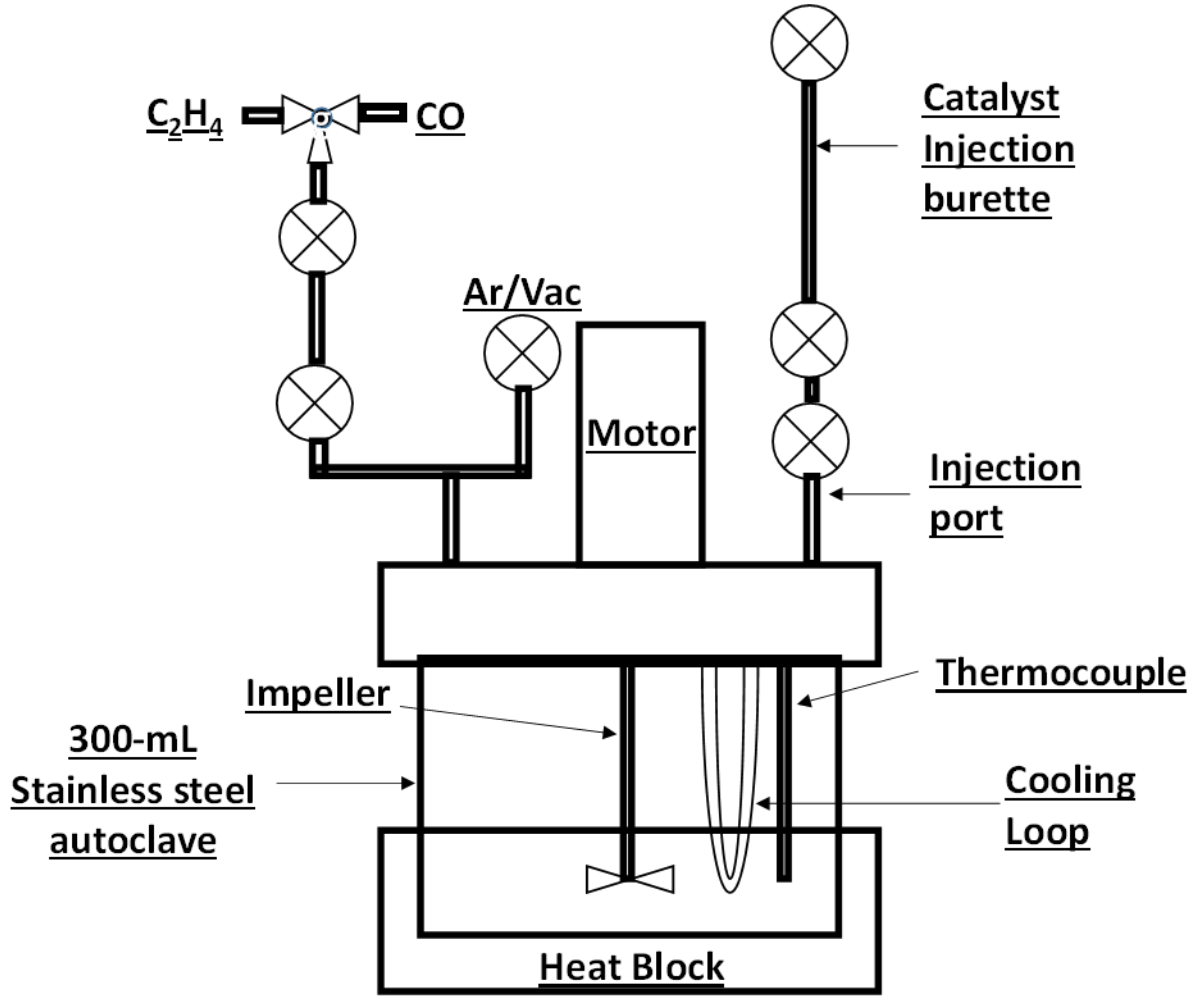

Figure 26*. Schematic of Parr reactor modified to better quantify CO in ethylene/CO copolymerizations*

To better quantify very small quantities of CO, a 7-mL stainless steel gas burette was added for CO pressurization. During pressurization, the burette was pressurized with a high pressure of CO and sealed off from the CO line. Using the known pressure and volume the mass of CO was calculated from reported densities of CO. Then the CO was released into the reactor, followed by

ethylene pressurization through the burette (via a three-way valve) to improve mixing. Since the volume of the burette is negligible compared to the reaction vessel, it can be assumed that all the CO was transferred.

Upon repeating the copolymerization experiments with the new CO pressurization method, it became evident that very small amounts of CO were required to cause massive changes in copolymer composition, with the difference between two different copolymers being on the milligram scale. This is shown in **Figure 27**, where the mole fraction of CO in the polymer is plotted as a function of the mole fraction of CO in the feed. Even small changes in feed composition (0.05% CO) can mean the difference between a 1% CO polyketone and a 27% CO polyketone. The extreme CO sensitivity and high reactivity of L2PdMePy adds significant challenges to the determination of copolymerization parameters and requires more sensitive feed quantification techniques.

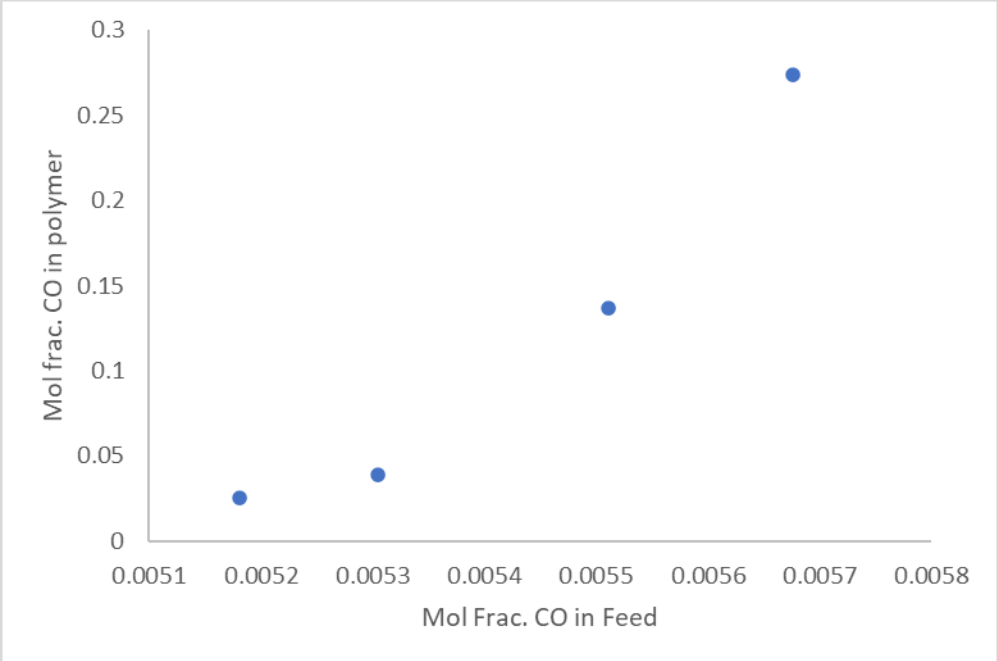

***Figure 27**. Mole fraction of CO in the polymer plotted as a function of the mole fraction of CO in the feed using the improved reactor design*

3.7 Conclusions

L2PdMePy is an extremely active and sensitive catalyst for the non-alternating copolymerization of ethylene and CO. The increases in molecular weight and catalyst activity compared to L1PdMePy that were previously observed[12] in ethylene homopolymerizations were demonstrated to also apply to ethylene/CO copolymerizations. L2PdMePy has the highest activity of any reported catalyst for these polymerizations by a factor of a 1000, and can synthesize copolymers with M_n values up 70,000 g/mol. Additionally, it can synthesize copolymers with a wide range of CO content – between 0.3 and 50% CO. These metrics make it a particularly attractive catalyst for the industrial scale-up of these polymerizations, compared to the state -of-the-art. More work is needed to elucidate the origins of its bias towards alternating copolymerization and control its high sensitivity to small quantities of CO.

CHAPTER 4: CATIONIC NICKEL(II) DIIMINE COMPLEXES FOR STEREOCONTROLLED PROPYLENE/VINYL SILYL ETHER COPOLYMERIZATION

4.1 Introduction

PEX_b, a crosslinked ethylene/vinyl silyl ether (VSE) copolymer, is used in construction applications as a piping material and wire insulator.[45] Commercially, this PEX_b is made through free-radical processes, either by functionalizing PE with a VSE via grafting or from the direct copolymerization of ethylene and a VSE followed by cross-linking via the condensation of the silyl ether groups (**Scheme 15**). Brookhart and coworkers developed an alternative method of

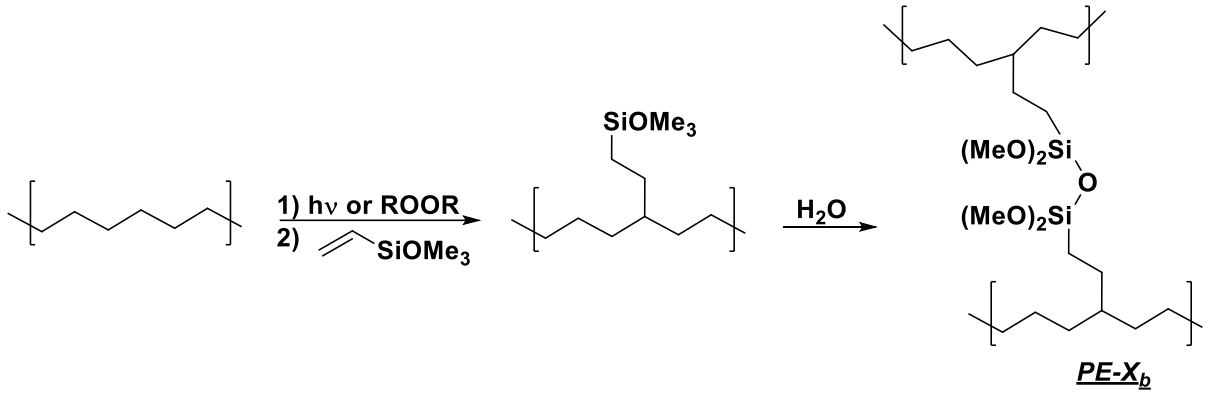

Scheme 15. Synthesis of PEX_b via radical grafting and condensation

synthesizing ethylene/VSE copolymers via the coordination-insertion copolymerization of ethylene and VSEs catalyzed by a cationic diimine Ni(II) complex (**Scheme 16**).[46-48] This method is advantageous over traditional free radical methods because of the significantly lower

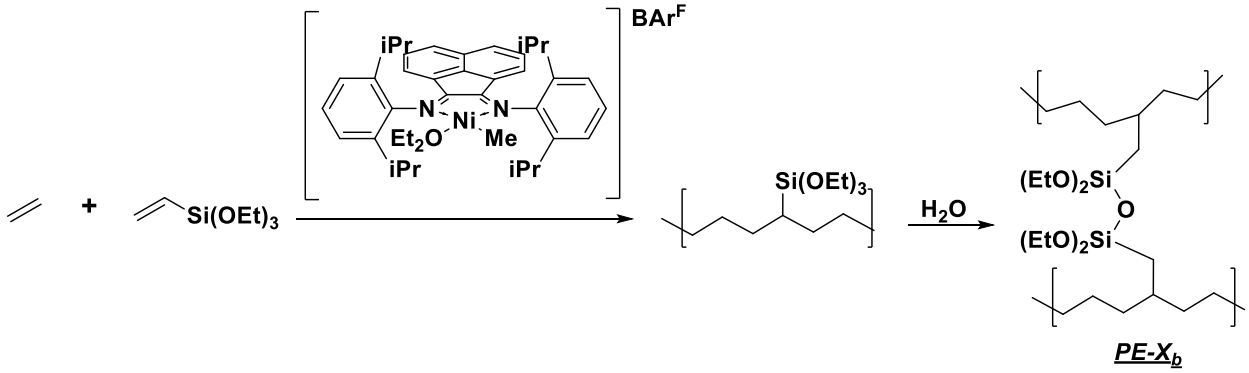

Scheme 16. *Synthesis of PEX_b via direct coordination-insertion polymerization catalyzed by a cationic Ni(II) diimine complex*

temperatures and pressures it employs and the potential for control of the polymer architecture inherent to single-site metal catalysis.

While PEX_b is widely utilized, the isotactic polypropylene (iPP) analogue has not yet been reported. The crystallinity imparted by the isotactic relationship between methyl substituents in iPP makes it less resistant to creep and improves its mechanical properties when compared to PE.[49] Because of these differences in mechanical properties, a novel cross-linked iPP would be a material of interest. However, the direct synthesis of an iPP analogue containing cross-linkable silyl ether groups is limited by the current catalytic methods used to produce isotactic polypropylene, which rely on early-transition metal catalysis. The Lewis basic nature of VSEs make them incompatible with highly oxophillic early-transition metals. Late-transition metals such as Ni or Pd are capable of tolerating Lewis basic moieties in VSEs, as demonstrated by Brookhart's Ni(II) diimine catalyzed ethylene/VSE copolymerization. The challenge with late-transition metals is their tendency to "chain-walk" – repeatedly undergo β-hydride elimination and re-insertion – which scrambles the stereochemistry of the growing polypropylene polymer.[50]

In 2005, Coates and coworkers reported a C_2-symmetric bulky Ni(II) dibromide diimine complex that could polymerize propylene in a stereocontrolled manner (**Scheme 17**).[51] This was

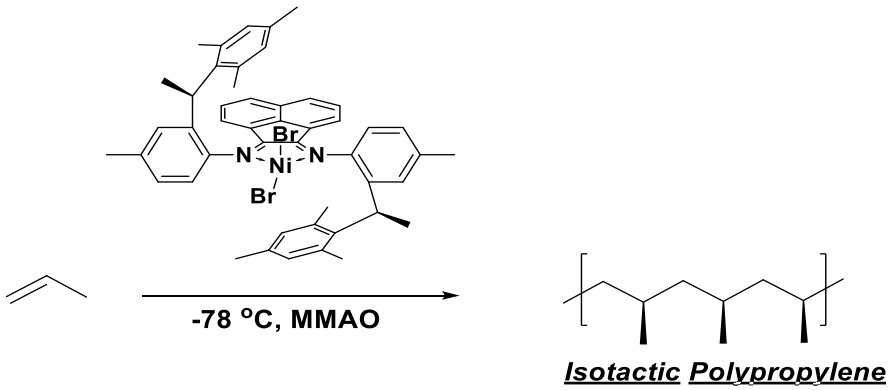

Scheme 17. *Synthesis of iPP by a C_2-symmetric (diimine)$NiBr_2$ complex activated by MMAO*

possible due to the low temperatures and high-axial bulk preventing chain walking from occurring.

This catalyst appeared to be an ideal candidate for isotactic propylene/VSE copolymerizations – it shares a similar ligand with the [(diimine)NiMe(OEt_2)]BAr^F complexes reported by Brookhart to copolymerize ethylene and VSEs with high activity and at low temperatures, it would polymerize propylene in a stereocontolled manner. The downside of this catalyst was that it required an alkyl aluminum activator – MMAO – to transmetalate the bromide ligands to alkyl groups capable of insertion polymerization. MMAO is extremely oxophillic, and therefore incompatible with most polar comonomers. Additionally, since MMAO has an undefined structure, its use complicates mechanistic studies since the identity of the active catalyst is unknown. To eliminate the need for MMAO and enable the copolymerization with vinyl comonomers, we set out to synthesize a cationic Ni-Me derivative with an ancillary diethyl ether ligand, like the metal center in the catalyst reported by Brookhart and coworkers. Initially, we planned to accomplish this by metalating the C_2-symmetric diimine ligand reported by Coates with (tmeda)$NiMe_2$, followed by protonation with Brookhart's acid (**Scheme 18**). Once this catalyst was on hand, its ability to copolymerize ethylene/VSEs in a stereocontrolled manner would be investigated.

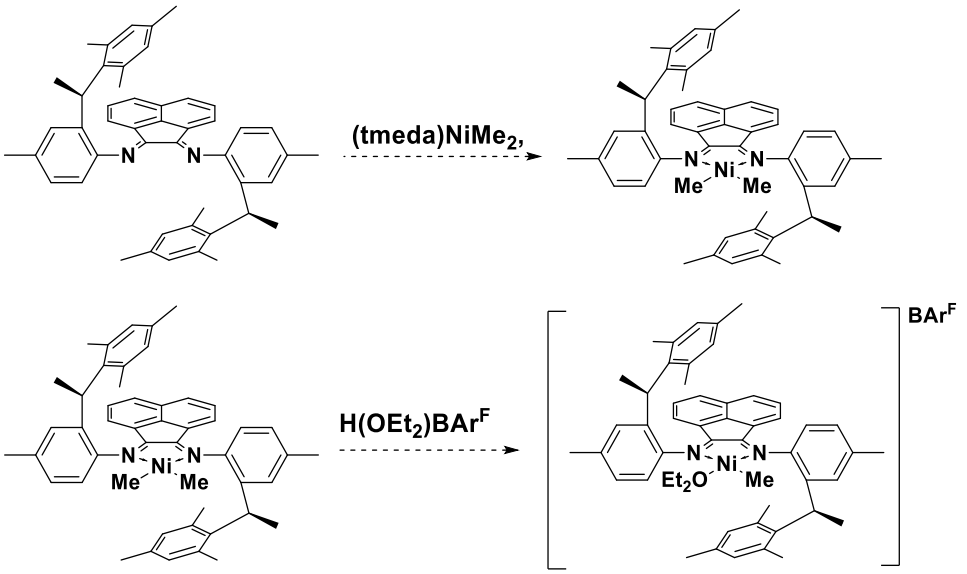

Scheme 18. *Proposed synthesis of a C_2-symmetric cationic [(diimine)NiMe(OEt_2)]BAr^F complex.*

4.2 Synthesis of a C_2-symmetric cationic [(diimine)NiMe(OEt_2)]BAr^F complex

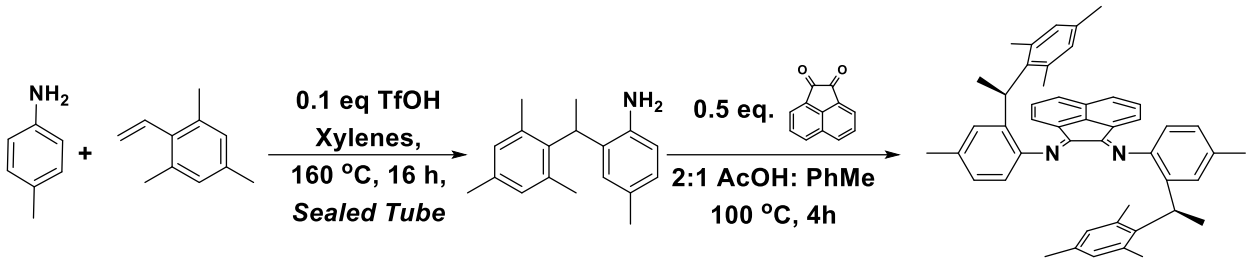

Scheme 19. *Synthesis of the C_2-symmetric diimine ligand (METAD)*

The C_2-symmetric diimine ligand (METAD) was synthesized according to literature procedures[51] in 16% yield over two steps as a yellow powder (**Scheme 19**). The yield is lower than what would normally be considered acceptable due to a diastereoselective precipitation of the desired racemic diastereomer. With the pure ligand in hand, NMR-scale attempts at Ni metalation began, starting with treating the diimine ligand with 1.5 equivalents of (tmeda)$NiMe_2$ in C_6D_6 at room temperature (**Scheme 20**). Visible decomposition to Ni black was observed immediately upon addition of the (tmeda)$NiMe_2$. Over the course of 30 min, the reaction mixture developed a purple hue, then began to precipitate as a green solid, which is likely a decomposed Ni salt.

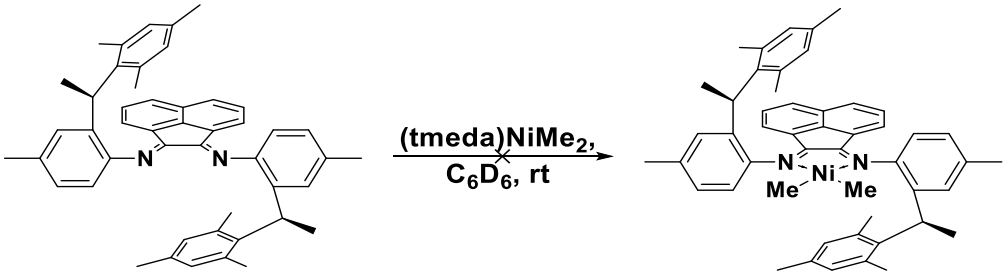

Scheme 20. *Attempted metalation of METAD with (tmeda)$NiMe_2$*

Analysis of the ^{1}H NMR spectra of the crude reaction mixture (**Figure 28**) reveals several new benzylic methine peaks between 5-7 ppm that suggest some sort of interaction with the ligand causing hindered rotation of the axial mesityl groups. No clear Ni-Me was identified other than

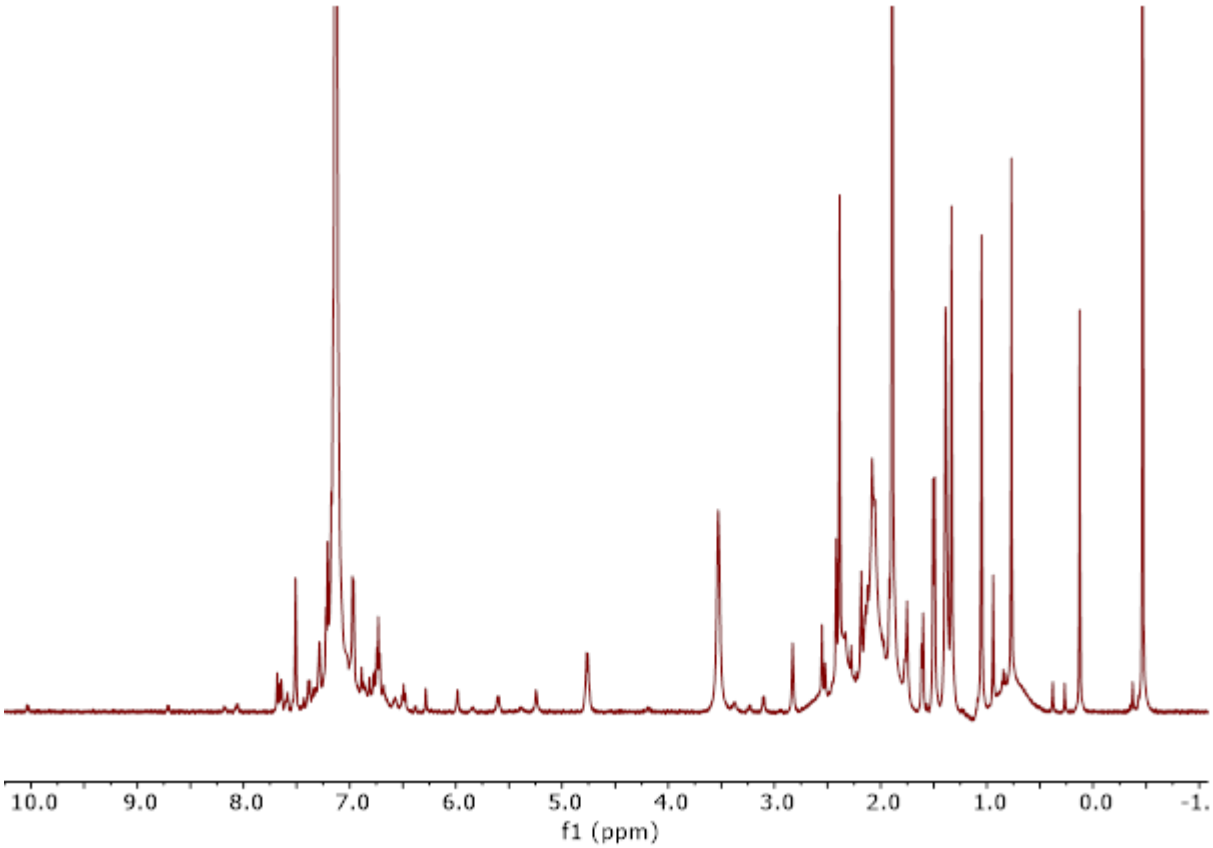

Figure 28. *^{1}H NMR (C_6D_6, 25 °C, 500 MHz) of attempted (METAD)$NiMe_2$ synthesis with impure (tmeda)$NiMe_2$*

residual (tmeda)$NiMe_2$ at -0.44 ppm. The purity of the (tmeda)$NiMe_2$ is a likely contributor to the failure of this reaction, especially the potential presence of leftover methyl lithium which would act as a nucleophile and attack the apo-diimine ligand. Following this approach, an alternative method utilizing a novel binuclear Ni(II) dimethyl complex, $[NiMe_2(thf)]_2$(tmeda), synthesized

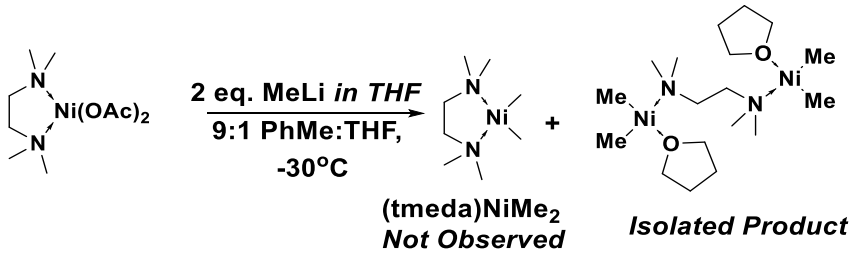

Scheme 21. *Synthesis of $[NiMe_2(thf)]_2$(tmeda)*

using a THF solution of MeLi instead of the commercial Et_2O solution used in the literature (**Scheme 21**).[52] $[NiMe_2(thf)]_2$(tmeda) was synthesized in 12.9% yield and isolated as an air, moisture, and temperature yellow powder. The ^{1}H NMR of this complex appears to be extremely

similar to that of mononuclear (tmeda)$NiMe_2$, with the exception of the coordinated THF signals at 3.59 and 1.29 ppm, and the 2:1 stoichiometry of the Ni-Me signal at -0.67 ppm to the TMEDA signals at 1.84 and 2.20 ppm (**Figure 29**). A small methyl lithium impurity can be observed at -1.5 ppm, which may be the cause of the rapid decomposition of this complex. Metalation with $[NiMe_2(thf)]_2(tmeda)$ were carried out in Et_2O at -78 ºC to discourage decomposition (**Scheme**

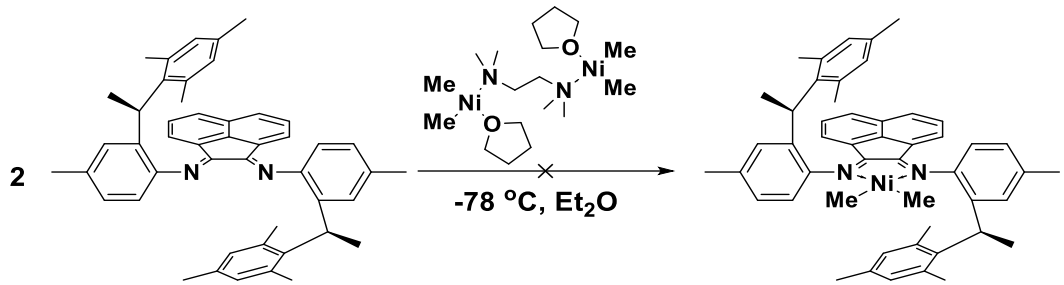

Scheme 22. *Attempted metalation of METAD with $[NiMe_2(thf)]_2(tmeda)$*

22). These attempts were also unsuccessful, although at lower temperatures, the purple species

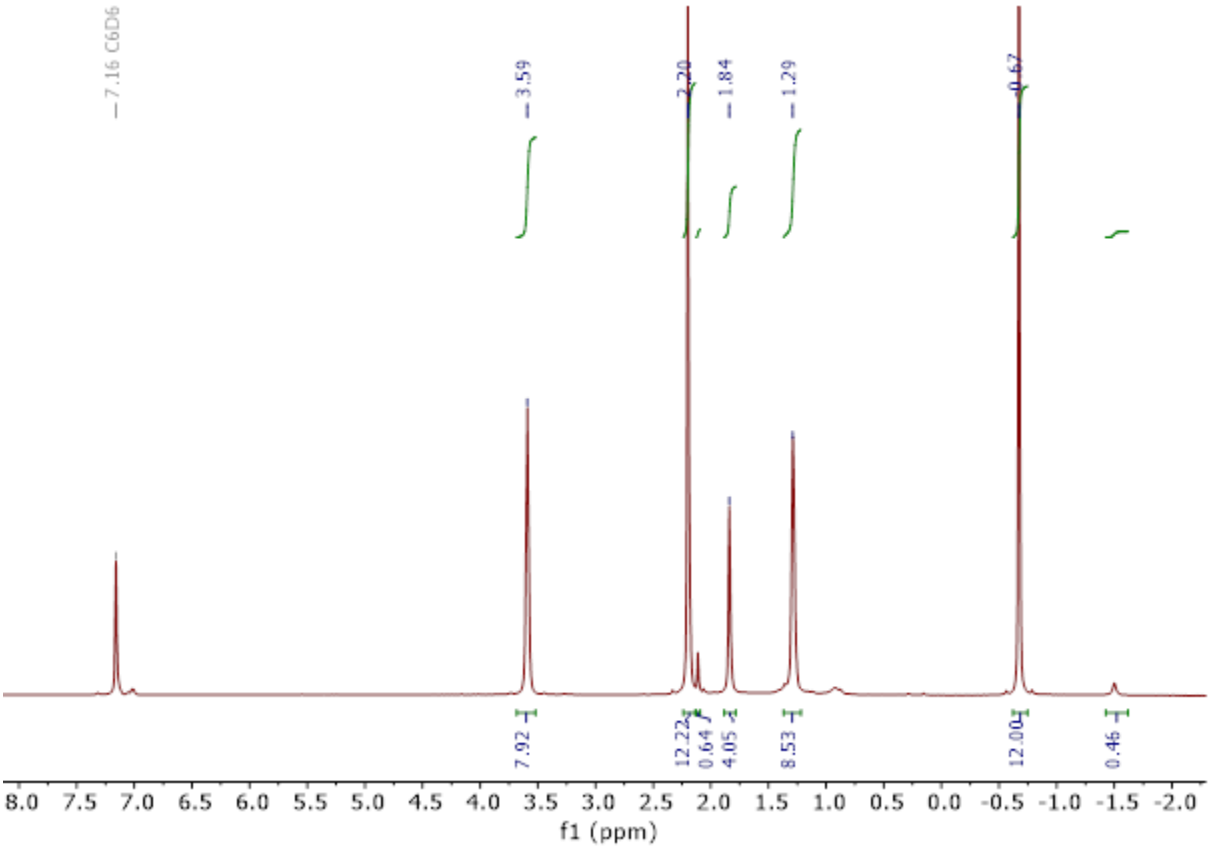

Figure 29. *^1H NMR (C_6D_6, 25 ºC, 500 MHz) of $[NiMe_2(thf)]_2(tmeda)$*

observed in the complexation persisted longer that the room temperature attempts, however it began to decompose upon warming to room temperature after solvent removal. ^{1}H NMR analysis of the crude reaction mixture shows that there are multiple new peaks between 5-7 ppm suggesting that there is some interaction with the METAD ligand (**Figure 30**). Based on the integrations of these peaks at 5.31, 4.79, and 4.45 ppm being in a 1:1.5:1 ratio it may be the case that these are

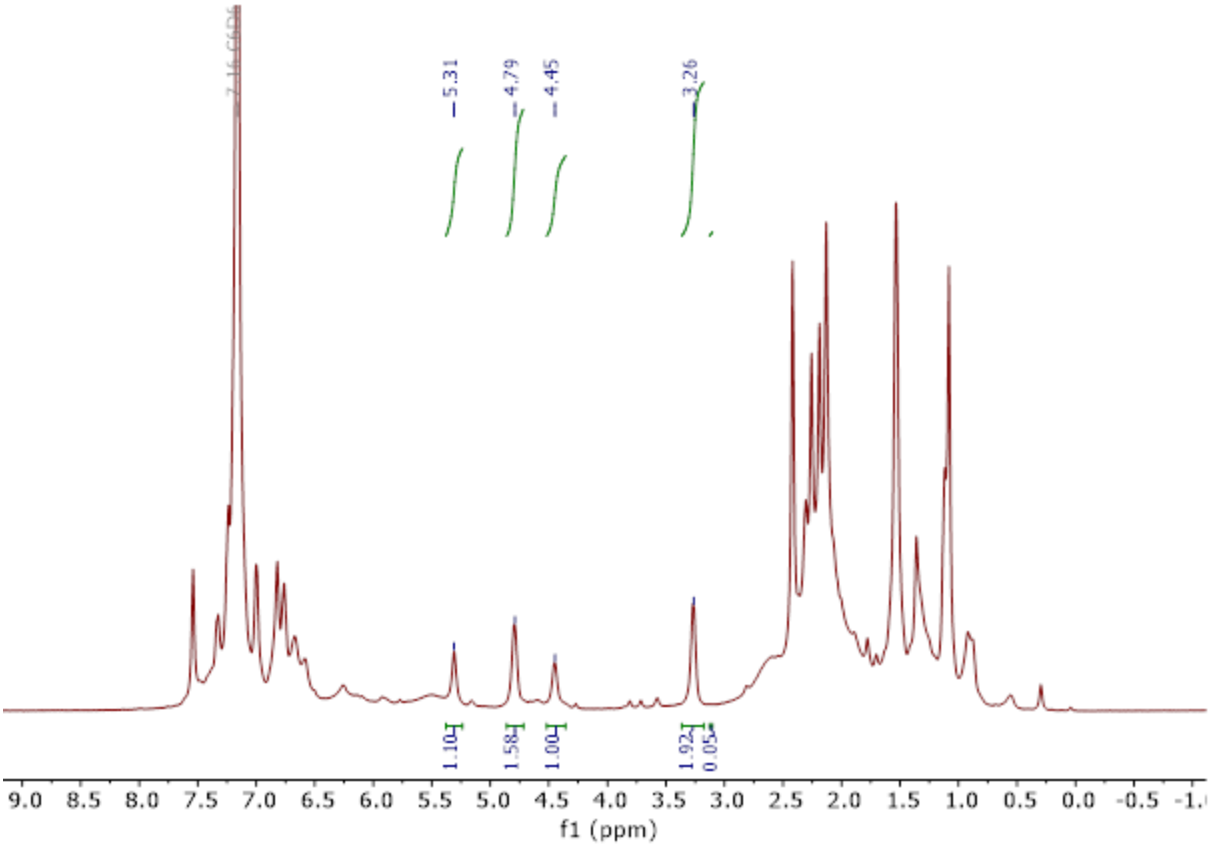

Figure 30. *^{1}H NMR (C_6D_6, 25 °C, 500 MHz) of attempted (METAD)$NiMe_2$ synthesis with $[NiMe_2(thf)]_2$(tmeda)*

the *m*-hydrogens and methyl groups on the mestityl rings, as well as the benzylic methine signals. These would be directly impacted by a coordinated metal since crystal structure of the reported dibromide complex show that the mesityl rings sit directly above the metal center, with each *m*-hydrogen and *o*-methyl group sitting in electronically inequivalent environments.[48] This is evident in the reported ^{1}H NMR of METAD$NiBr_2$ as well. However, due to the clear absence of a Ni-Me peak, this reaction was ultimately unsuccessful.

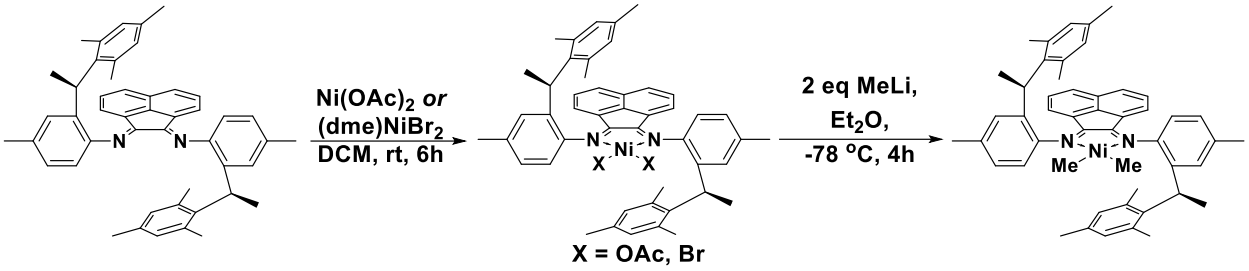

Scheme 23. *Proposed two-step synthesis of METADNiMe$_2$*

The lack of success using dimethyl Ni(II) precursors to metalate the METAD ligand prompted a 2-step transmetalation approach with MeLi (**Scheme 23**). First, an Ni(II) precursor (either $Ni(OAc)_2$ or $(dme)NiBr_2$) was treated with equimolar METAD ligand to synthesize the corresponding diacetate or dibromide complex. These complexes were then transmetalated with 2 equivalents of MeLi at -78 ºC with the intent of synthesizing the dimethyl complex. This approach is commonly taken in the synthesis of cationic Ni methyl diimine complexes.[53] $(METAD)NiBr_2$, the catalyst reported by Coates and coworkers in 2005, was synthesized using the first step of this route.[51]

The attempted synthesis of $(METAD)Ni(OAc)_2$ was initially believed to be successful. Due to poor solubility of the $Ni(OAc)_2$ precursor, the metalation was allowed to run overnight in an argon-atmosphere glovebox, after which the yellow solution deepened into an orange color. Comparison of the ^1H NMR of the apo-METAD ligand (**Figure 31**, green) and putative $(METAD)Ni(OAc)_2$ complex (red) shows new peaks in the 4.5-7 ppm region that are similar to

the split peaks in the published METADNiBr$_2$ NMR, as well as two new signals at 4.14 and 4.24 ppm.

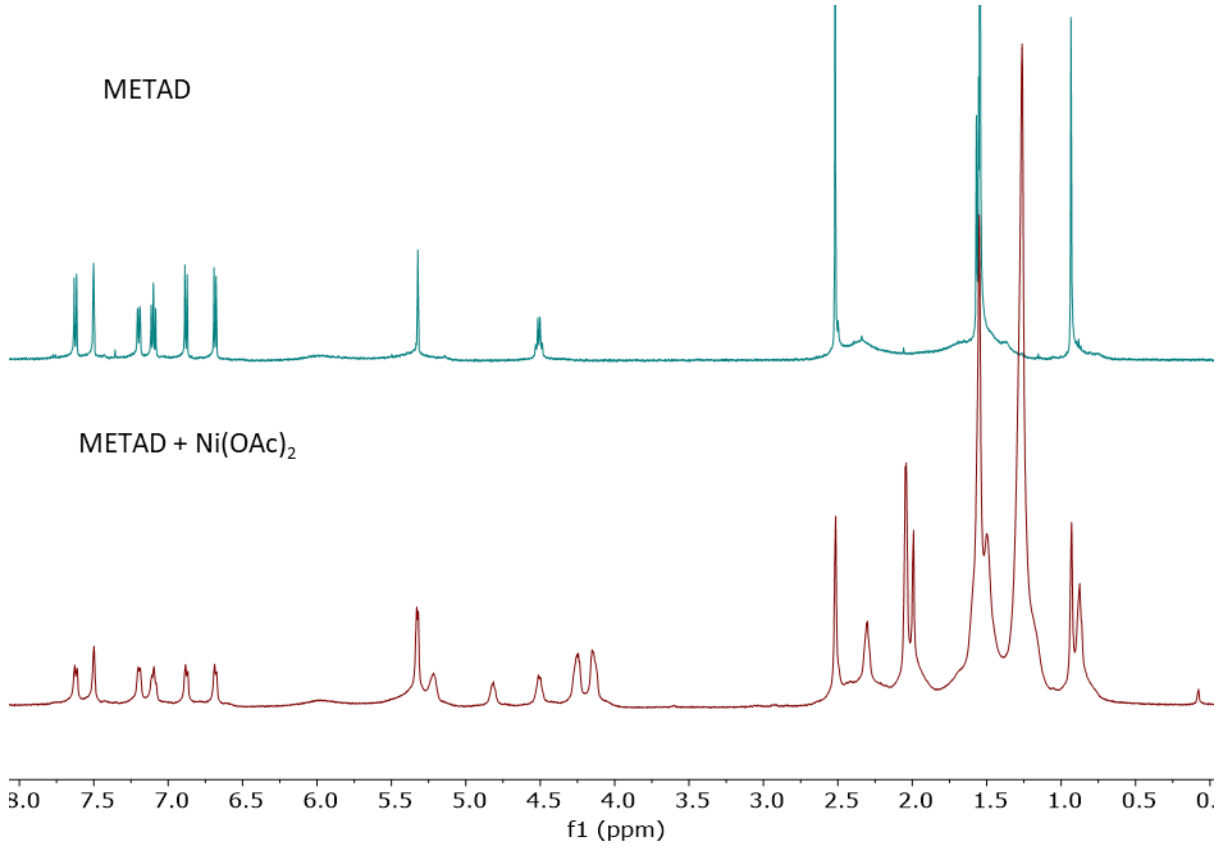

Figure 31. *^{1}H NMR (d_2-DCM 25 °C, 500 MHz) of attempted (METAD)Ni(OAc)$_2$ synthesis. Top (green): apo METAD ligand; Bottom (red): Putative (METAD)Ni(OAc)$_2$ complex.*

On closer examination of the peak integrations of the (METAD)Ni(OAc)$_2$ ^{1}H NMR spectra, it is apparent that there are multiple species present in the product mixture (**Figure 32**). Whereas the aromatic signals integrate as expected with the signals attributed to the mesityl *o*-methyl groups and benzylic methine signals, the two new peaks at 4.14 and 4.24 ppm integrate to 5 protons each, and several alkyl peaks integrate in an impossibly large ratio with respect to the aromatic signals.

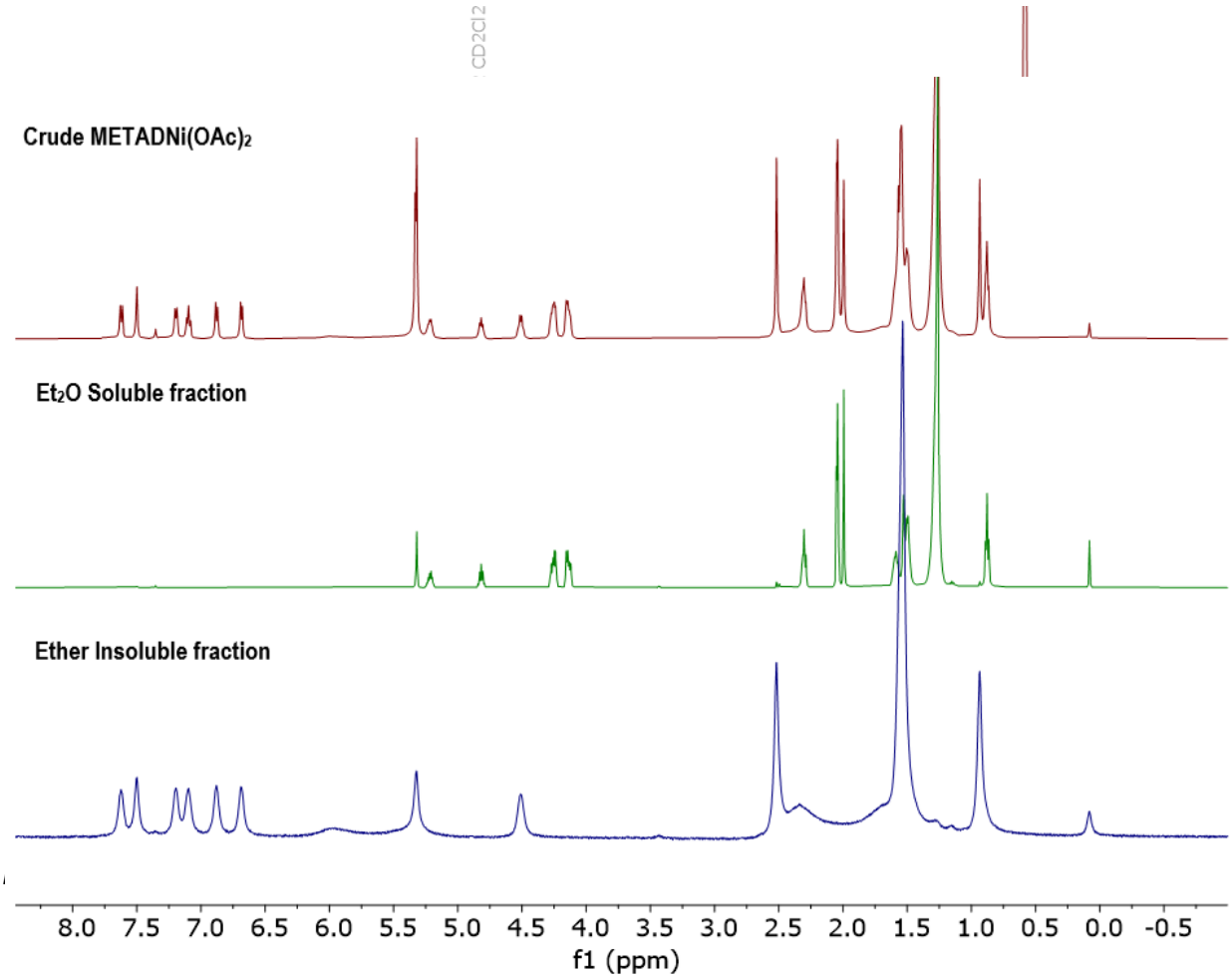

Figure 32. *^{1}H NMR (d_2-DCM 25 °C, 500 MHz) of the ether-washed crude (METAD)Ni(OAc)$_2$ complex. Top (red): crude complex mixture; Middle (green): ether-soluble fraction, unknown impurity/decomposition product; Bottom (blue): ether-insoluble fraction, apo-METAD*

The crude (METAD)Ni(OAc)$_2$ reaction mixture was washed with ether, leaving behind a yellow precipitate. The solvent was removed *in vacuo* from the ether fraction, and both it and the insoluble portion were characterized by ^{1}H NMR (**Figure 33**). The results were surprising, while two separate species were expected based on the ^{1}H NMR of the crude mixture, the ether-soluble fraction contained peaks previously believed to be the mesityl methyl groups and benzylic hydrogens, the new signals at 4.14 and 4.24 ppm, and most of the alkyl region signals. Noticeably absent were any aromatic peaks, which was strange considering METAD is almost entirely

aromatic. The insoluble portion was determined to be apo-METAD, indicating that the mixture was the result of either decomposition or an incomplete reaction.

Following this unsuccessful approach, the (dme)$NiBr_2$ complexation with METAD reported by Coates and coworkers was carried out. (METAD)$NiBr_2$ was synthesized in 42% yield according to literature procedures[48] and isolated as air-stable blood red crystals. From here, the crystals were dissolved in anhydrous, degassed diethyl ether and cooled to -78 ^oC. Two equivalents of 1.6 M MeLi in ether were added dropwise causing the solution to chainge in color from deep red to deep purple. The reaction was stirred under argon for 4h at -78 ^oC. The ether was removed *in vacuo* at 0 ^oC and the remaining mixture was redissolved in anhydrous, degassed benzene and filtered through a Schlenk frit packed with celite. The remaining solution was flash frozen in liquid nitrogen and the benzene was sublimed off *in vacuo* to yield a fluffy purple powder (66% yield). The product was characterized by ^1H, ^{13}C, HSQC, and HMBC NMR techniques (**Figures 33-36**).

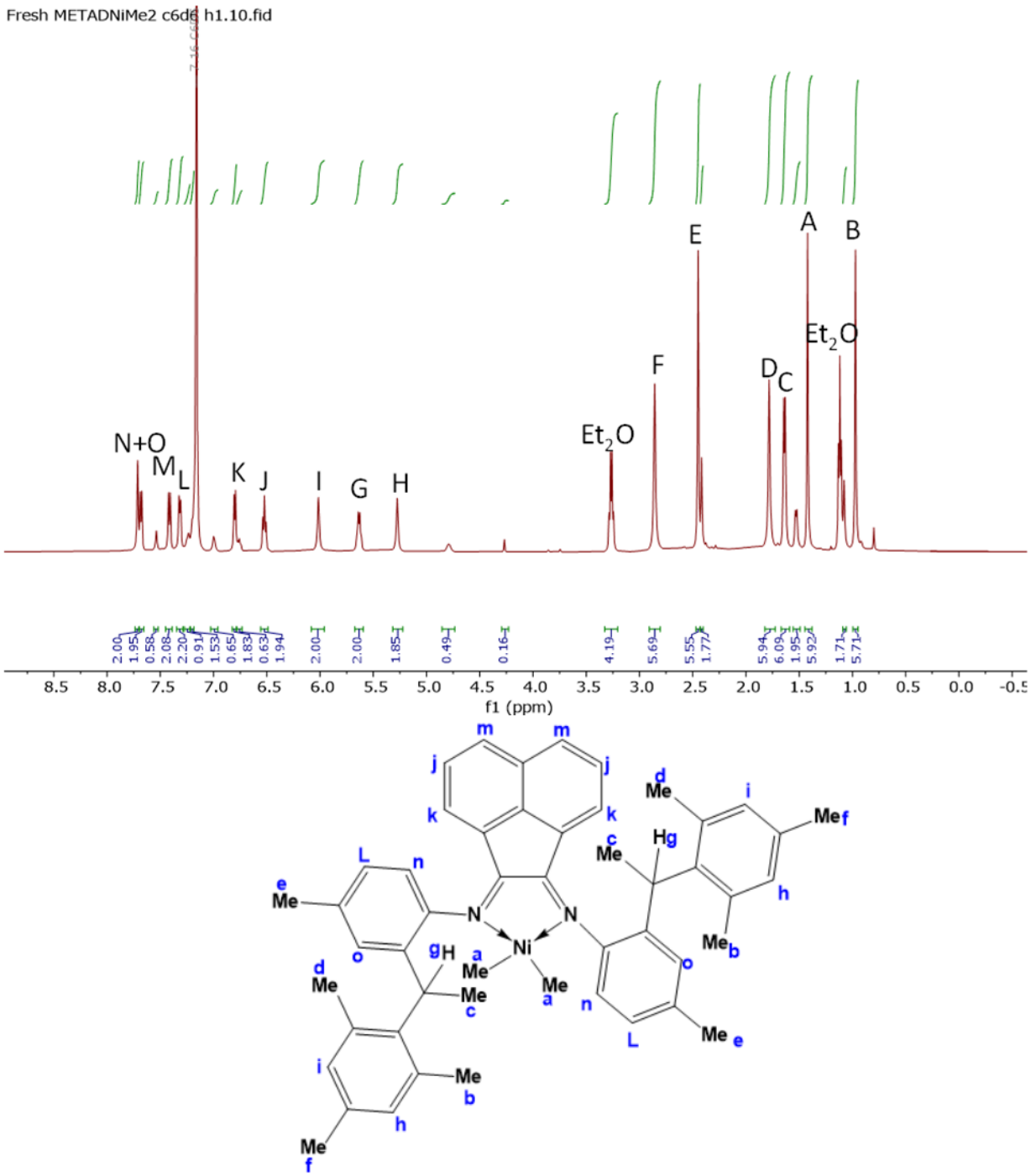

Figure 33. *^{1}H NMR of (METAD)$NiMe_2$ (C_6D_6, 25 ^{o}C, 500MHz) with peak assignments*

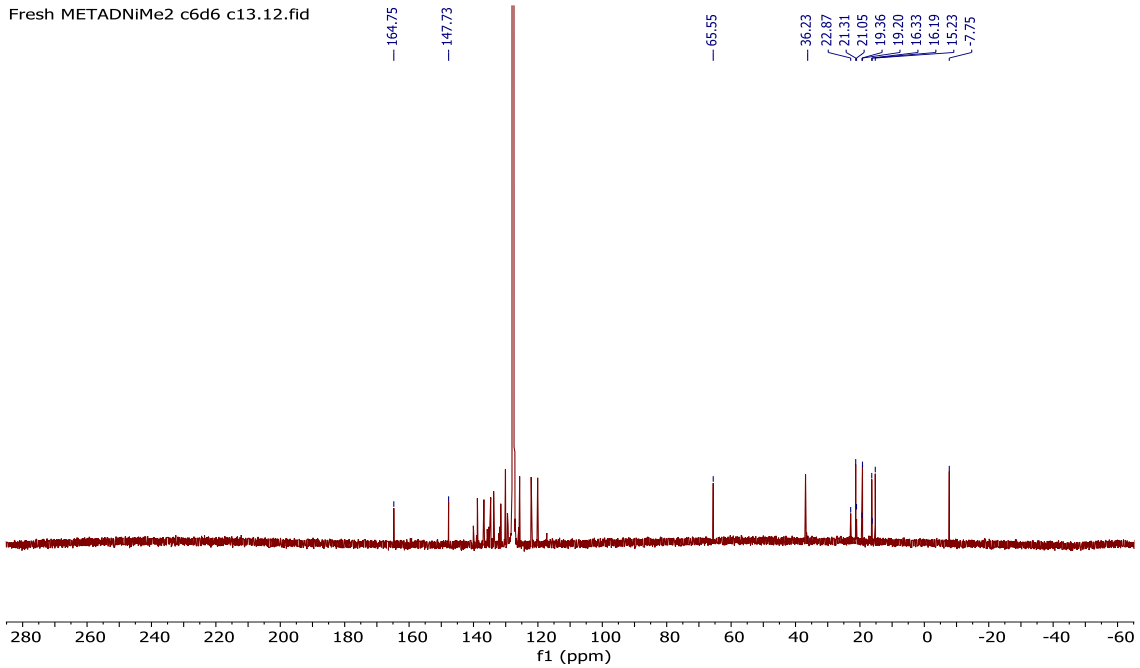

Figure 34. *^{13}C NMR (C_6D_6 25 ^oC, 500 MHz) of the isolated (METAD)$NiMe_2$*

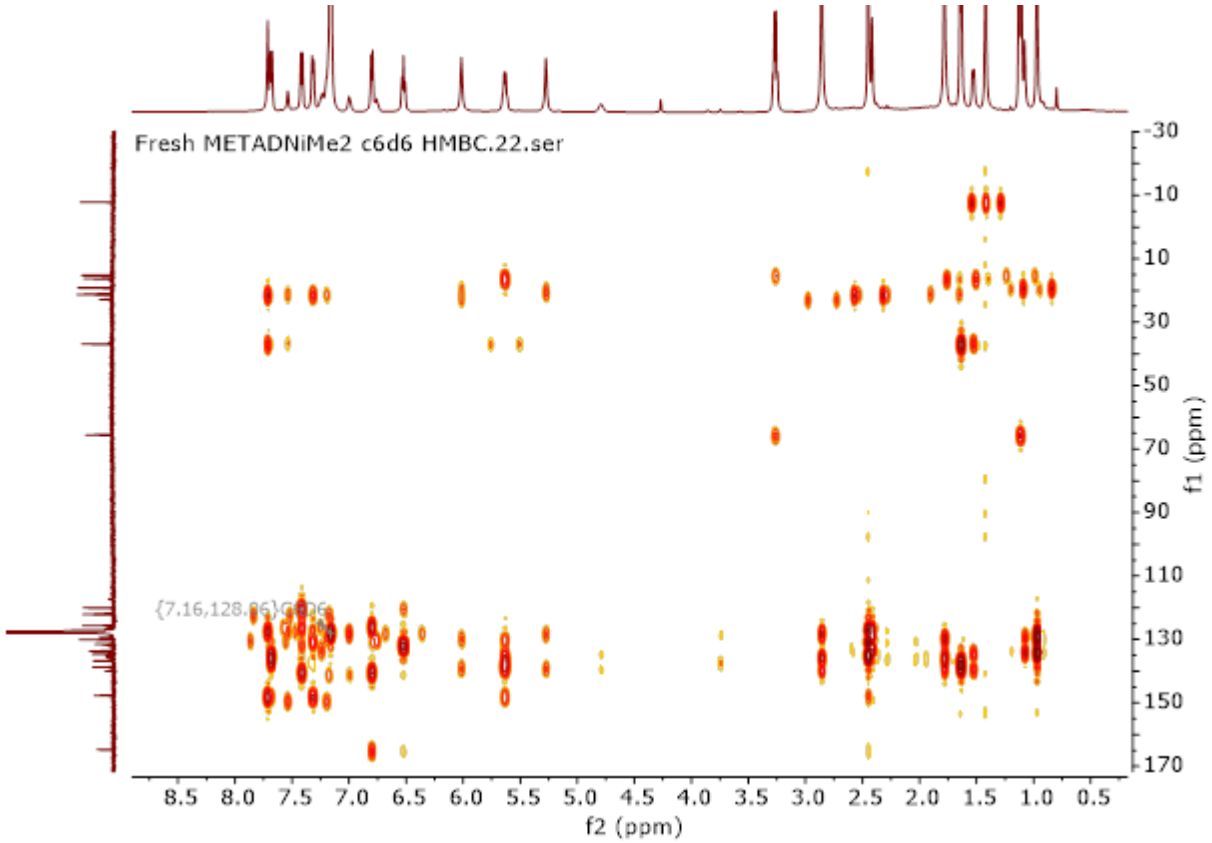

Figure 35. *^1H-^{13}C HMBC spectra (C_6D_6 25 ^oC, 500 MHz) of the isolated (METAD)$NiMe_2$*

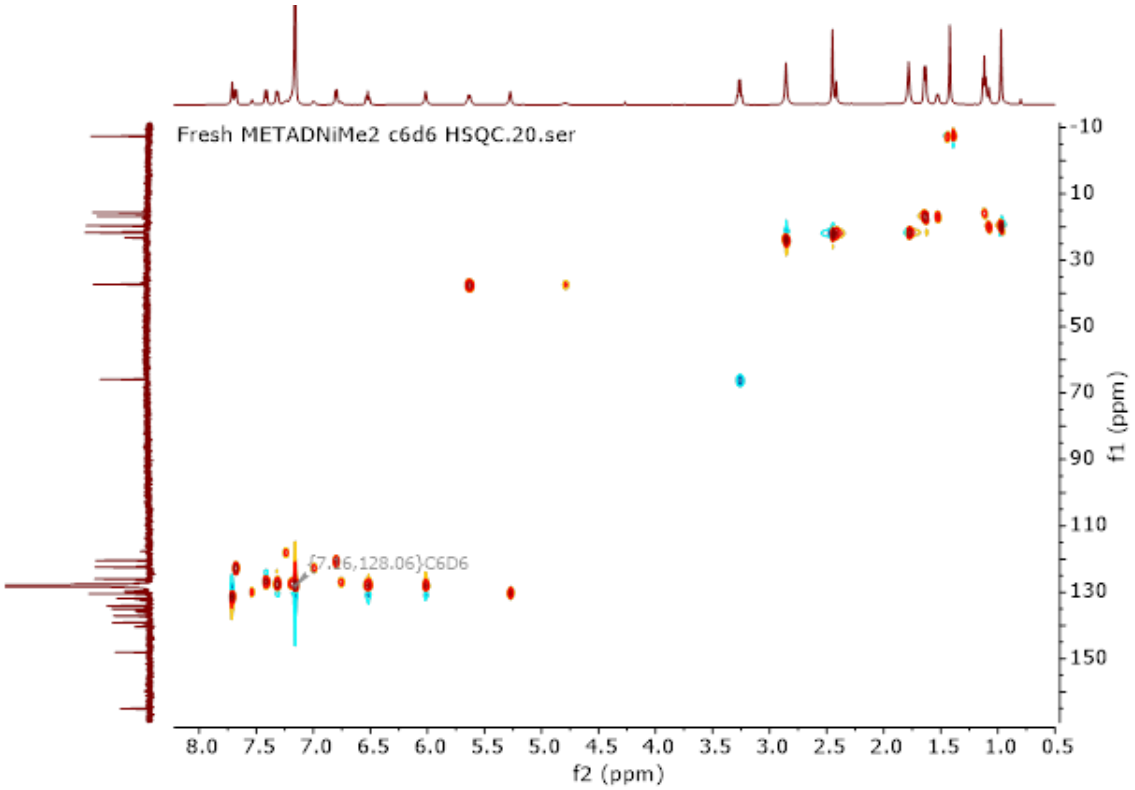

Figure 36. *^{1}H-^{13}C HSQC NMR spectra (C_6D_6, 25 °C, 500 MHz) of (METAD)$NiMe_2$*

The ^{1}H NMR spectra of (METADNiMe_2 lacks an upfield Ni-Me peak (**Figure 33**). Using HSQC analysis, the Ni-Me peak is assigned to be at 1.41 ppm, with a negative ^{13}C cross-peak at -7.7 ppm (**Figure 35**). This signal is extremely downfield compared to other Ni-Me complexes and implies higher electron density on the methyl ligands. The characteristic signals between 5 and 7 were also able to be assigned. The ^{1}H signals at 6.8 and 6.52 ppm were assigned as the 3- and 4-position hydrogens on the anthraquinone backbone. The signals at 6.01 and 5.26 ppm was assigned to be the *m*-hydrogens on the axial mesitylene rings, which were in unequal electronic environments over the Ni center as expected. The quartet at 5.62 ppm was assigned to be the benzylic hydrogen with cross peaks in the HMBC spectra (**Figure 36**) to both *ipso*-carbons on the toludinyl and mesityl rings (140 and 129.2 ppm, respectively) and the benzylic methyl group (19.5 ppm). Similar to the *m*-mesityl hydrogens, the *o*-mesityl methyl groups also experienced unequal electronic environments, and were assigned to be the signals at 0.96 (potentially over the electron-

withdrawing Ni center) and 1.77 ppm (potentially over the diimine ligand backbone). The *p*-methyl group on the mesityl rings was assigned to the signal at 2.83 ppm. The remaining alkyl peak at 2.45 ppm was determined to be the toludinyl *p*-methyl group. Attempts to grow diffraction quality crystals of (METAD)$NiMe_2$ were unsuccessful.

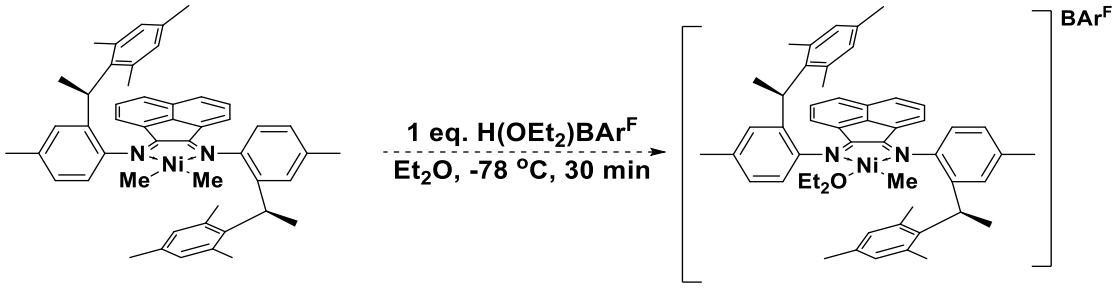

Scheme 24. *Protonation of (METAD)$NiMe_2$ with Brookhart's Acid*

After synthesizing the novel (METAD)$NiMe_2$ complex, the final synthetic step of protonating a methyl ligand with Brookhart's acid to yield the cationic Ni(II)Me(OEt_2) complex was investigated. Brookhart's acid was synthesized using a modified literature procedure,[54] where an HCl diethyl ether solution was used in place of $HCl_{(g)}$. Afterwards, a solution of the prepared Brookhart's acid was added dropwise to a (METAD)$NiMe_2$ solution in ether at -78 °C (**Scheme**

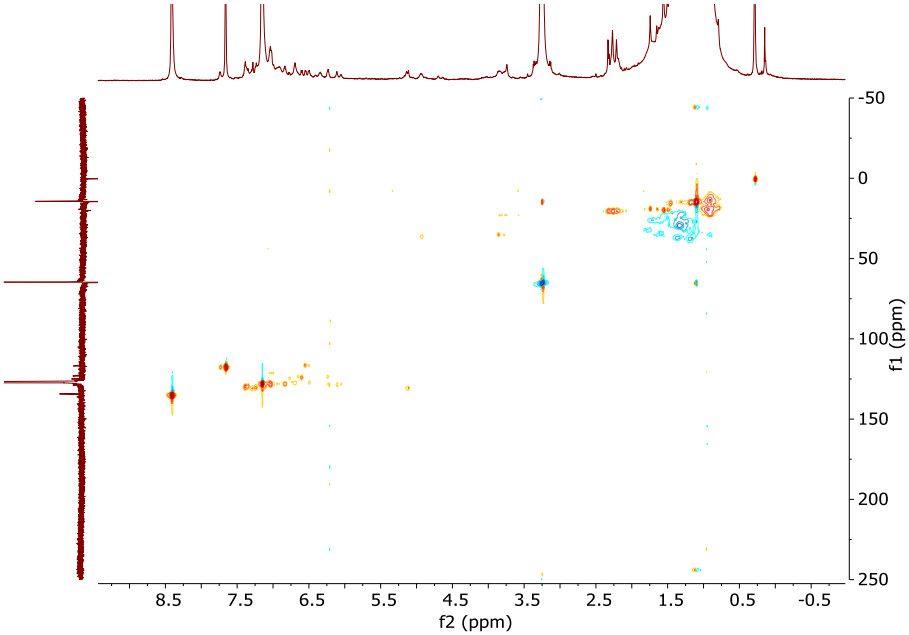

Figure 37. *^1H-^{13}C HSQC NMR spectra (C_6D_6, 25 °C, 600 MHz) of (METAD)$NiMe_2$ treated with Brookhart's acid at -78 °C*

24).. This solution was stirred for 30 min, the solvent was removed *in vacuo*. No upfield Ni-Me peaks were observable in the ^{1}H NMR spectrum, nor negative ^{13}C cross-peaks in the HSQC spectra (**Figure 37**).

4.3 Future work

Future efforts in this project will be focused on synthesizing the [(METAD)NiMe(OEt_2)]BAr^F complex that is predicted to stereoselectively copolymerize propylene and VSEs. The order of acid addition may play a role – in the synthesis of other cationic diimine Ni(II) complexes with BAr^F counterions,[9] the dialkyl Ni complex is added to a solution of Brookhart's acid, instead of the acid to the complex. In addition to this, other ethereal solvents (1,4-dioxane, methyl *t*-butyl ether) could be explored. If the ether complex proves to be unstable, the [(METAD)NiMe(MeCN)]BAr^F complex could be prepared by addition of MeCN to the protonation reaction. The stronger MeCN ligand may impart extra stability towards the cationic complex, however it would compete with VSE monomers for coordination to the Ni center more effectively than ether.

After the cationic complex is synthesized, three important experiments must be performed – analysis of the solid-state structure by x-ray diffraction, homopolymerization of propylene to verify isotactic iPP can be made by the cationic complex, and low-temperature NMR studies into the insertion behavior of VSEs in to the Ni-Me bond. The XRD structure of the complex will verify it's identity and structure, and would be useful if a new stereochemical model would need to be developed. The catalyst must also homopolymerize propylene isostatically, otherwise new ligand structures would need to be investigated. Finally, insertion of VSEs at low temperatures must be feasible enough to produce copolymers with sufficient silyl ether content (2-3%). Brookhart reports that the insertion of triethoxyvinylsilane did not occur at -80 ^{o}C in his cationic Ni diimine

complexes, and only occurred slowly when warmed to -60 °C.[48] This may cause issues since these low temperatures are required to discourage chain-walking by Ni diimine complexs – Coates reports a 20% increase in chain-walking between -60 and -78 °C by his diimine complex.[51]

REFERENCES

1. Stürzel, M., Mihan, S. & Mülhaupt, R. From Multisite Polymerization Catalysis to Sustainable Materials and All-Polyolefin Composites. *Chem. Rev.* **2016,** *116*, 1398–1433.
2. Sauter DW, Taoufik M and Boisson C, Polyolefins: A Success Story. *Polymer* **2017**, *9*, 185-198.
3. Walsh, D. J.; Hyatt, M. G.; Miller, S. A.; and Guironnet, D. Recent Trends in Catalytic Polymerizations. *ACS Catal.* **2019**, *9*, (12), 11153–11188.
4. Franssen, N. M. G.; Reek, J. N. H.; and de Bruin, B. Synthesis of functional 'polyolefins': state of the art and remaining challenges. *Chem. Soc. Rev*. **2013**, *42*, 5809-5833.
5. Kaminsky, W. Trends in Polyolefin Chemistry. *Macromol. Chem. Phys.* **2008**, *209*, 459–466.
6. Coiai, S.; Passaglia, E.; Aglietto, M.; Ciardelli, F. Control of Degradation Reactions during Radical Functionalization of Polypropylene in the Melt. *Macromolecules*, **2004** *37* (22), 8414-8423.
7. Carrow, B. P. and Nozaki, K. Transition-Metal-Catalyzed Functional Polyolefin Synthesis: Effecting Control through Chelating Ancillary Ligand Design and Mechanistic Insights. *Macromolecules* **2014**, 47, (8), 2541–2555.
8. Nakamura, A.; Ito, S.; and Nozaki, K. Coordination-Insertion Copolymerization of Fundamental Polar Monomers. *Chem. Rev.* **2009**, *109*, 5215–5244.
9. Johnson, L. K.; Mecking, S.; Brookhart, M. Copolymerization of Ethylene and Propylene with Functionalized Vinyl Monomers by Palladium(II) Catalysts. *J. Am. Chem. Soc.* **1996**, *118*, 267-268.
10. Wang, C.; Friedrich, S.; Younkin, T. R.; Li, R.T.; Grubbs, R. H.; Bansleben, D. A.; and Day, M. W. Neutral Nickel(II)-Based Catalysts for Ethylene Polymerization. *Organometallics* **1998**, *17*, (15), 3149–3151
11. Drent, E.; van Dijk, R.; van Ginkel, R.; van Oort, B.; and Pugh, R. I. Palladium Catalyzed Copolymerisation of Ethene with Alkylacrylates: Polar Comonomer Built Into the Linear Polymer Chain. *Chem. Commun.*, **2002**, 744-745.
12. Guironnet, D.; Roesle,P,; Rünzi, T.; Göttker-Schnetmann, I.; and Mecking S. Insertion Polymerization of Acrylate. *J. Am. Chem. Soc.* **2009**, *131*, (2), 422–423.
13. Gao, J.; Yang, B.; Chen, C. Sterics versus electronics: Imine/Phosphine-Oxide-Based Nickel Catalysts for Ethylene Polymerization and Copolymerization *J. Catal.* **2019,** *369*, 233–238.
14. Zou, C.; Tan, C.; Pang, W.; and Chen, C. Amidine/Phosphine-Oxide-Based Nickel Catalysts for Ethylene Polymerization and Copolymerization. *Chem. Cat. Chem.* **2019**, *11*, 5339–5344.
15. Wigbers, C.; Prigge, J.; Mu, Z.; Fröhlich, R.; Chi, L.; and Würthwein, E. Synthesis, Structures, and Aggregation Properties of N-Acylamidines. *Eur. J. Org. Chem.* **2011**, 861-877.

16. Chen, J.; Gao, Y.; Marks, T. J. Early Transition Metal Catalysis for Olefin–Polar Monomer Copolymerization. *Angew. Chem.* **2020**, *132*, 14834 – 14843.
17. Makio, H.; Terao, H.; Iwashita A.; and Fujita, T. FI Catalysts for Olefin Polymerization—A Comprehensive Treatment. *Chem. Rev.* **2011**, *111*, 3, 2363–2449.
18. Liu, D.; Wang, S.; Wang, H.; Chen, W. Trialkylaluminums: Efficient cocatalysts for bis(phenoxy-imine)zirconium complexes in ethylene polymerization *J. Mol. Catal. A* **2006**, *246*, 53-58.
19. Goerdeler, J. and Richter, R. Imidoyl-isocyanate und ihre Folgeprodukte *Synthesis* **1978**, *10*, 760-762.
20. Jubinville, D.; Esmizadeh, E.; Saikrishnan, S.; Tzoganakis, C.; and Mekonnen, T.; A comprehensive review of global production and recycling methods of polyolefin (PO) based products and their post-recycling applications. *Sustainable Materials and Technologies*, **2020**, *25*, e00188.
21. Chamas, A.; Moon, H.; Zheng, J.; Qiu, Y.; Tabassum, T.; Jang, J. H.; Abu-Omar, M.; Scott, S. L.; and Suh, S.; Degradation rates of plastics in the environment. *ACS Sustainable Chem. Eng.* **2020**, *8*, (9), 3494-3511.
22. Gewert, B.; Plassmann, M. M.; MacLeod, M. Pathways for Degradation of Plastic Polymers Floating in the Marine Environment. *Environ. Sci. Process. Impacts*, **2015**, *17*, (9), 1513−1521.
23. Albertsson, A.-C.; Karlsson, S. The Influence of Biotic and Abiotic Environments on the Degradation of Polyethylene. *Prog. Polym. Sci.* **1990**, *15*, (2), 177−192.
24. Morgen, T.O.; Baur, M.; Göttker-Schnetmann, I.; and Mecking, S. Photodegradable branched polyethylenes from carbon monoxide copolymerization under benign conditions. *Nat. Comm.* **2020,** *11*, 3693-3700.
25. *Catalytic Synthesis of Alkene-Carbon Monoxide Copolymers and Cooligomers*; Sen, A., Ed.; Kluwer Academic: Dordrecht, The Netherlands, 2003.
26. F. Ballauf, O. Bayer, L. Leichmann, G. Pat., 863 711, **1941**.
27. Bianchini C. and Meli, A. Alternating copolymerization of carbon monoxide and olefins by
single-site metal catalysis. *Coordination Chemistry Reveiws*, **2002**, *225*, 35-66.
28. Drent, E.; Van Broekhoven, J. A. M.; and Doyle, M.J.; Efficient palladium catalysts for the copolymerization of carbon monoxide with olefins to produce perfectly alternating polyketones. *J. Orgmet. Chem.* **1991,** *417*, 235-251.
29. Shell, Carilon Thermoplastic Polymers, Information Sheet, **1994**.
30. Soomro, S. S.; Cozzula, D.; Leitner, W.; Vogta, H.; and Müller, T. E. The Microstructure and Melt Properties of CO–Ethylene Copolymers with Remarkably Low CO Content. *Polym. Chem.*, **2014**, *5*, 3831–3837.
31. Drent, E.; van Dijk, R.; van Ginkel, R.; van Oort, B.; and Pugh, R. I. The first example of palladium catalyzed non-perfectly alternating copolymerisation of ethene and carbon monoxide *Chem. Commun.* **2002**, 964–965.
32. Haras, A.; Michalak, A.; Rieger, B; and Ziegler, T.; Theoretical Analysis of Factors Controlling the Nonalternating CO/C2H4 Copolymerization. *J. Am. Chem. Soc.* **2005**, *127*, (24), 8765–8774.

33. Luo, R. Newsham, D. K. and Sen, A. Palladium-Catalyzed Nonalternating Copolymerization of Ethene and Carbon Monoxide: Scope and Mechanism. *Organometallics* **2009**, *28*, 6994–7000.
34. Hearley, A. K.; Nowack, R.J.; and Rieger, B. New Single-Site Palladium Catalysts for the Nonalternating Copolymerization of Ethylene and Carbon Monoxide. *Organometallics* **2005,** *24*, 2755-2763.
35. Soomro, S. S.; Cozzula, D.; Leitner, W.; Vogta, H.; and Müller, T. E. The Microstructure and Melt Properties of CO–Ethylene Copolymers with Remarkably Low CO Content. *Polym. Chem.* **2014**, *5*, 3831–3837.
36. Baur, M.; Lin, F.; Morgen, T. O.; Odenwald, L.; and Mecking, S. Polyethylene Materials with In-Chain Ketones from Catalytic Copolymerization. *Science* **2021**, *374*, (6557), 604-607.
37. Kacker, S. and Sen, A. Nonterminating Alternating Copolymerization of Ethene with Carbon Monoxide and the Synthesis of Graft Polymers with alt-Ethene-Carbon Monoxide Blocks. *J. Am. Chem. Soc.* **1995**, *117*, (42), 10591–10592.
38. Voccia, M.; Odenwald, L.; Baur, M.; Lin, F.; Falivene, L.; Mecking, S.; and Caporaso, L. Mechanistic Insights into Ni(II)-Catalyzed Nonalternating Ethylene–Carbon Monoxide Copolymerization. *J. Am. Chem. Soc.* **2022**, *144*, (33), 15111–15117.
39. Chen, S.; Pan, R.; Chen, M.; Liu, Y.; Chen, C.; and Lu, X. Synthesis of Nonalternating Polyketones Using Cationic Diphosphazane Monoxide-Palladium Complexes. *J. Am. Chem. Soc.* **2021**, *143*, (28), 10743–10750.
40. Zhu, L.; Gaire, S.; Ziegler, C.J.; and Jia, L. Nickel Catalysts for Non-Alternating CO-Ethylene Copolymerization. *ChemCatChem* **2022**, *14*, e2022009.
41. Tang, S.; Seidel, F.W.; and Nozaki, K. High Density Polyethylenes Bearing Isolated In-Chain Carbonyls. *Angew. Chem. Int. Ed.* **2021**, *60*, 26506–26510.
42. Skupov, K. M.; Marella, P. R.; Simard, M.; Yap, G. P A.; Allen, N.; Conner, D.; Goodall, B. L.; Claverie, J. P. Palladium Aryl Sulfonate Phosphine Catalysts for the Copolymerization of Acrylates with Ethene. *Macromol. Rapid Commun.* **2007**, *28*, 2033–2038.
43. Mayo, F. R. and Lewis, F. M. Copolymerization. I. A Basis for Comparing the Behavior of Monomers in Copolymerization; The Copolymerization of Styrene and Methyl Methacrylate. *J. Am. Chem. Soc*. **1944**, *66*, (9), 1594 – 1601.
44. Merz, E.; Afrey, T.; and Goldfinger, G. Intramolecular reactions in vinyl polymers as a means of investigation of the propagation step. *J.* Polym. Sci., **1946**, *1*, (2), 75-82.
45. Rado, R. and Zelenak, P. Applications of crosslinked polyethylene. *International Polymer Science and Technology*, **1992,** *19*, (4), 72-77.
46. Johnson, L. K.; McLain, S. J.; Sweetman, K. J.; Wang, Y.; Bennett, A. M. A.; Wang, L.; McCord, E. F.; Lonkin, A.; Ittel, S. D.; Radzewich, C. E.; Schiffino, R. S. WO 2003044066, **2003.**
47. Chen, Z.; Liu, W.; Daugulis, O.; Brookhart, M. Mechanistic Studies of Pd(II)-Catalyzed Copolymerization of Ethylene and Vinylalkoxysilanes: Evidence for a β-Silyl Elimination Chain Transfer Mechanism *J. Am. Chem. Soc.* **2016**, *138*, 16120−16129.

48. Chen, Z.; Leatherman, M. D.; Daugulis, O.; and Brookhart, M. Nickel-Catalyzed Copolymerization of Ethylene and Vinyltrialkoxysilanes: Catalytic Production of Cross-Linkable Polyethylene and Elucidation of the Chain-Growth Mechanism. *J. Am. Chem. Soc.* **2017**, *139*, (44), 16013–16022.
49. Tripathi, D. Practical guide to polypropylene. Shrewsbury: RAPRA Technology. 2001.
50. Luckham, S. L. J. and Nozaki, K. Toward the Copolymerization of Propylene with Polar Comonomers. *Acc. Chem. Res.* **2021**, *54*, (2), 344–355.
51. Cherian, A. E.; Rose, J. M.; Lobkovsky, E. B.; Coates, G. W. A C2-Symmetric, Living α-Diimine Ni(II) Catalyst: Regioblock Copolymers from Propylene. *J. Am. Chem. Soc.* **2005**, *127*, 13770− 13771.
52. Göttker-Schnettmann, I. and Mecking, S. A Practical Synthesis of [(tmeda)Ni(CH_3)$_2$], Isotopically Labeled [(tmeda)Ni($^{13}CH_3$)$_2$], and Neutral Chelated-Nickel Methyl Complexes. *Organometallics* **2020**, *39*, (18), 3433–3440.
53. Johnson, L.K.; Killian, C. M.; and Brookhart, M. New Pd(II)- and Ni(II)-Based Catalysts for Polymerization of Ethylene and a-Olefins. *J. Am. Chem. Soc.* **1995**, *117*, 6414-6415.
54. Brookhart, M.; Grant, B.; Volpe, A. F. [(3,5-(CF_3)$_2$$C_6H_3$)$_4$B]$^-$[H($OEt_2$)$_2$]$^+$: A convenient reagent for generation and stabilization of cationic, highly electrophilic organometallic complexes. *Organometallics*, **1992,** *11*, (11), 3920-3922.